D1-82-0423

BOEING SCIENTIFIC RESEARCH LABORATORIES

Obstacle-Induced Flow Recirculation

G. K. Timm

March 1965

D1-82-0423

BOEING SCIENTIFIC RESEARCH LABORATORIES

FLIGHT SCIENCES LABORATORY REPORT NO. 94

OBSTACLE-INDUCED FLOW RECIRCULATION

by

G. K. Timm

March 1965

OBSTACLE-INDUCED FLOW RECIRCULATION

by

G. K. Timm

Abstract

The results of a series of tests studying obstacle-induced flow recirculation are presented. A small scale rotor creates a slipstream which impinges on a ground plane and then encounters an obstacle. The principal test technique is that of flow visualization using sawdust particles, but in addition some power measurements are made.

I. INTRODUCTION

The need for a means of describing and predicting jet impingement and flow recirculation phenomena is well established[1]. These phenomena are of particular importance for aircraft operating near the ground, i.e. within the ground effect regime. They may be created, under certain circumstances, either by a pure jet or by the slipstream of a rotor impinging on the ground[2].

The present paper deals mainly with flow visualization and is in support of theoretical work connected with the flow recirculation problem[1,3]. However, some quantitative data of power required in the presence of flow recirculation are also included.

The complexity of the problem necessitated an extension of this work from simply furnishing a model for a mathematical analysis to that of also investigating flow recirculation in more general terms[4,5,6]. Thus, tests were conducted not only with a progression of prism obstacles[1], which have a simple geometry, but also with various other obstacles.

Further tests are planned to better understand the flow patterns observed in the present tests, to check that the types of recirculation seen here are actually flow recirculation as well as particle recirculation, and to explore further cases.

II. FLOW VISUALIZATION

Jet impingement and flow recirculation induced by various obstacles as well as the general flow field in the neighborhood of a rotor were investigated with the help of the particle track method[7,8,9]. This flow visualization technique requires that, if the flow field is to be mapped with any accuracy, the tracer material should be relatively light (low inertia) and that the individual particles should have high drag[9].

Various light-weight materials, with particle sizes between 0.295 mm and 0.147 mm, were tried and discarded in favor of sawdust. The best results were obtained with sugar pine or spruce sawdust from a relatively fine-toothed band saw[10]. Fir sawdust was the only other material performing almost equally as well as the above two and was used exclusively in this study. Other tracer particles tested for flow visualization purposes were:

1) corn meal (also Farina) -- recollected into larger clumps after introduction into the flow field through the screen of the sifter,
2) balsa dust -- was too fine and too susceptible to extraneous air movement, resulting in poor particle tracks,
3) flour (also Wondra) -- commercially available flour was too fine; it also recollected into larger clumps (refer to corn meal, above),
4) cork -- was too fine and had too low a reflectance to yield good photographs.

5) styrene beads (styrene divinylbenzene copolymer) -- were too heavy, however had good reflectance.

The characteristics and selection of the proper sawdust have been discussed previously[1].

III. EXPERIMENTAL EQUIPMENT

The following components comprised the experimental equipment (Figure 1):

a) Rotor.

b) Ground plane and rotor drive mechanism.

c) Light source and chopper.

d) Sifter.

e) Recording equipment and material.

f) Control unit.

g) Instrumentation

a) Rotor

The rotor was a Top-Flite wooden model airplane propeller of 12" diameter with a fixed geometric pitch of 5". The rotor had been reworked to provide a smooth surface and painted flat black to eliminate as much glare as possible. The tips were painted white in order to indicate the limits of the rotor disc on the photographs.

b) Ground Plane and Rotor Drive

The 36" x 36" top surface of a table, covered with flat black Formica, was used as the ground plane. The ground plane also served as a support for the rotor drive mechanism.

The rotor drive mechanism consisted of the following major components: rotor drive shaft, Dayton model 5K006, 1/20 HP synchronous electric motor, and a support for shaft and motor.

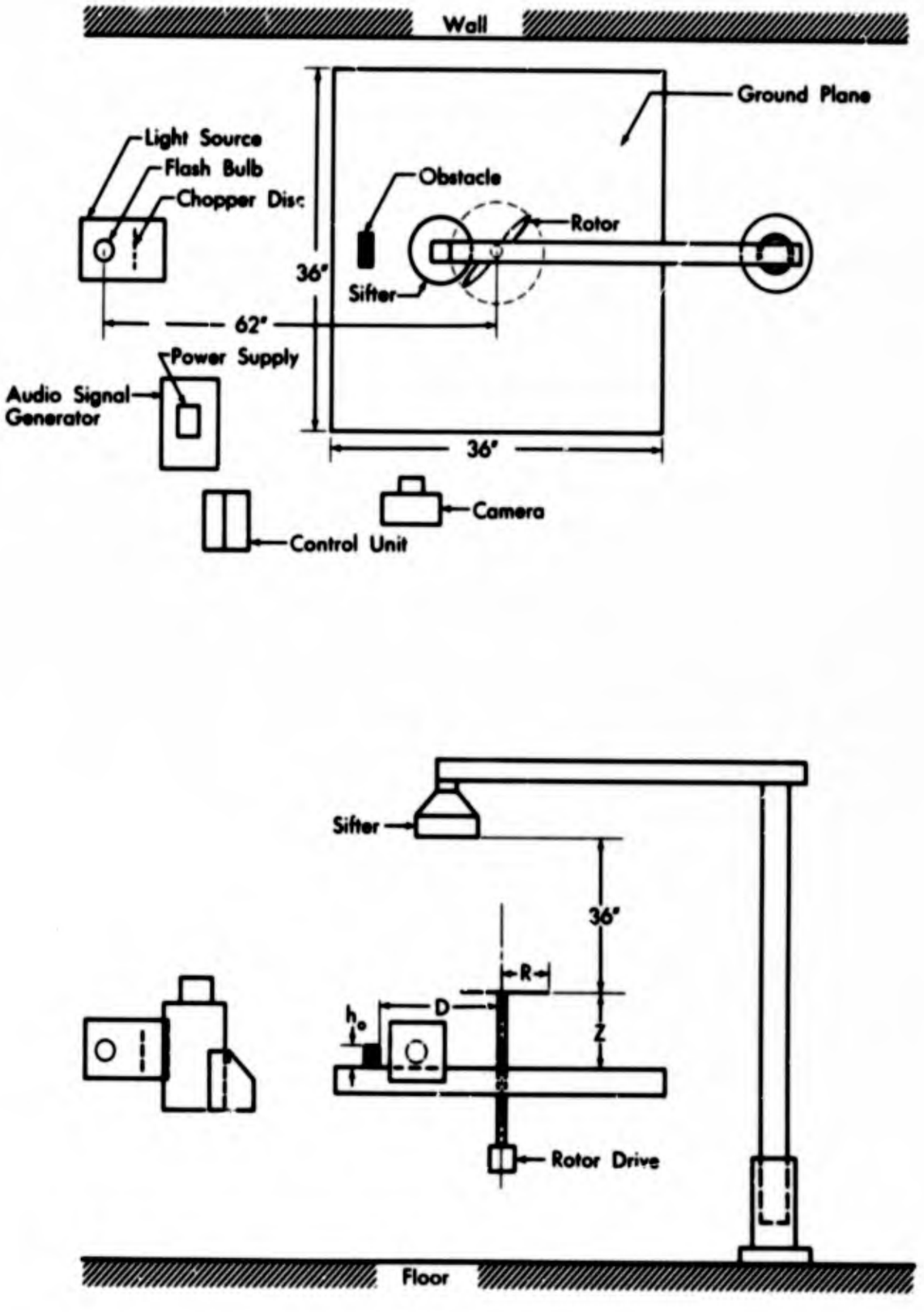

Fig. 1 General arrangement.

The height of the rotor drive shaft could be adjusted. The limits of the rotor disc plane were between approximately 2.25" and 15" above the ground plane. The shaft could also be tilted through ± 45° in a plane normal to the ground plane. However, all runs were made with the rotor disc plane between 3" and 12" and the shaft normal to the ground plane, i.e. rotor disc plane parallel to the ground plane.

The line voltage to the rotor drive motor, as well as to all 115 VAC equipment, was regulated by a Sorensen model 2501 AC voltage regulator. This reduced the fluctuations in the supply voltages to the more sensitive components. The motor was operated at 110.29 ± 0.02 VAC and turned 1800 ± 10 RPM (counter-clockwise).

The support provided a base for the rotor drive motor and incorporated the height and inclination adjustment for the rotor.

c) Light Source and Chopper

The light source (Figure 2) consisted of two 8" spherical second surface mirrors (f = 3.5") with the actual light source, GE PH/31 focal plane flash bulbs, at the common focal point between the two mirrors. An area of 3/32" x 1-3/4" of the silver coating on the front mirror had been removed in order to provide a light slot. This slot was followed by a collecting lens system, which focused the narrow light beam onto the chopper disc.

After passing through the chopper disc the beam was

collimated by a cylindrical lens. The dimensions of the light beam, measured between 9" and 15" from the center line of the rotor drive shaft, were approximately 1" in width and 15" in height.

The chopper (Figure 3) consisted of two pieces of Plexiglas (3/32" thick and 6" diameter) with an "open-closed" pattern. The chopper was driven by a miniature DC motor. Power to the DC motor was supplied by a Kepco model 15-1 M DC power supply, which permitted a reasonably close regulation of the motor revolutions. The chopper disc speed was, for the most part, 1450 ± 50 RPM. The "open-closed" pattern aided in determining the direction of the flow and the velocity of the tracer particles. The light transmission time through the pattern was:

Table 1

"Open-Closed" Pattern of Chopper

Segment	Degrees Open	Light Transmission Time x 10^3 (sec)		
		1400 RPM	1450 RPM	1500 RPM
I	6.25	0.744	0.718	0.694
II	41.75	0.970	4.799	4.639
III	6.50	0.774	0.747	0.722
IV	51.20	6.095	5.885	5.689
V	60.75	7.232	6.983	6.750

The distance between the center of the rotor drive shaft and the center of the flash bulb was approximately 62".

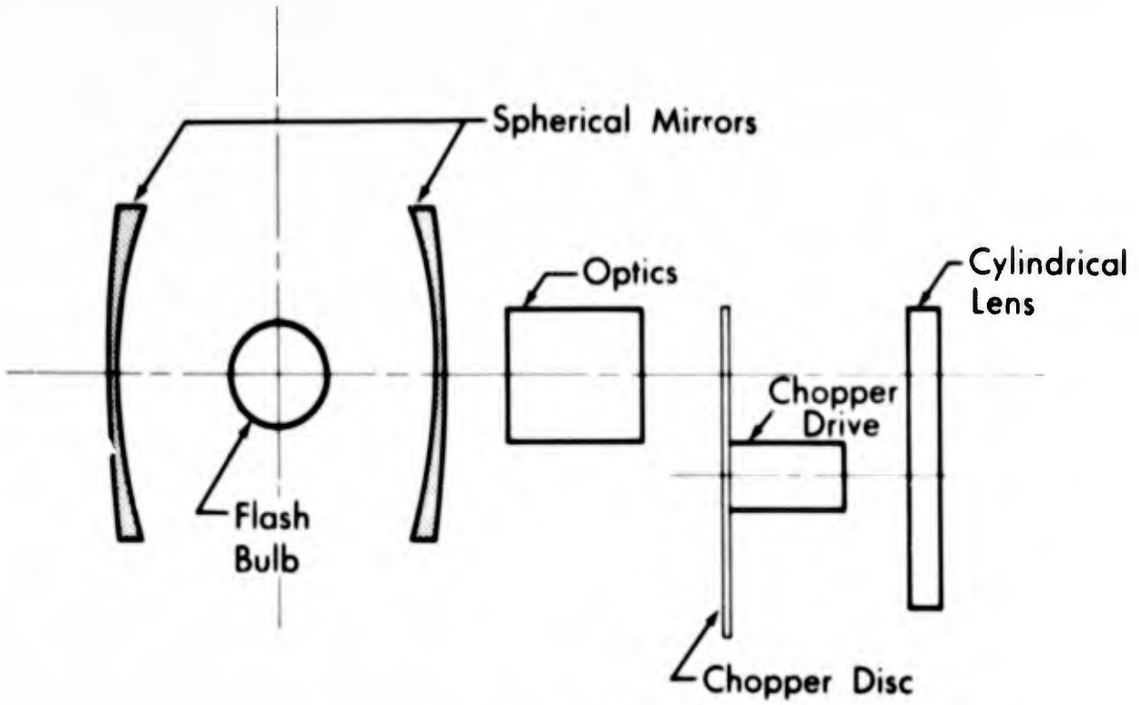

Fig. 2 Light source (side view).

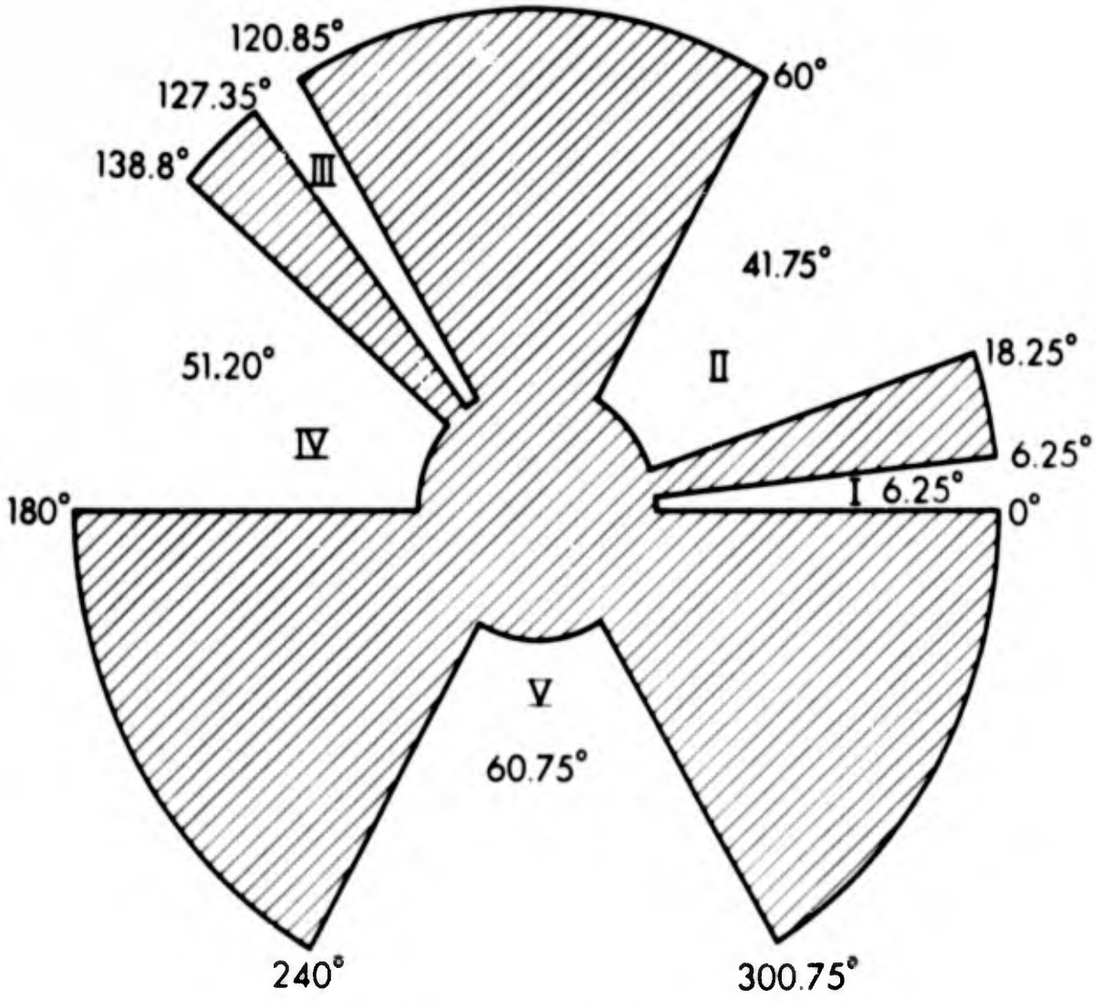

Fig. 3 Chopper.

d) Sifter

The sifter assembly consisted of a Hewlett-Packard model 205 AG audio signal generator, a Jensen Poly-Tech plane piston $10\frac{1}{4}$" speaker, a Tyler standard mesh screen, US equivalent series 50 and a support for the last two components.

The screen, mounted directly to the loudspeaker, contained the presifted sawdust.

The screen-loudspeaker unit (Figure 4) was attached to the support which could be adjusted in height and positioned over any desired location above the ground plane.

The distance between the sifter screen and the rotor disc plane was maintained at 36", regardless of the distance between the ground plane and the rotor disc plane. The position of the sifter screen in the plane parallel to the ground plane was such that the rotor tips passed through the extended vertical axis of the screen-loudspeaker unit (Figure 4).

Optimum sifting, with regard to uniformity of area covered by and volume flow of sawdust, was achieved for this particular setup at approximately 30 to 35 Hz.

e) Recording Equipment and Material

Pictures of the flow field under the various test conditions were taken with a 4 x 5 Speed-Graphic camera with shutter activation by means of a remote solenoid trigger. The film material was Polaroid Type 57 film with a rating of 3000 ASA. The exposure latitude and the grain of this photographic material were adequate. The possibility of an immediate visual check of

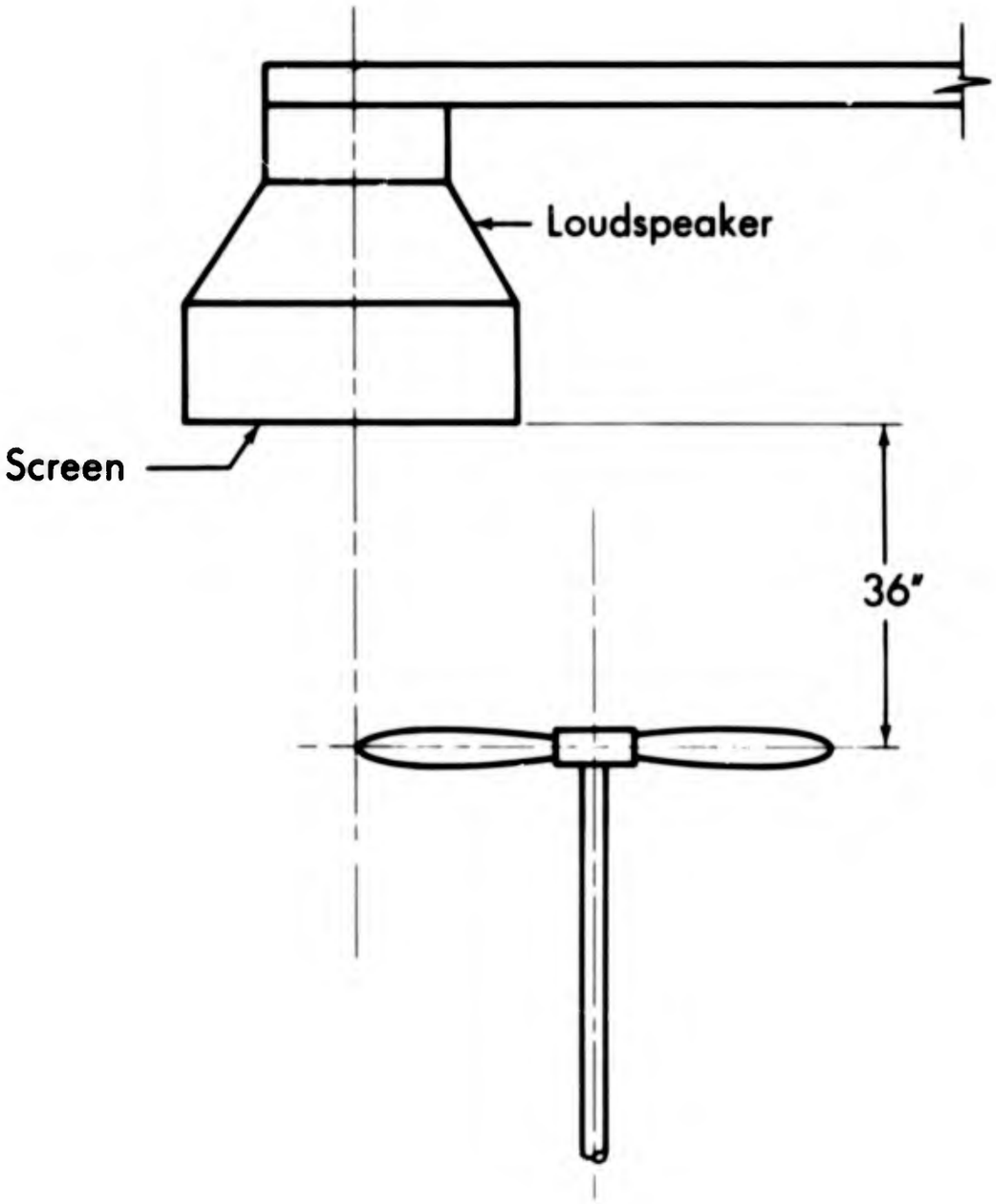

Fig. 4 Sifter.

a test run were, together with the high exposure rating, a great asset. Any minor adjustments between runs could thus be effected without delay.

The remote solenoid camera trigger was necessary for the overhead camera locations. It also allowed the operator to move away from the immediate vicinity of the ground plane, thus reducing the chance of inducing extraneous recirculation.

The camera was always positioned as close to the rotor drive shaft as possible under the circumstances. But great care had to be taken to keep it away from the flow coming off the ground plane, so as to eliminate any possibility of the camera itself inducing recirculation.

f) Control Unit

The control unit provided a central location for all controls necessary to conduct a test by remote control, thus allowing the operator to stand back from the immediate vicinity of the ground plane during a run. It included controls for the rotor drive, the sifter, the camera shutter and the flash trigger.

The major portion of the test was conducted under the following conditions:

Rotor	$N = 1800 \pm 10$ RPM (counter-clockwise)
Chopper	$n = 1450 \pm 50$ RPM
Sifter screen	$h_S = 36"$ above rotor disc plane
Flash bulb	$D_F = 62"$ from rotor drive shaft center line

All runs were photographed such that one picture was taken with the chopper stationary (the particles appear as

streaks) while the others, usually 5 pictures, were taken with the chopper turning at the above RPM.

g) Instrumentation

The rotational speed of the rotor and the chopper were measured with a General Radio Strobotac type 1531A.

The power data were obtained by measuring the voltage drop across a $\frac{1}{2}\Omega$, 1 W. wire-wound resistor ($\pm$ 1.0% accuracy) with a Fluke model 803 AC-DC differential voltmeter.

A Fuess micromanometer model 134b and a total head tube were used during a brief velocity survey behind (below) the rotor disc. The total head tube was traversed along a radial line (Appendix II).

IV. OBSTACLES AND TEST GEOMETRY

All obstacles were made out of Lucite and were, with the exception of the wedge obstacle, d_o = 1" thick (measured radially outward, Figure 5). They were placed on the ground plane (Figure 5), normal to the radial outflow from the rotor at D = 9, 12 and 15", i.e. at 1.5, 2.0 and 2.5 times the rotor radius R, from the rotor drive shaft center line.

The rotor disc was located at Z = 3, 4, 6, 9 and 12" above and parallel to the ground plane, i.e. at 0.5000, 0.667, 1.000, 1.500 and 2.000 times the rotor radius R from the ground plane (Table II).

There were 16 prism obstacles:

Obstacle	Height h_o	Width w_o	Obstacle	Height h_o	Width w_o
1	1"	1"	9	3"	1"
2	1"	2"	10	3"	2"
3	1"	3"	11	3"	3"
4	1"	4"	12	3"	4"
5	2"	1"	13	4"	1"
6	2"	2"	14	4"	2"
7	2"	3"	15	4"	3"
8	2"	4"	16	4"	4"

In addition, the following obstacles were used:

Obstacle	Description
17	1" diameter cylinder, longitudinal axis normal to ground plane, h_o = 2"
18	Same as 17, h_o = 3"

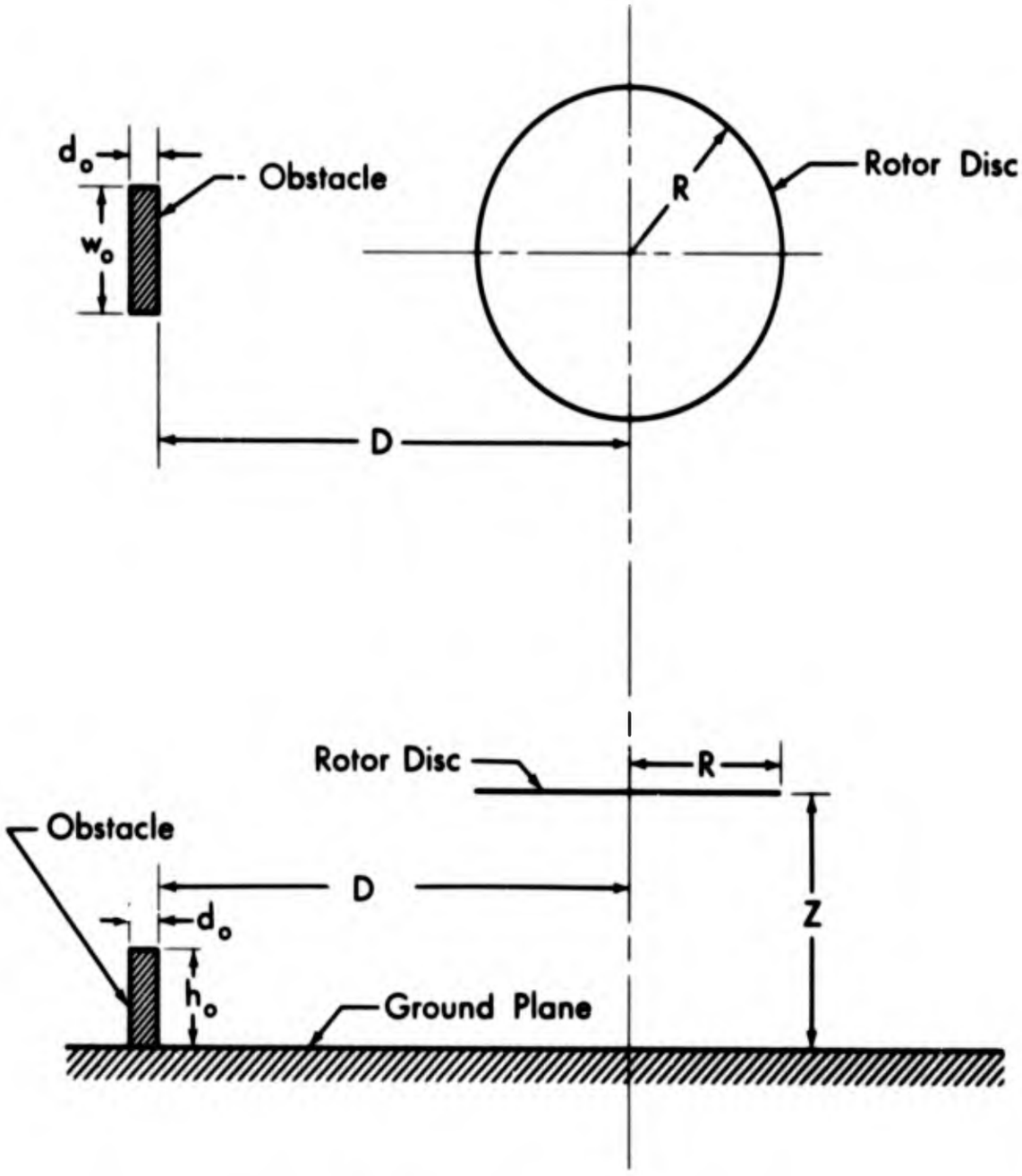

Fig. 5 Test geometry.

Obstacle	Description
19	1" diameter cylinder, longitudinal axis parallel to ground plane and normal to radial outflow, w_o = 2"
20 + 0	Same as 19, w_o = 3"
20 + 3	Obstacle 20 mounted on top of obstacle 3
20 + 7	Obstacle 20 mounted on top of obstacle 7
20 + 11	Obstacle 20 mounted on top of obstacle 11
21 + 0	Wedge obstacle (Figure 6)
21 + 3	Obstacle 21 mounted on top of obstacle 3
21 + 7	Obstacle 21 mounted on top of obstacle 7
21 + 11	Obstacle 21 mounted on top of obstacle 11
22	Rod obstacle (Figure 7)

Table II

Dimensions and Parameters

Rotor radius	R = 6.00"
Rotor chord (measured at 75% radius)	c = 1.06"
Rotor pitch (geometric)	b = 5.00"
Rotor solidity (c = 1.06")	σ = 0.1128
Rotor disc to ground plane	Z = 3.0" Z = 4.0" Z = 6.0" Z = 9.0" Z = 12.0"
$\frac{\text{Rotor disc to ground plane}}{\text{Rotor radius}}$	Z/R = 0.500 Z/R = 0.667 Z/R = 1.000 Z/R = 1.500 Z/R = 2.000
Obstacle to rotor drive shaft	D = 9.0" D = 12.0" D = 15.0"
$\frac{\text{Obstacle to rotor drive shaft}}{\text{Rotor radius}}$	D/R = 1.5 D/R = 2.0 D/R = 2.5

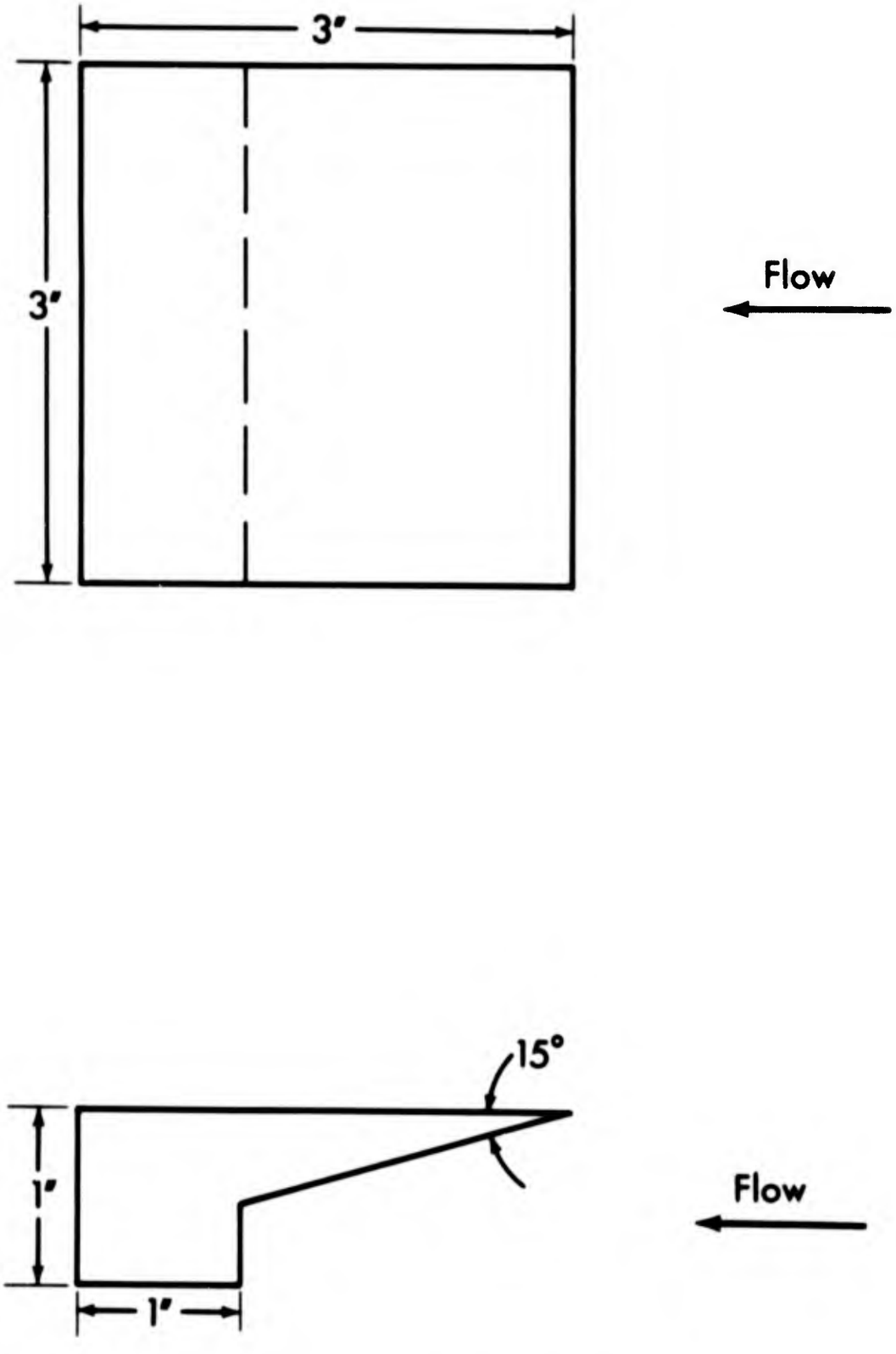

Fig. 6 Wedge obstacle.

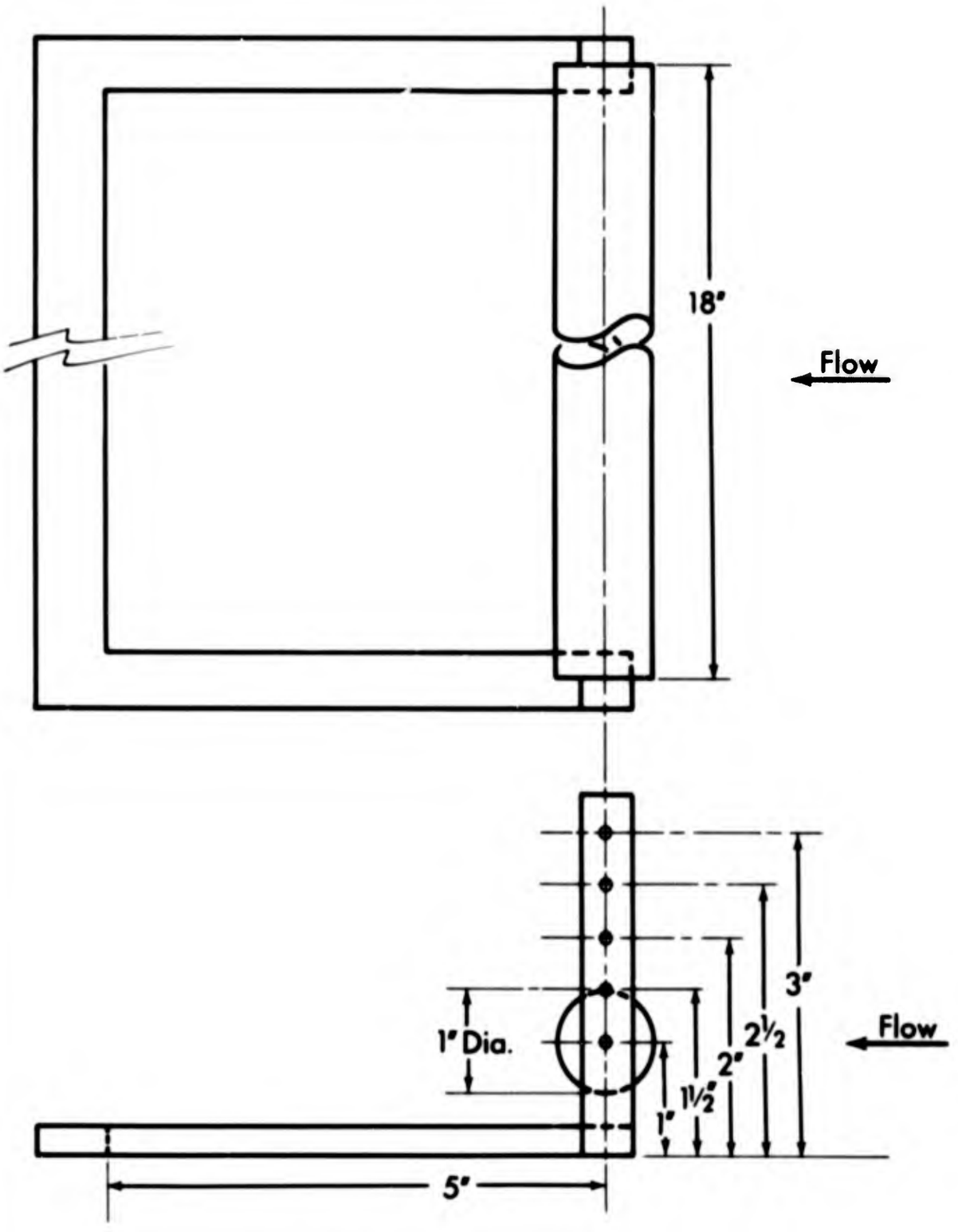

Fig. 7 Rod obstacle.

V. PRISM OBSTACLES

The projected series of flow visualization studies involving all of the 16 prism obstacles has been completed[1]. Also included in this series was a number of photographs with the camera positioned above the ground plane next to the sifter (overhead photographs) and the light source tilted through 90^{o} so as to produce a "flat" beam in a plane parallel to the ground plane (Figure 8). An additional number of photographs (end-on photographs) were taken with the camera and the light source locations interchanged (Figure 9).

In both cases (overhead and end-on), only one obstacle (obstacle 11) was used. The light beam divided the field near the obstacle into 1" wide planes (Figures 8 and 9).

The flow visualization photographs indicate that the flow field in the vicinity of the obstacles can be divided into three distinct groups:

Group 1: No recirculation, $h_j > h_o$ (Figure 10)*

Group 2: No recirculation, $h_o > h_j$ (Figure 11)

Group 3: Recirculation, $h_o > h_j$ (Figure 12)

where: h_j - height of the wall jet

h_o - height of the obstacle

Recirculation (Group 3) can further be divided into two distinct types along with an intermediate phase:

---

*Note: The arrow in the photographs indicates the position of the rotor tip in the picture plane.

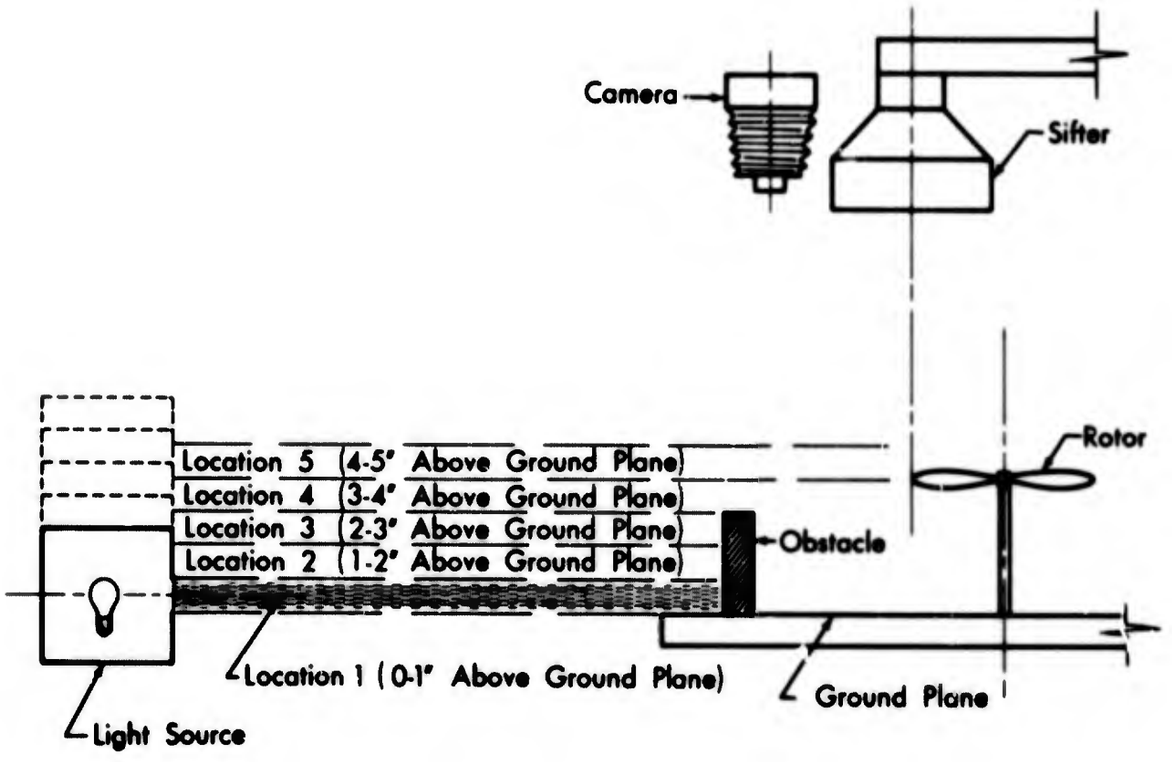

Fig. 8 "Overhead" locations.

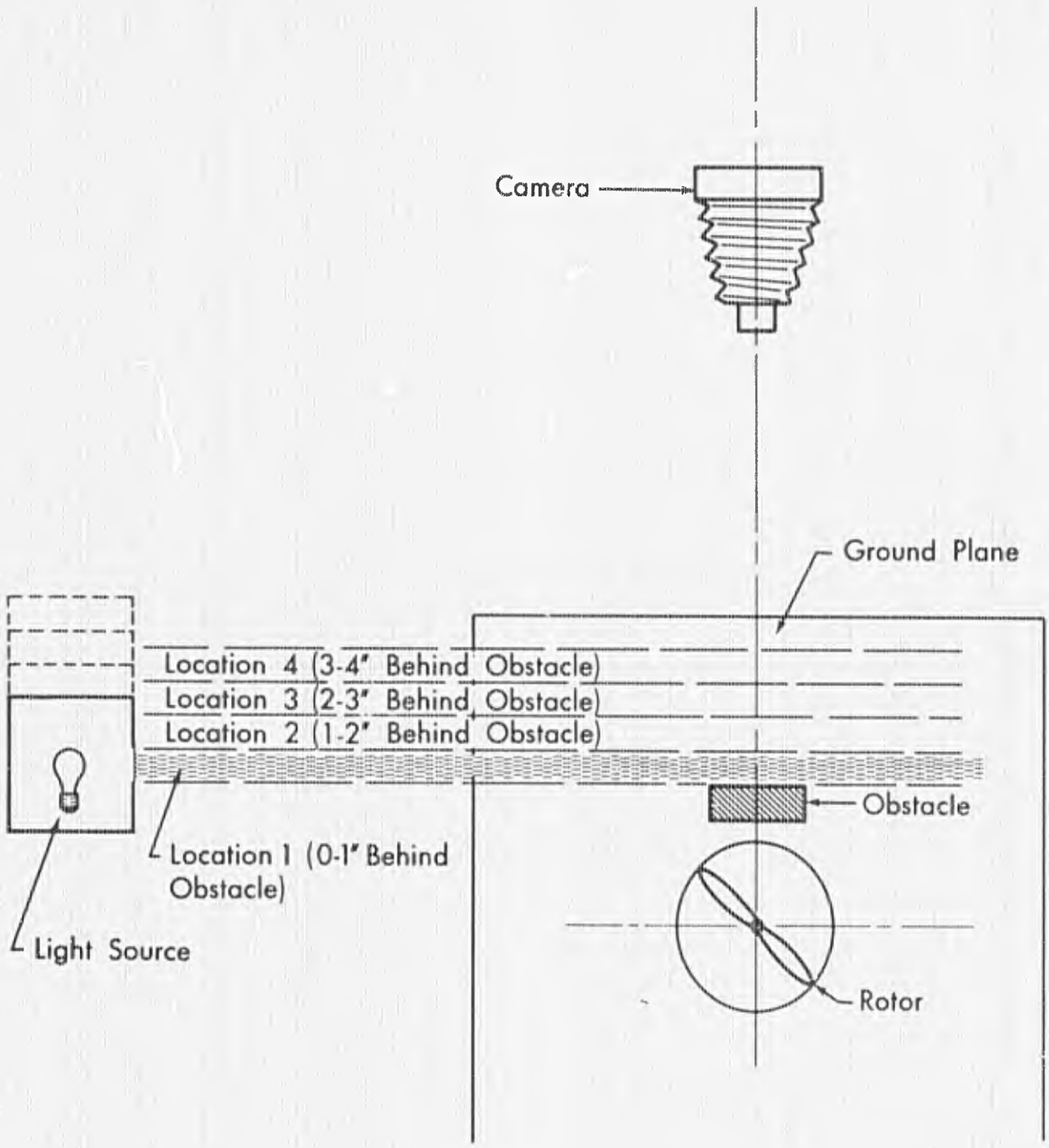

Fig. 9 "End-on" locations (sifter omitted).

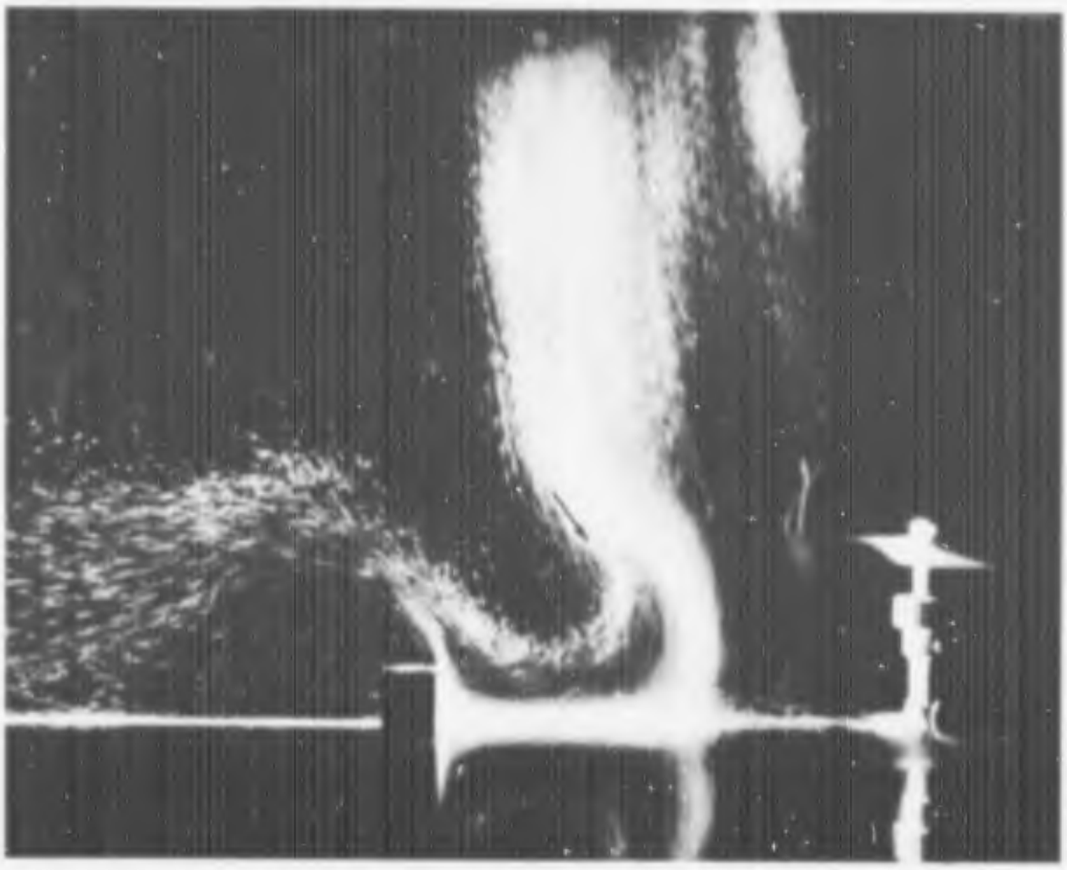

Fig. 10 Obstacle 3: Z/R = 0.500, D/R = 1.5; Group 1, no recirculation, $h_j > h_o$.

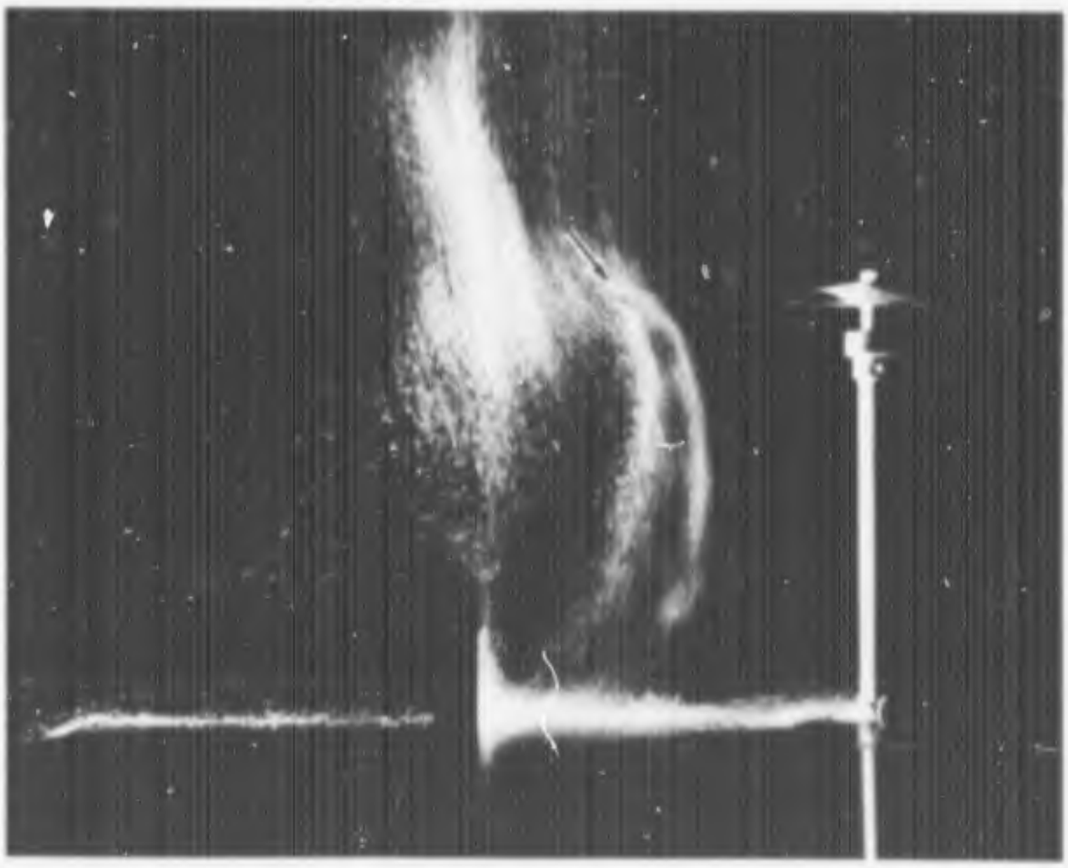

Fig. 11 Obstacle 7: Z/R = 1.500, D/R = 1.5; Group 2, no recirculation, $h_o > h_j$.

Type A: Recirculation inboard of the rotor tip, with the recirculating flow passing through the rotor disc (Figure 13).

Type B: Recirculation outboard of the rotor tip with the recirculating flow either passing through the rotor disc plane (Figure 14) or remaining below it (Figure 15).

Type C: Recirculation through the rotor tip, i.e., the flow turns in a rather narrow plane above and below the rotor disc plane, while the mainstream of the recirculating flow passes through the rotor tip area (Figure 16); essentially a combination of Types A and B.

Variation of the selected geometric parameters (D/R, Z/R, h_o and w_o) results in the development of definite trends in the flow field, which show up quite clearly in the flow visualization photographs.

Group 1 -- No Recirculation - $h_j > h_o$

As long as h_j remains greater than h_o no recirculation can be observed (Figure 17). Variation of the other parameters (Z/R, D/R and w_o) does not induce recirculation, but does alter the flow field somewhat.

An increase in the distance rotor disc to ground plane Z/R, seems to reduce the intensity of the flow pattern (Figure 18), i.e. a smaller number of tracer particles seems to show up on the photographs. The same results are obtained as the distance

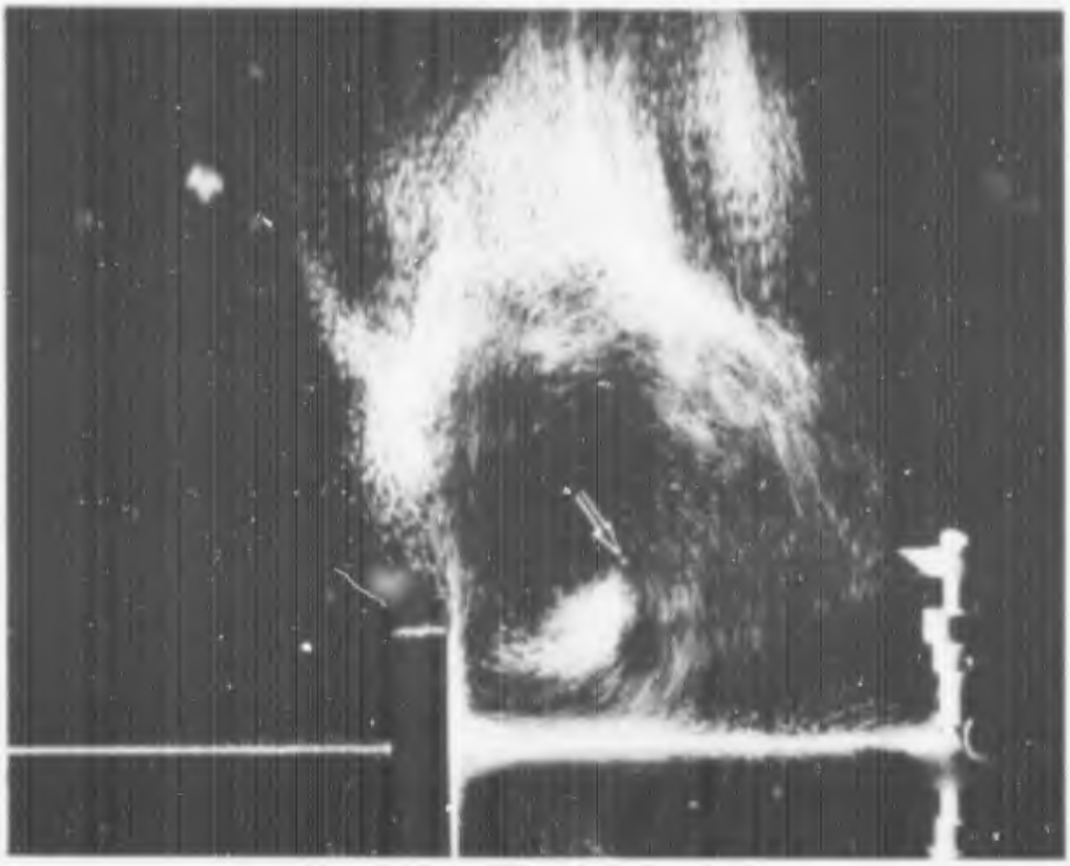

Fig. 12 Obstacle 7: Z/R = 0.500, D/R = 1.5; Group 3, recirculation, $h_o > h_j$, Type A.

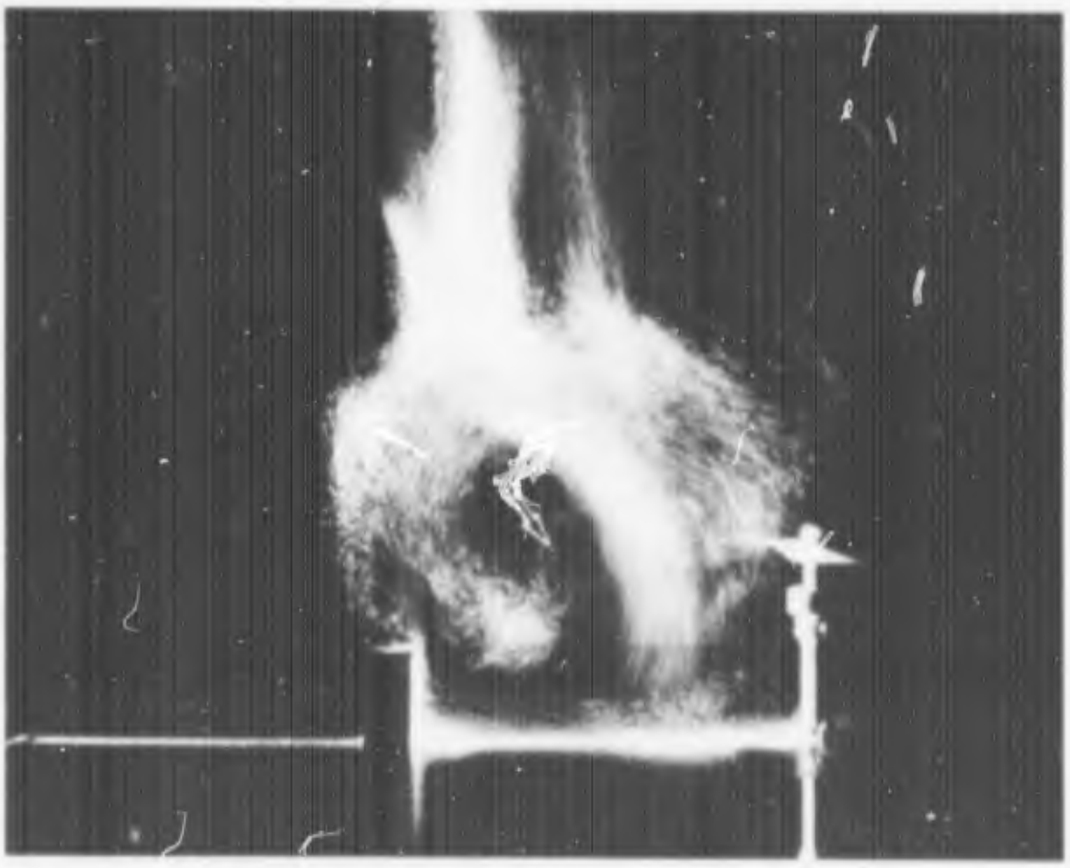

Fig. 13 Obstacle 7: Z/R = 0.667, D/R = 1.5; Group 3, recirculation, $h_o > h_j$, Type A.

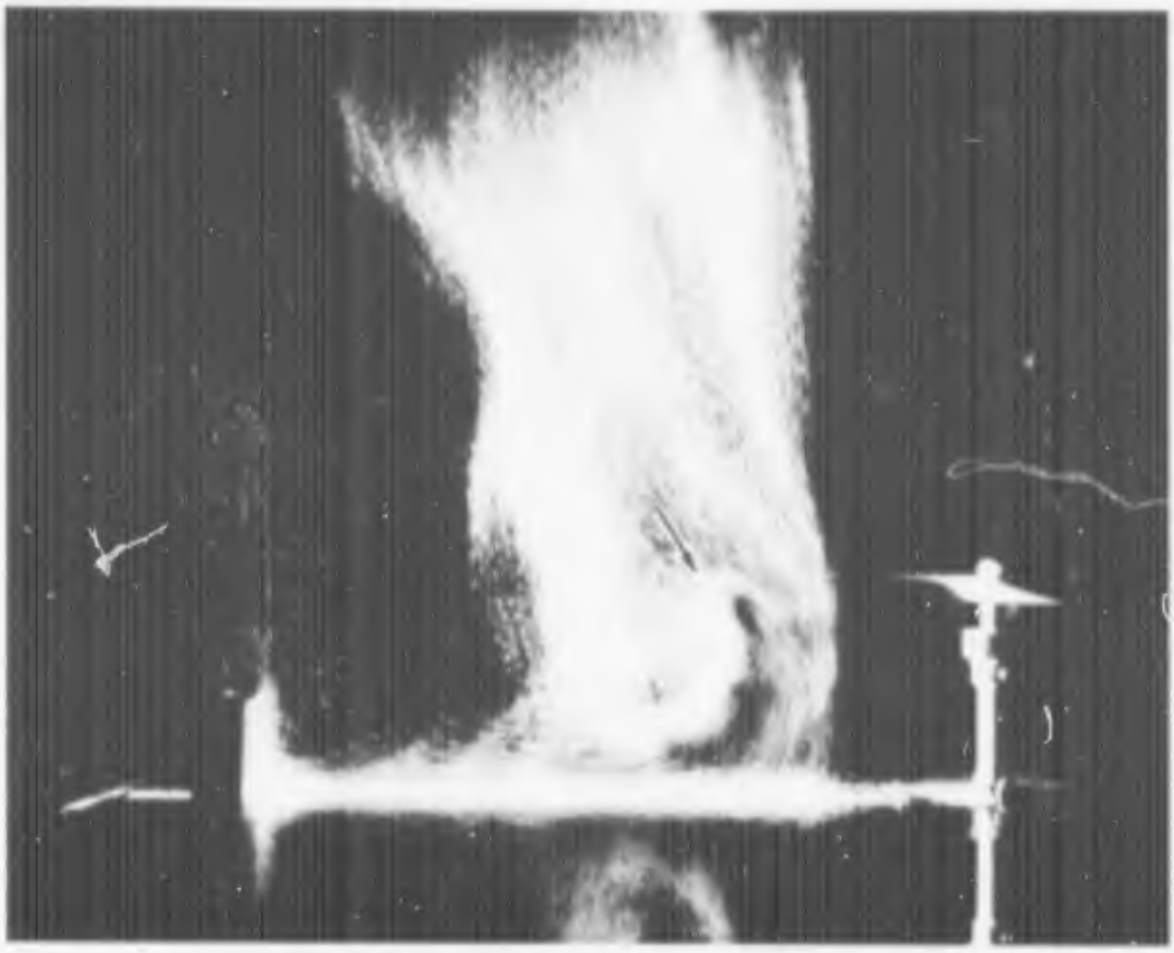

Fig. 14 Obstacle 7: Z/R = 0.667, D/R = 2.5; Group 3, recirculation, $h_o > h_j$, Type B.

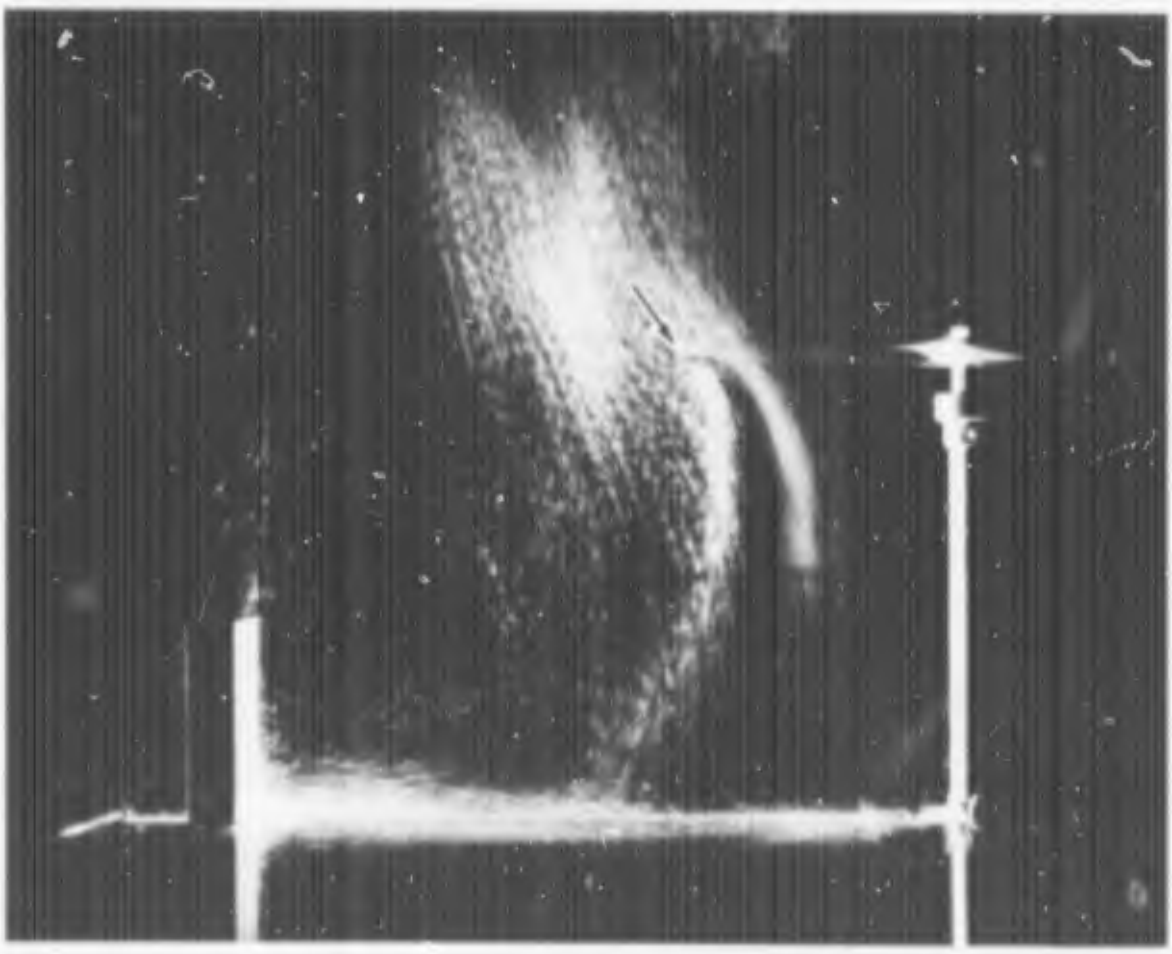

Fig. 15 Obstacle 14: Z/R = 1.500, D/R = 2.5; Group 3, recirculation, $h_o > h_j$, Type B.

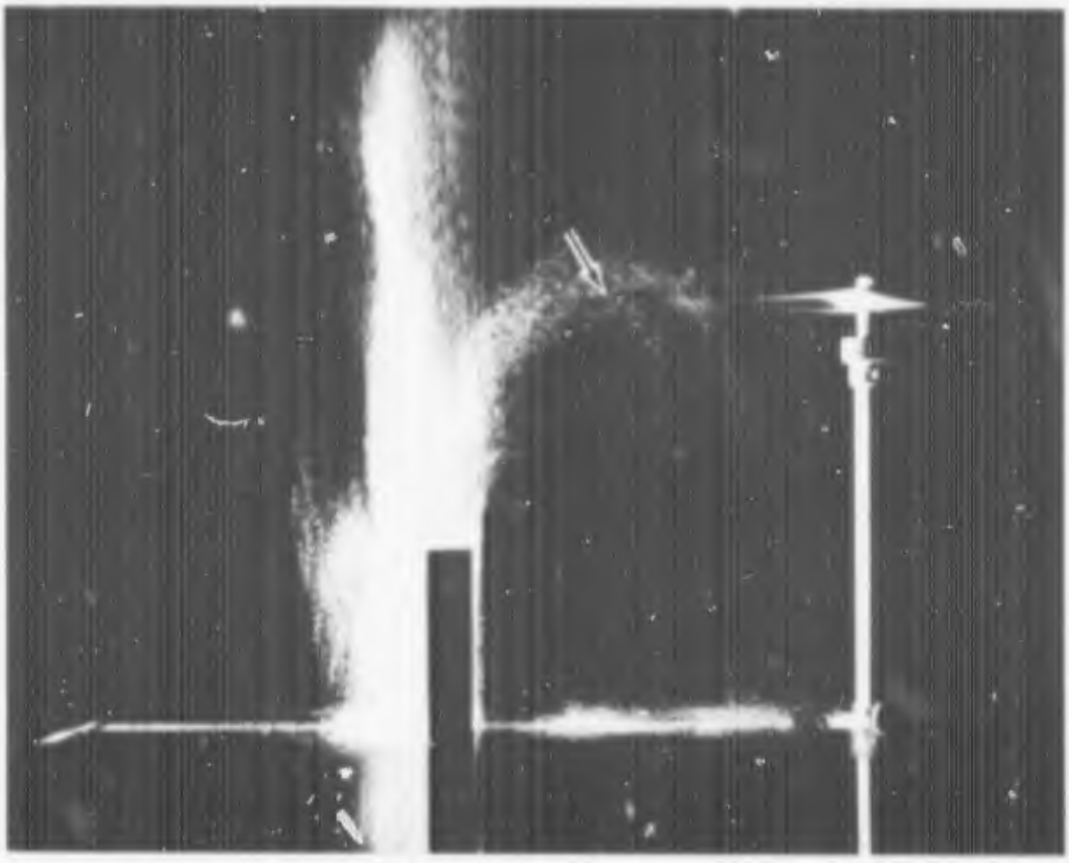

Fig. 16 Obstacle 16: Z/R = 1.500, D/R = 1.5; Group 3, recirculation, $h_o > h_j$, Type C.

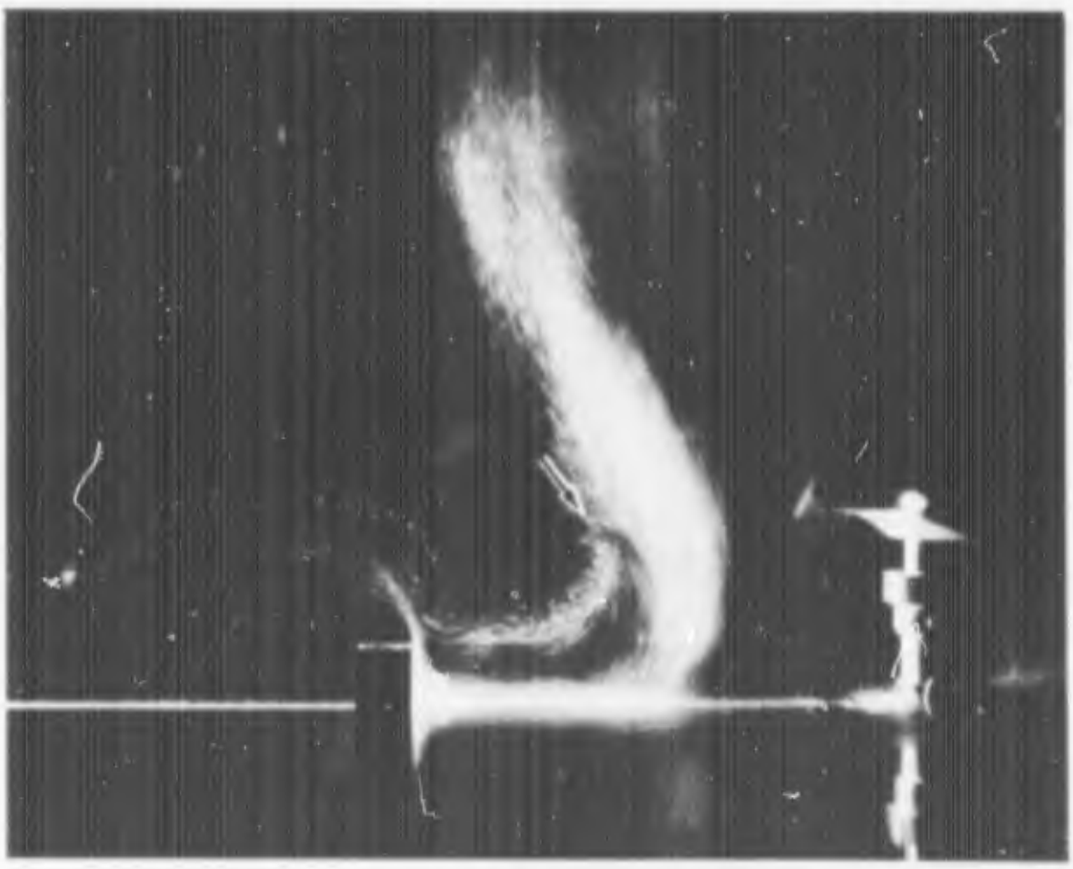

Fig. 17 Obstacle 2: Z/R = 0.500, D/R = 1.5; Group 1, no recirculation, $h_j > h_o$.

obstacle to rotor drive shaft, D/R, is increased (Figure 19). The opposite is true as the obstacle width w_o is increased (Figure 20). Thus, keeping D/R and, at the same time, Z/R constant and increasing w_o results in a more intense flow pattern.

The height of the obstacle face h_o normal to the approaching wall jet apparently determines whether or not recirculation sets in. The width of the obstacle w_o, on the other hand, seems to determine the intensity of the flow pattern. The thickness of the obstacle d_o is assumed to have no influence over the flow field and thus is kept at a constant value of 1".

Groups 2 & 3 -- No Recirculation, Recirculation - $h_o > h_j$

A primary condition for recirculation to set in appears to be the requirement that $h_o > h_j$ (Figure 12). However, the initial geometric conditions determine which flow pattern will be established.

a) $D/R = 1.5$ and $0.500 \leq Z/R \leq 2.000$

$Z/R = 0.500$: Recirculation passes inboard of the rotor tip through the rotor disc, regardless of obstacle height h_o (Figures 21, 22 and 23) or obstacle width w_o (Figures 24, 25, 26 and 27).

$Z/R > 0.500$: The flow changes, as Z/R is increased from 0.500 to 2.000, from recirculation type A to type B, with the mainstream remaining below the rotor disc plane (Figure 28) and eventually becomes very similar to the flow described under Group 1 (Figure 29).

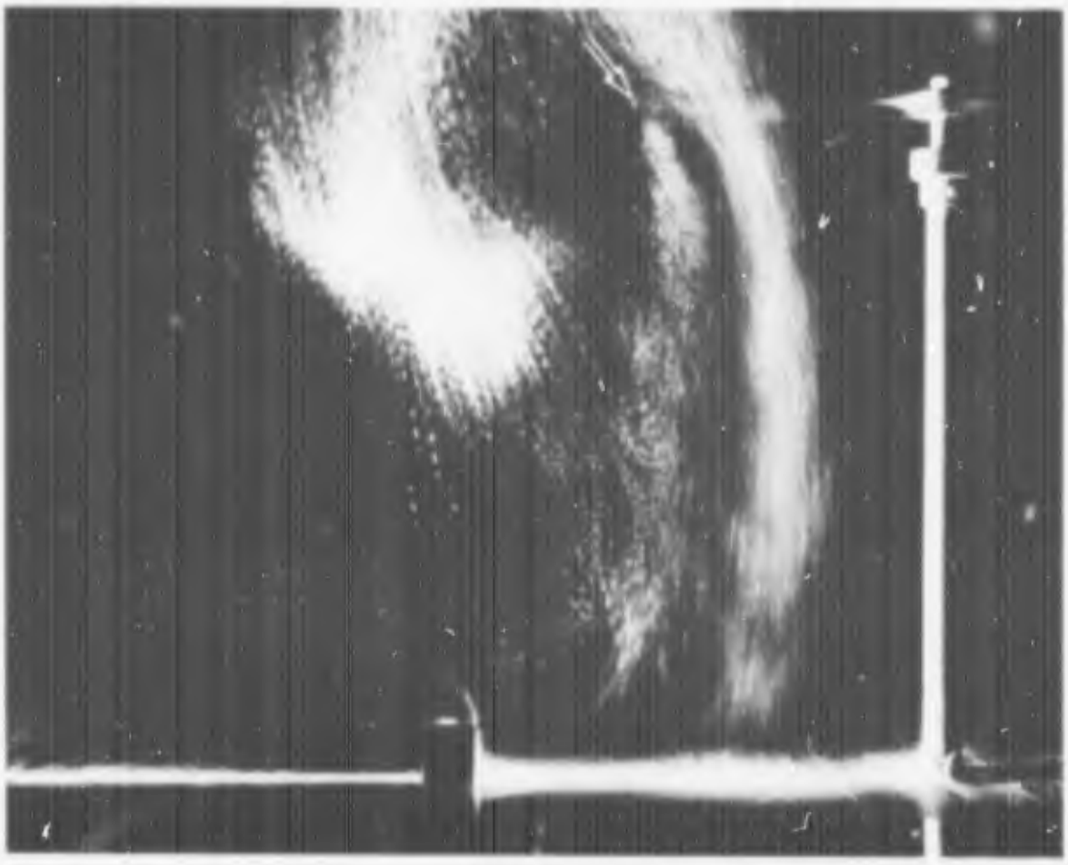

Fig. 18 Obstacle 2: Z/R = 2.000, D/R = 1.5; Group 1, no recirculation, $h_j > h_o$.

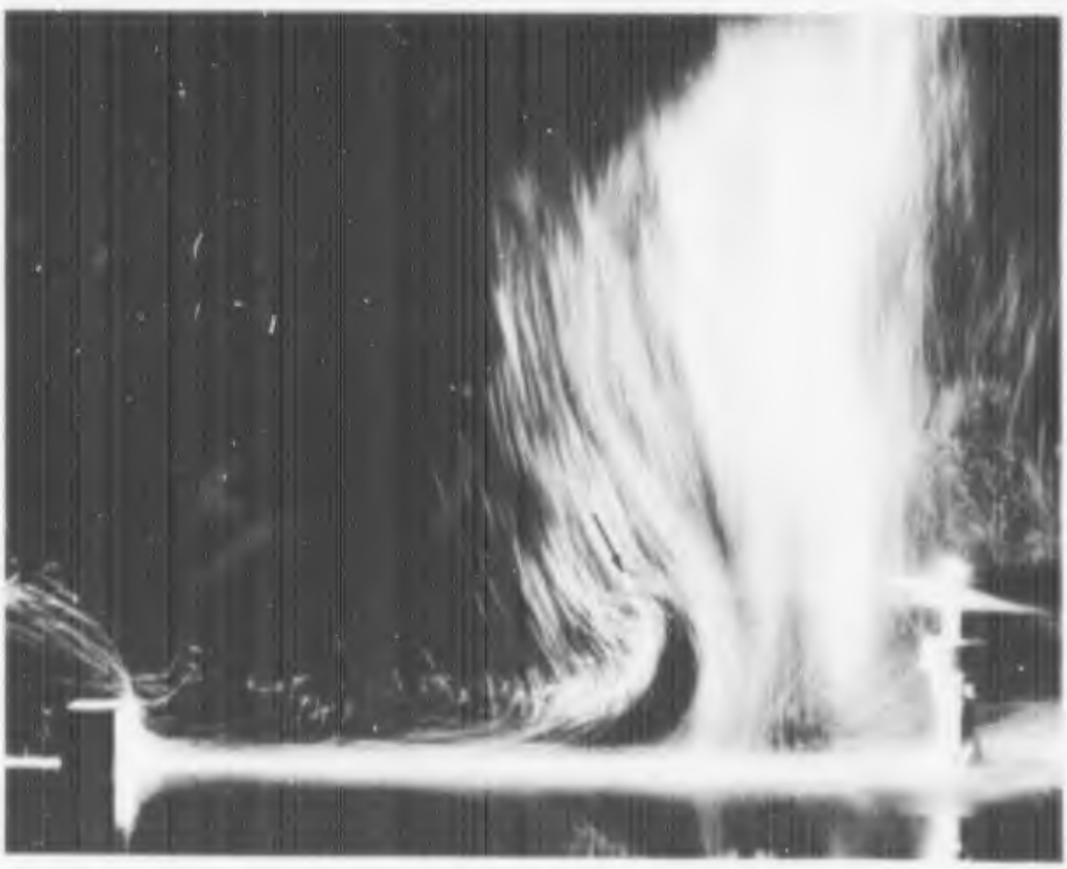

Fig. 19 Obstacle 2: Z/R = 0.500, D/R = 2.5; Group 1, no recirculation, $h_j > h_o$.

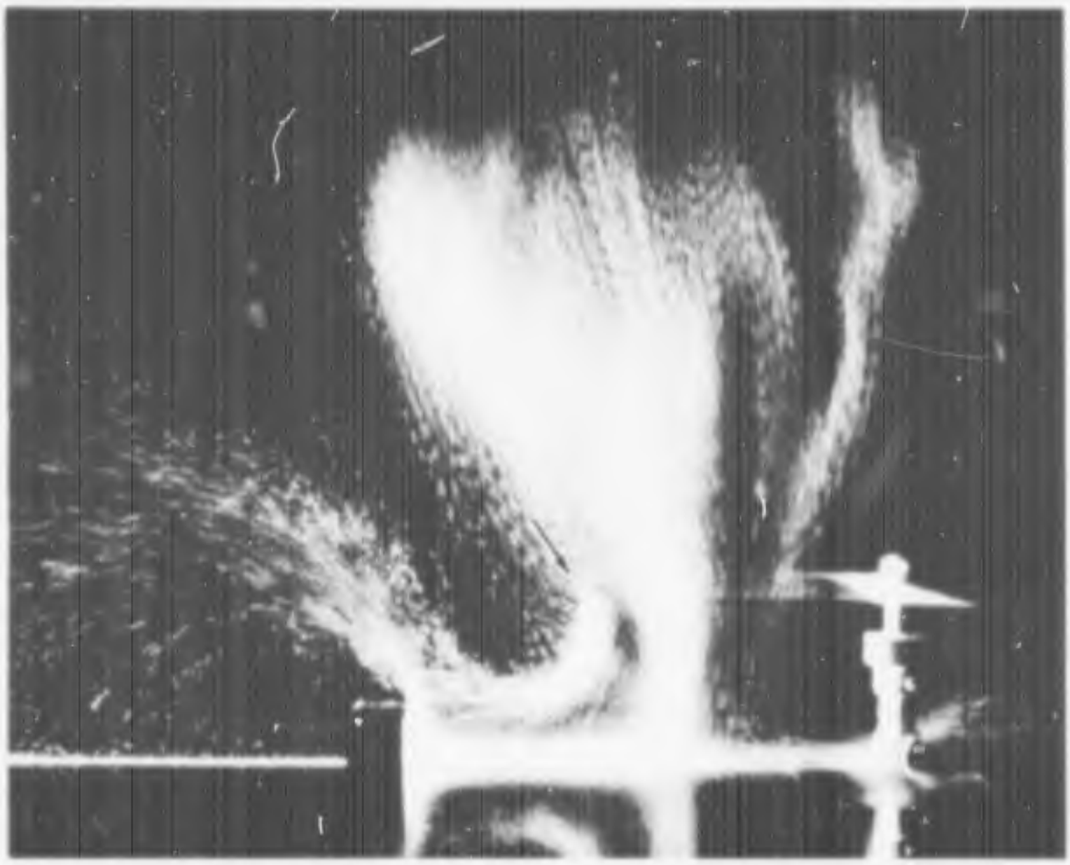

Fig. 20 Obstacle 4: Z/R = 0.500, D/R = 1.5; Group 1, no recirculation, $h_j > h_o$.

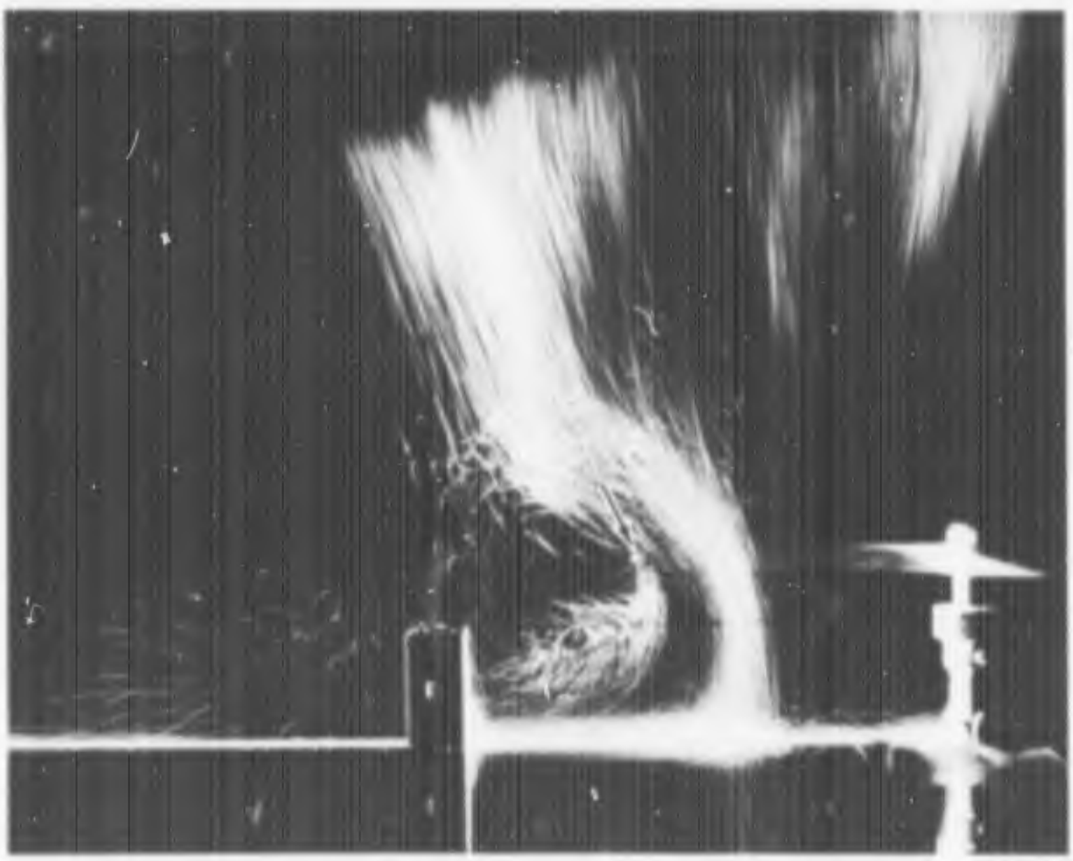

Fig. 21 Obstacle 5: Z/R = 0.500, D/R = 1.5; Group 3, recirculation, $h_o > h_j$, Type A.

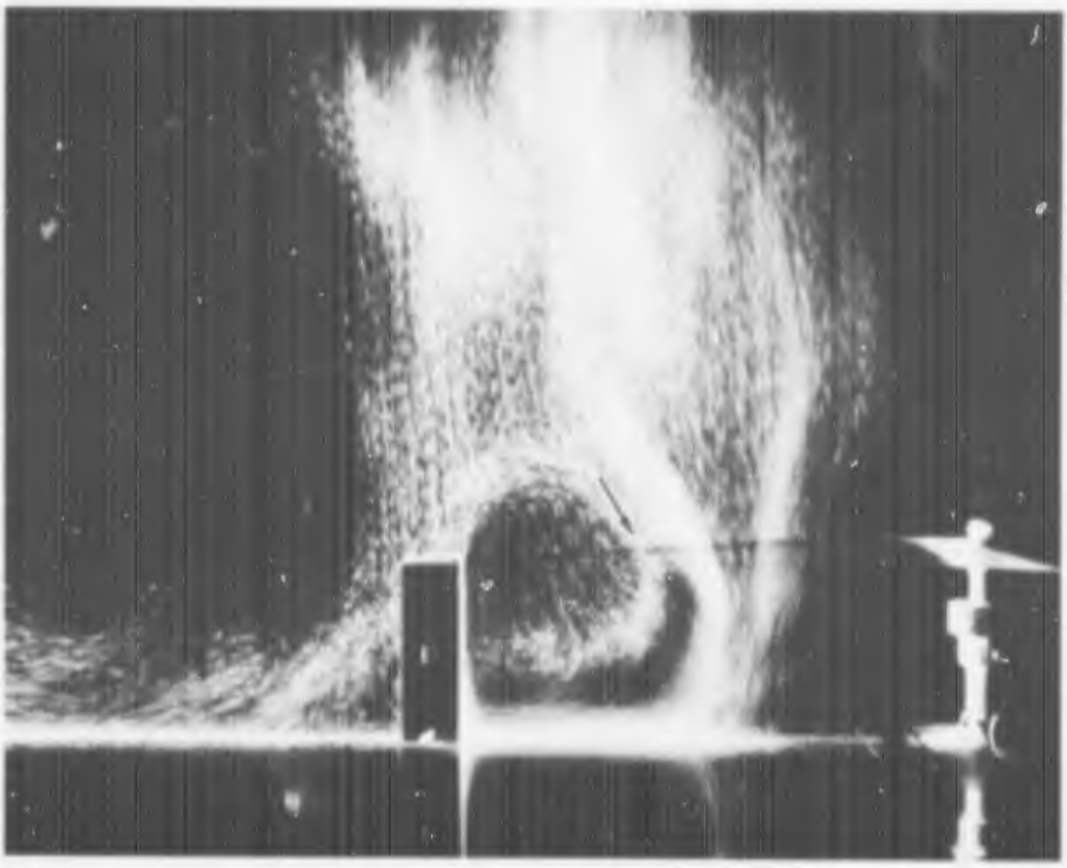

Fig. 22 Obstacle 9: Z/R = 0.500, D/R = 1.5; Group 3, recirculation, $h_o > h_j$, Type A.

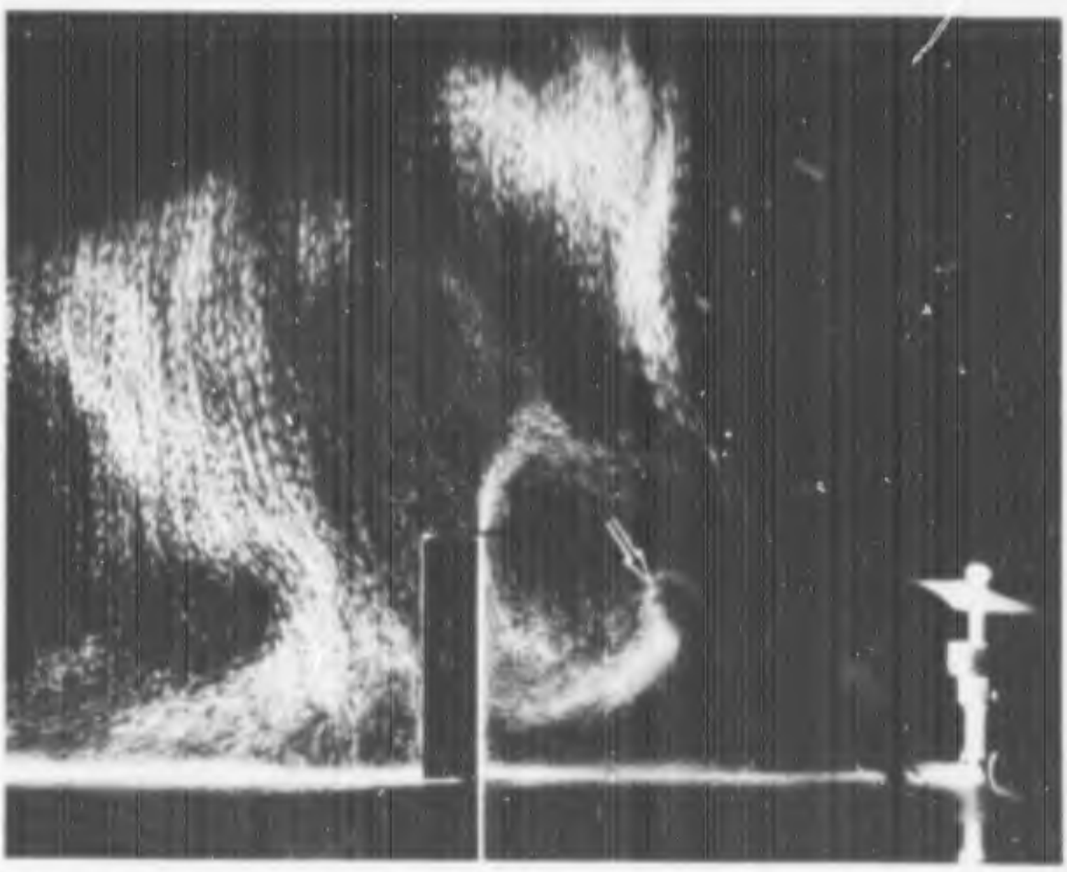

Fig. 23 Obstacle 13: Z/R = 0.500, D/R = 1.5; Group 3, recirculation, $h_o > h_j$, Type A.

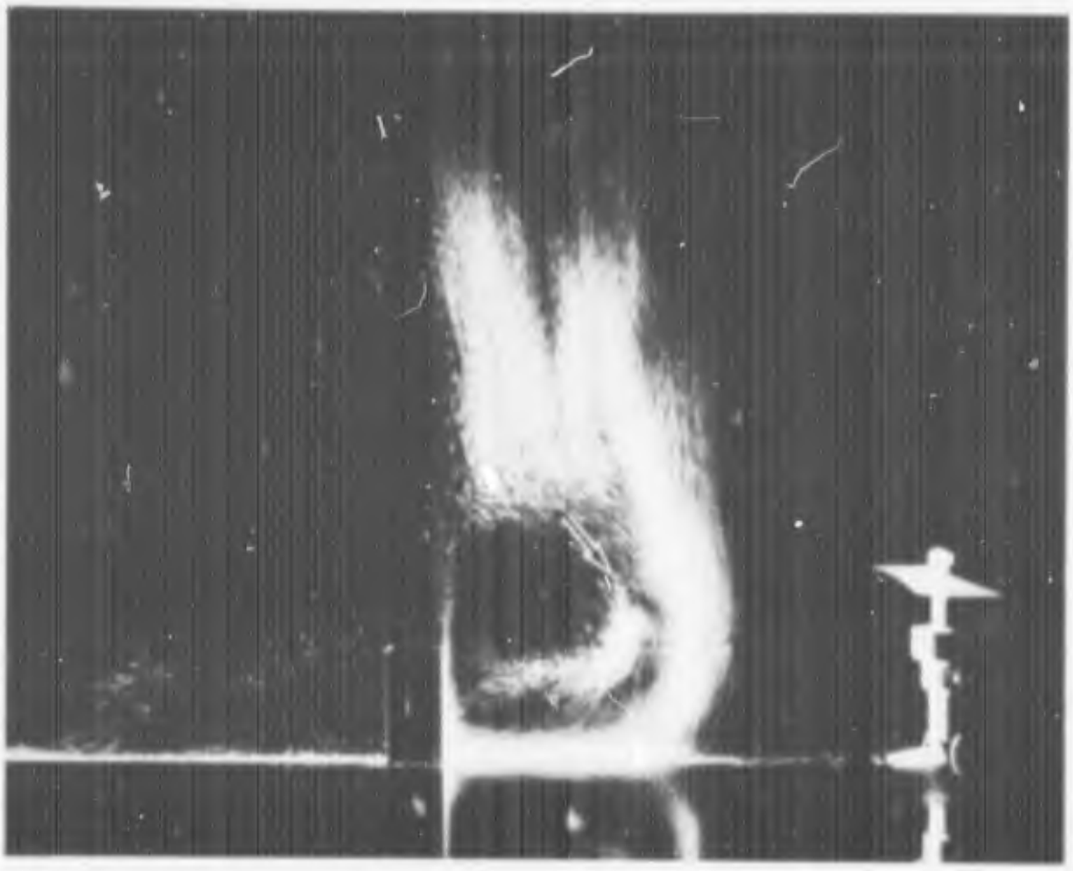

Fig. 24 Obstacle 5: Z/R = 0.500, D/R = 1.5; Group 3, recirculation, $h_o > h_j$, Type A.

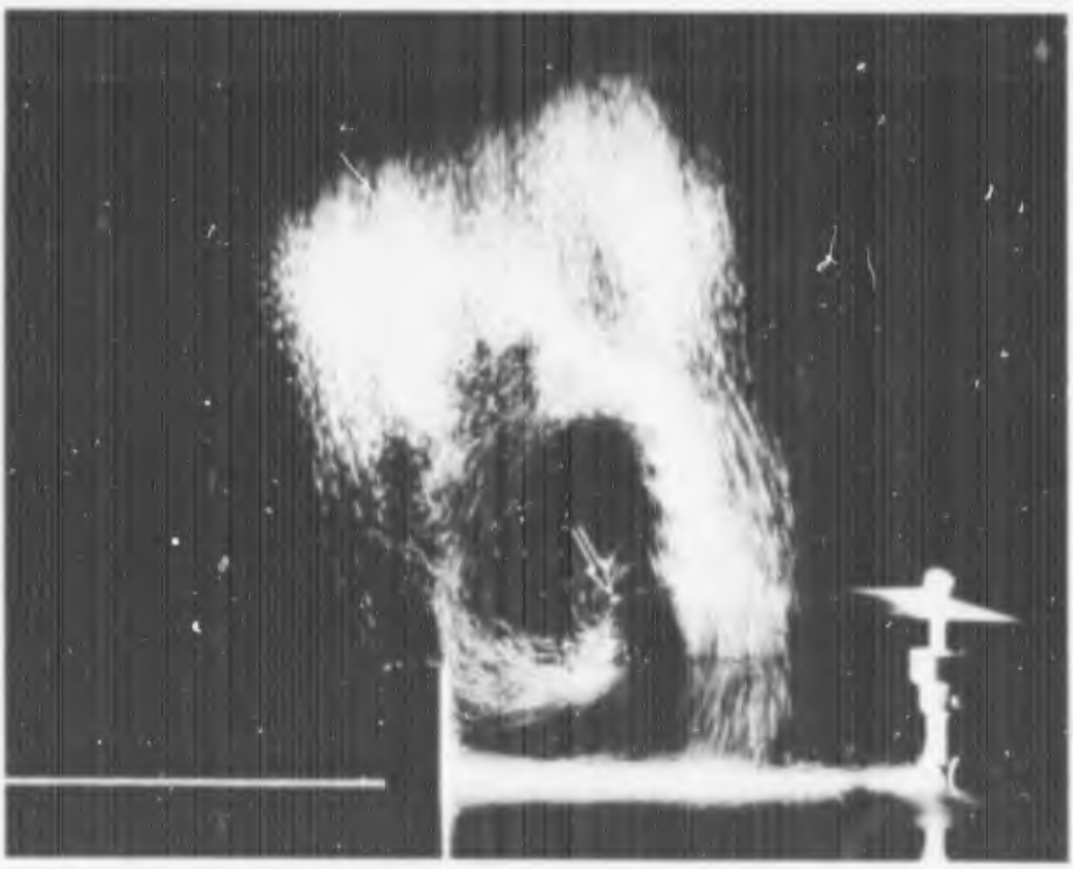

Fig. 25 Obstacle 6: Z/R = 0.500, D/R = 1.5: Group 3, recirculation, $h_o > h_j$, Type A.

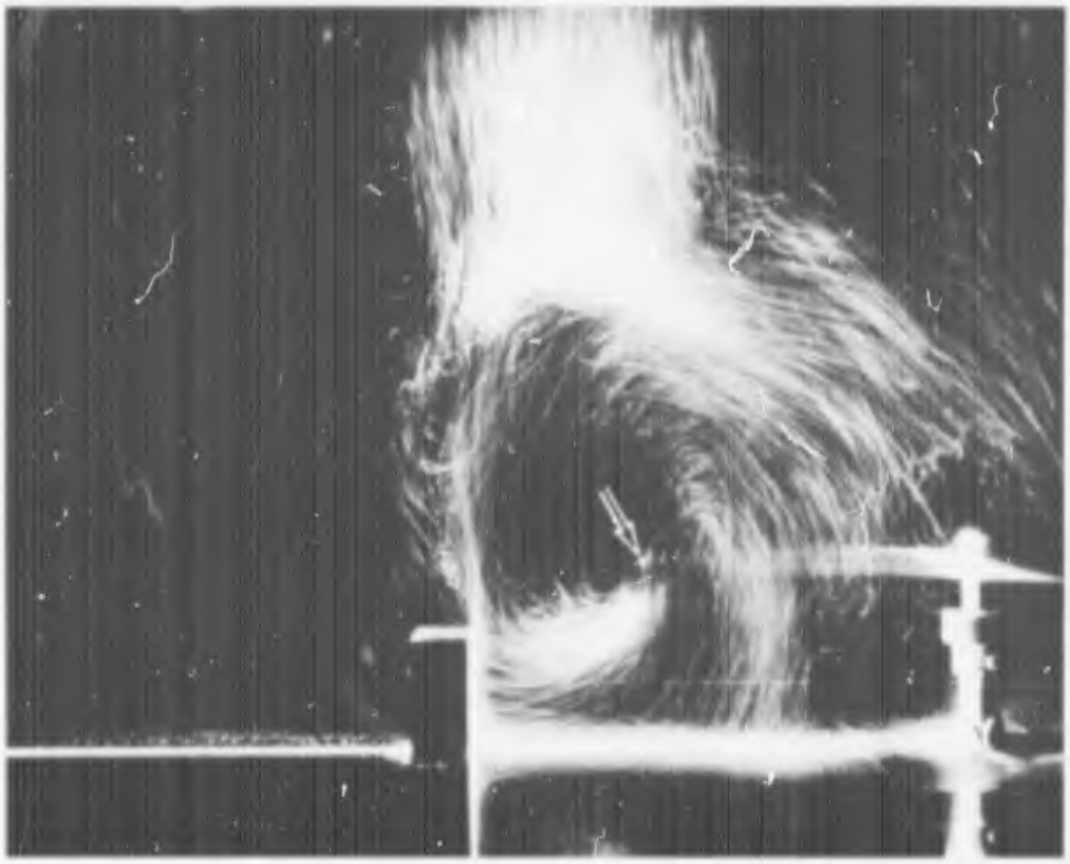

Fig. 26 Obstacle 7: Z/R = 0.500, D/R = 1.5; Group 3, recirculation, h_o h_j, Type A.

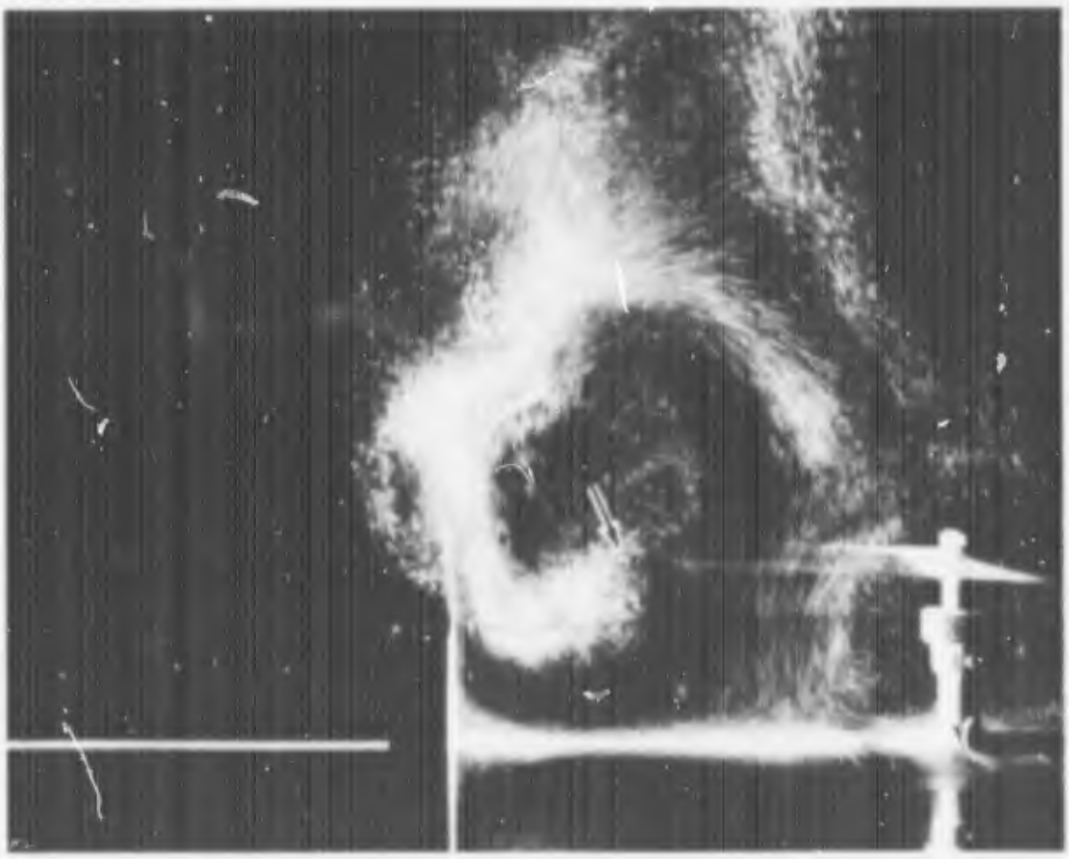

Fig. 27 Obstacle 8: Z/R = 0.500, D/R = 1.5; Group 3, recirculation, h_o h_j, Type A.

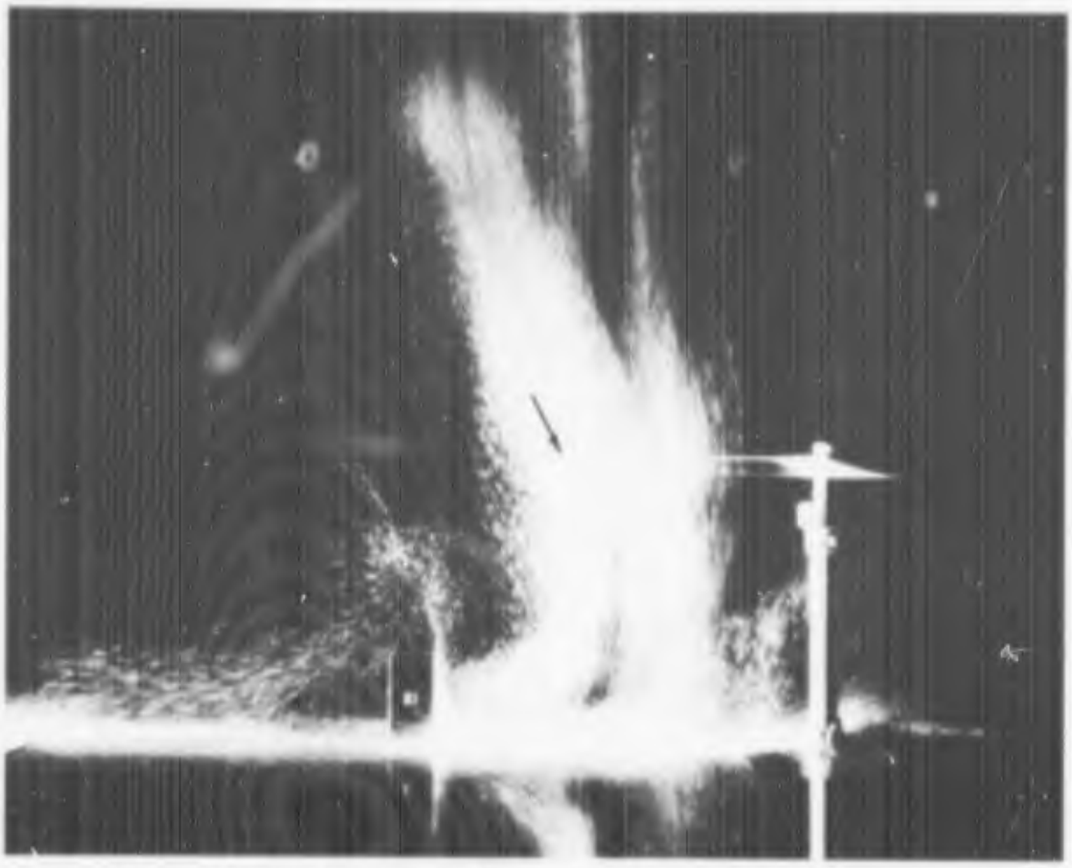

Fig. 28 Obstacle 5: Z/R = 1.000, D/R = 1.5; Group 3, recirculation, $h_o > h_j$, Type B.

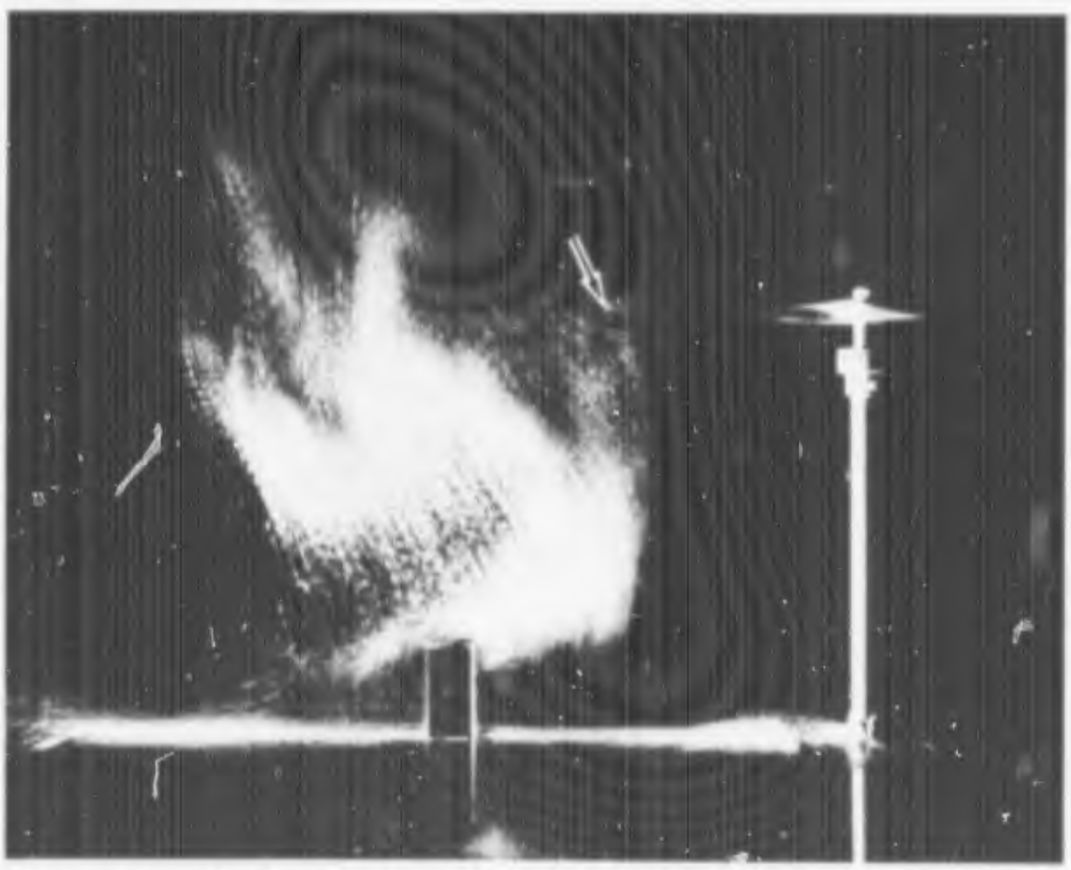

Fig. 29 Obstacle 5: Z/R = 1.500, D/R = 1.5; Group 2, no recirculation, $h_o > h_j$.

b) $D/R = 2.0$ and $0.500 \leq Z/R \leq 2.000$

$Z/R \leq 0.667$: Recirculation passes either outboard of the rotor tip through the rotor disc plane (narrow obstacle width w_o, Figure 30) or inboard of the rotor tip through the rotor disc (wider obstacle width w_o, Figure 31).

$Z/R > 0.667$: The flow behaves as described under a) for $Z/R > 0.500$.

c) $D/R = 2.5$ and $0.500 \leq Z/R \leq 2.000$

$Z/R \leq 0.667$: Recirculation passes outboard of the rotor tip through the rotor disc plane, regardless of the obstacle height h_o (Figures 32, 33 and 34) and obstacle width w_o (Figures 35, 36, 37 and 38).

$Z/R > 0.667$: The flow behaves as described under a) for $Z/R > 0.500$.

Obstacle 11 (h_o = 3", w_o = 3" and d_o = 1") was selected for the overhead (Figure 8) and end-on (Figure 9) photographs because of the well-defined recirculation inboard of the rotor tip through the rotor disc (Figure 39). The remaining parameters were selected as follows:

a) Overhead -- $Z/R = 0.667$
$D/R = 1.5$, 2.0 and 2.5

b) End-on -- $Z/R = 0.667$
$D/R = 1.5$

Overhead Photographs (All D/R Values)

Location 1: Radial flow along the ground plane up to about 1" ahead of the obstacle, where a "bow wave" forms (Figure 40). The flow then spills around the obstacle with an

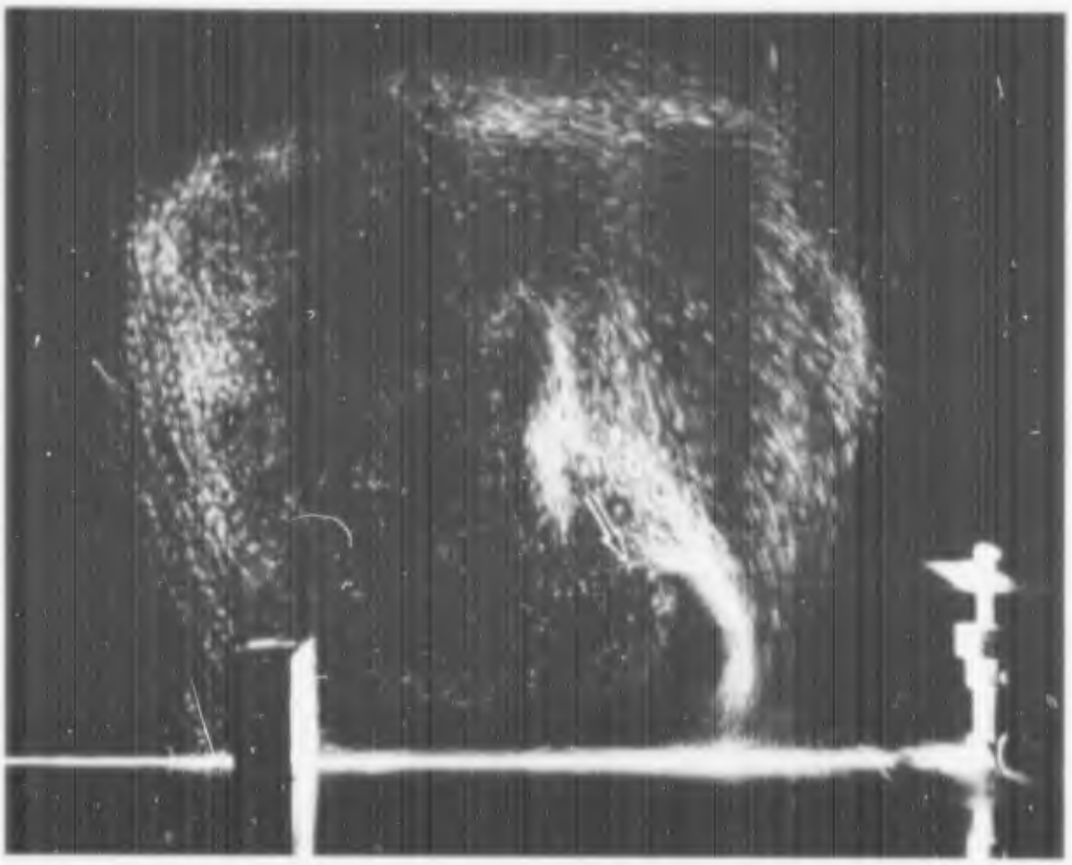

Fig. 30 Obstacle 5: Z/R = 0.500, D/R = 2.0; Group 3, recirculation, $h_o > h_j$, Type B.

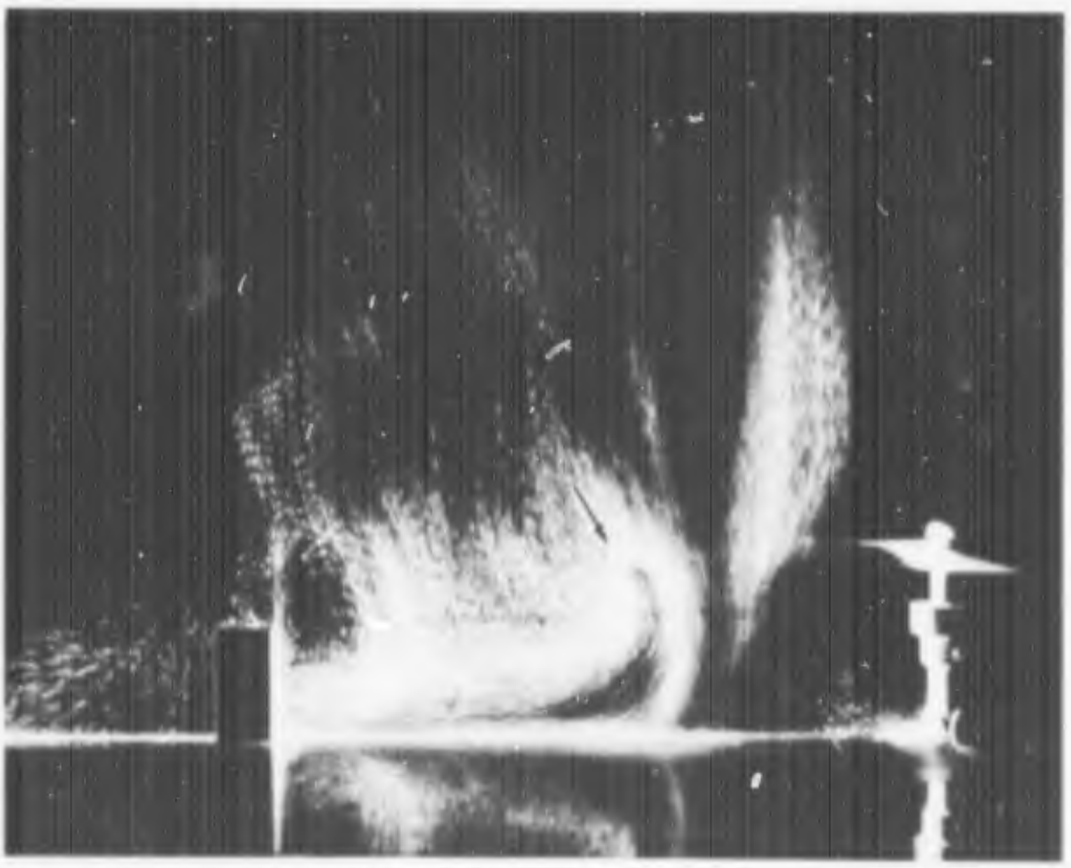

Fig. 31 Obstacle 8: Z/R = 0.500, D/R = 2.0; Group 3, recirculation, $h_o > h_j$, Type A.

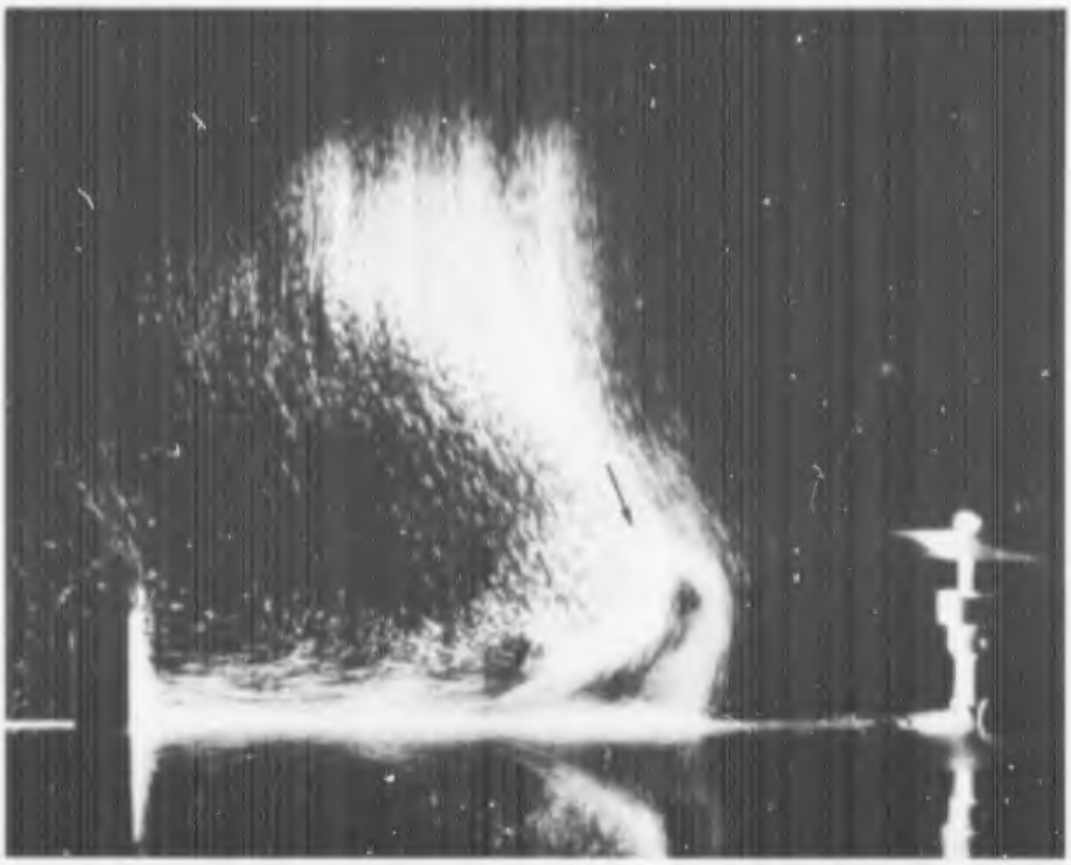

Fig. 32 Obstacle 5: Z/R = 0.500, D/R = 2.5; Group 3, recirculation, $h_o > h_j$, Type B.

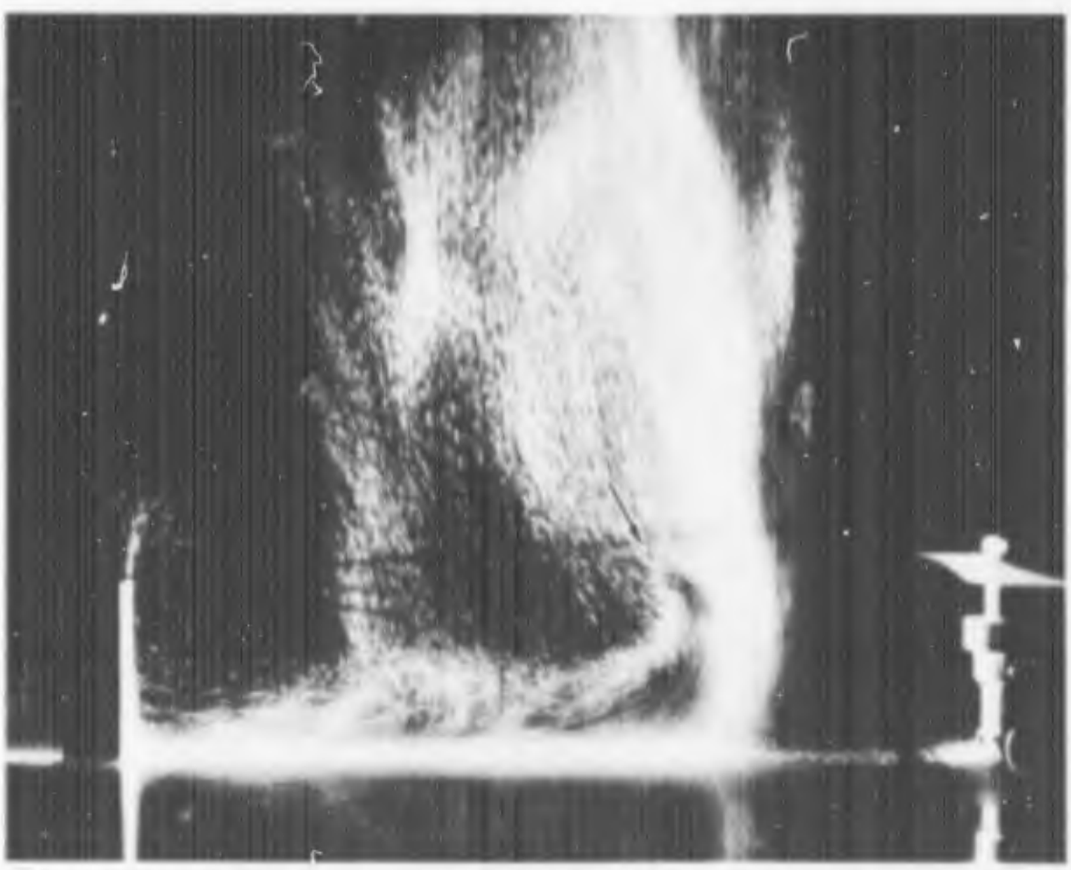

Fig. 33 Obstacle 9: Z/R = 0.500, D/R = 2.5; Group 3, recirculation, $h_o > h_j$, Type B.

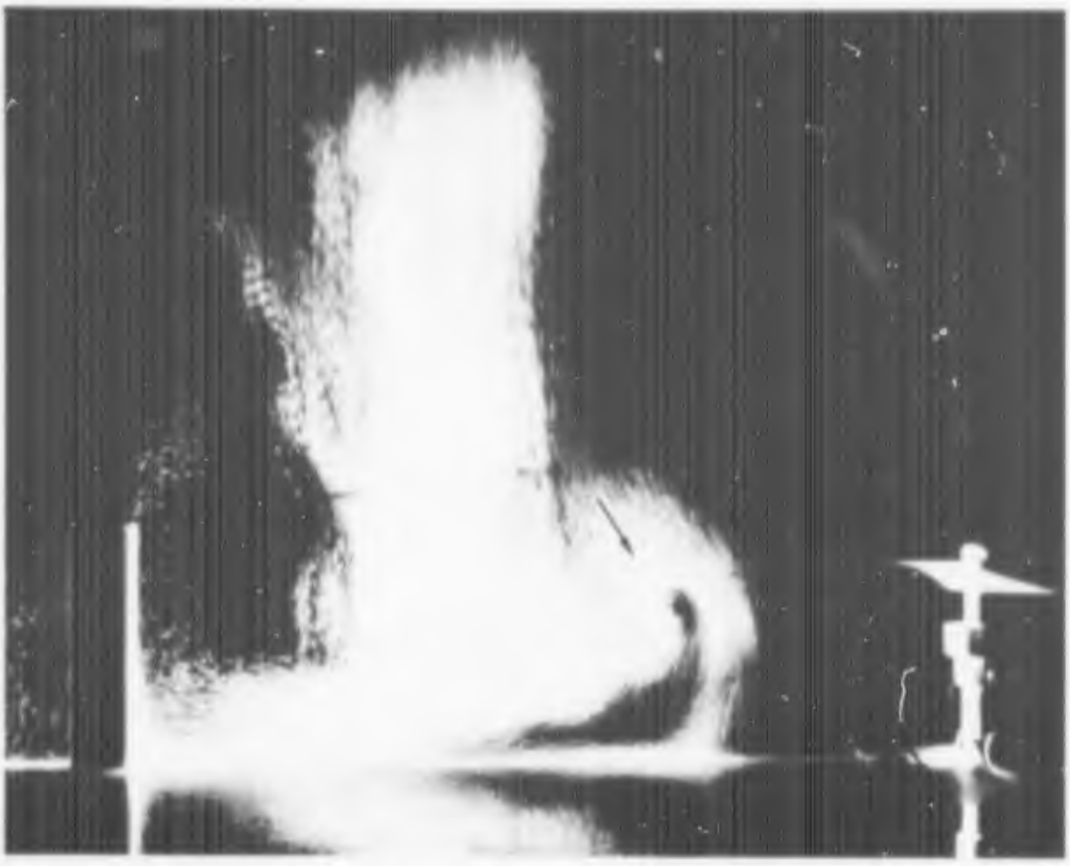

Fig. 34 Obstacle 13: Z/R = 0.500, D/R = 2.5; Group 3, recirculation, $h_o > h_j$, Type B.

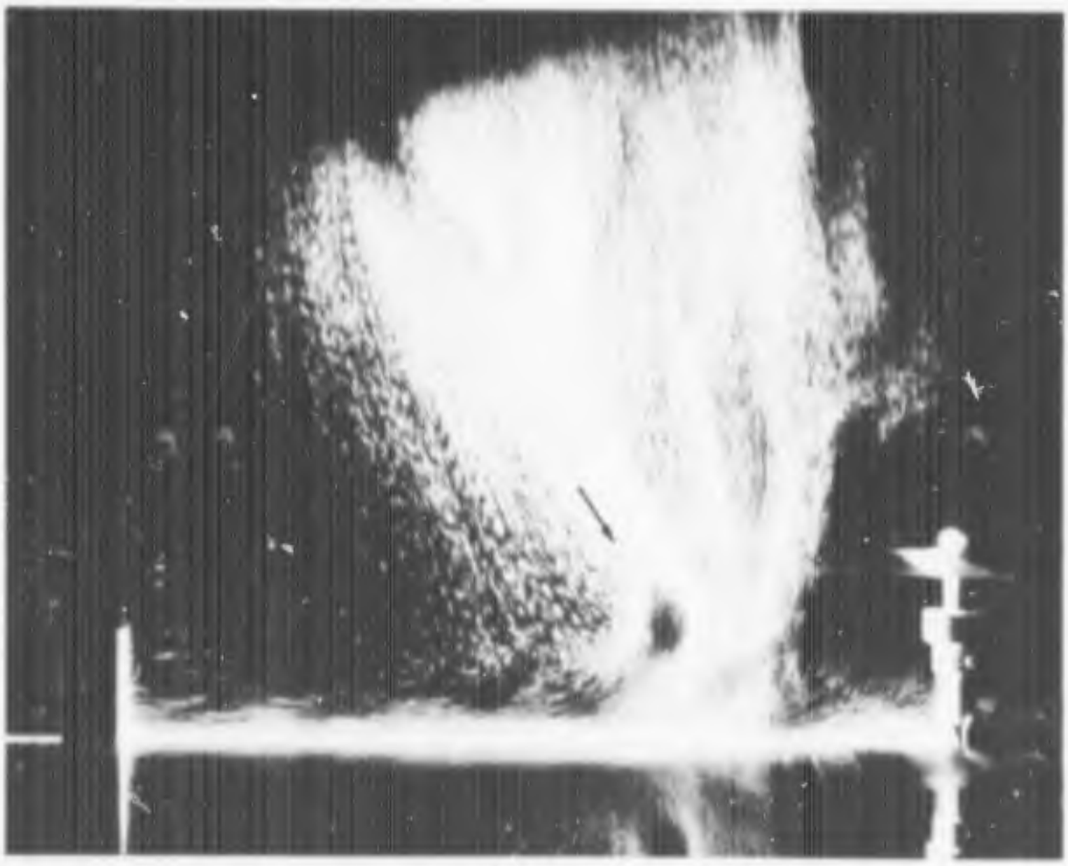

Fig. 35 Obstacle 5: Z/R = 0.500, D/R = 2.5; Group 3 recirculation, $h_o > h_j$, Type B.

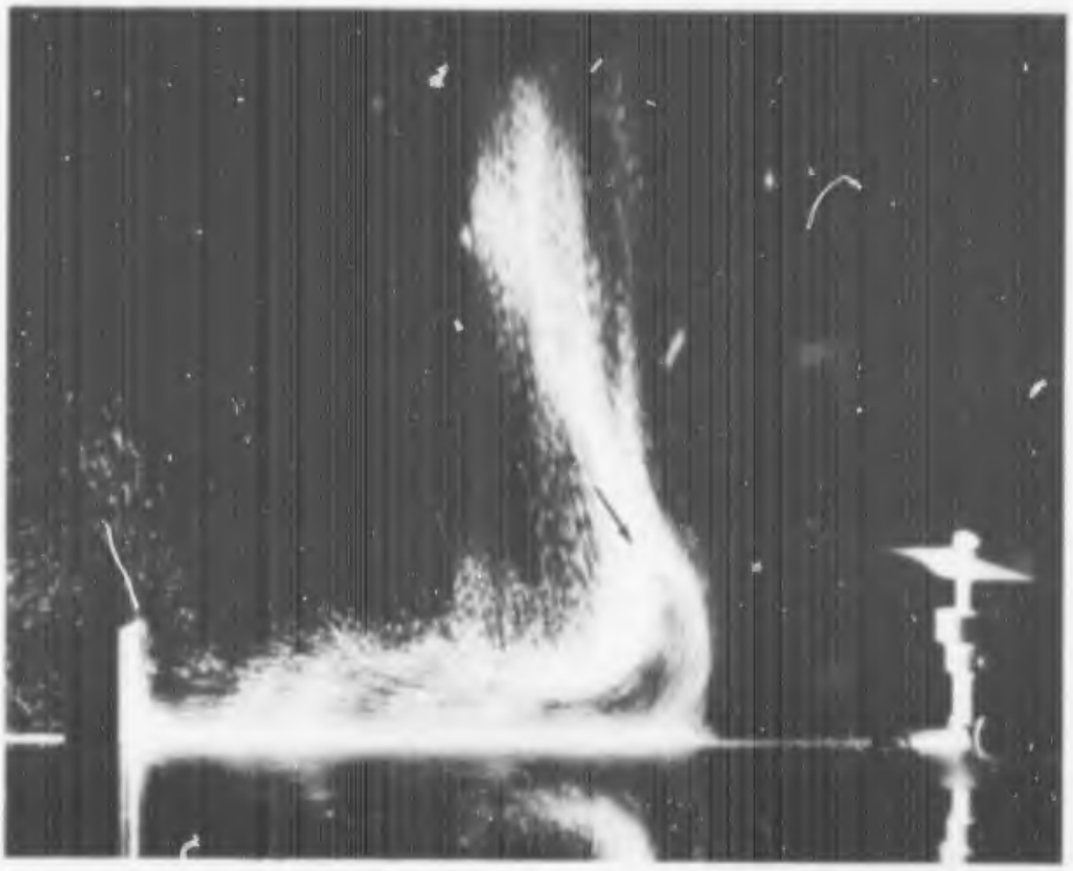

Fig. 36 Obstacle 6: Z/R = 0.500, D/R = 2.5; Group 3, recirculation, $h_o > h_j$, Type B.

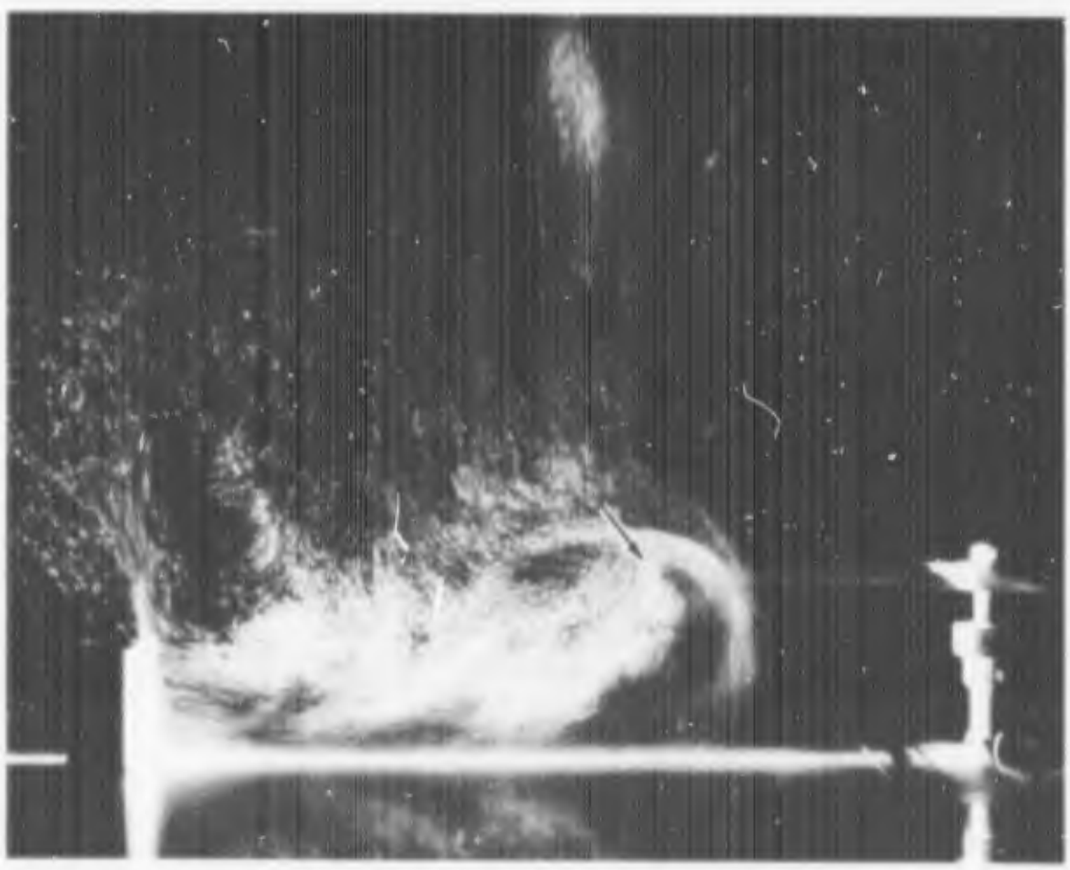

Fig. 37 Obstacle 7: Z/R = 0.500, D/R = 2.5; Group 3, recirculation, $h_o > h_j$, Type B.

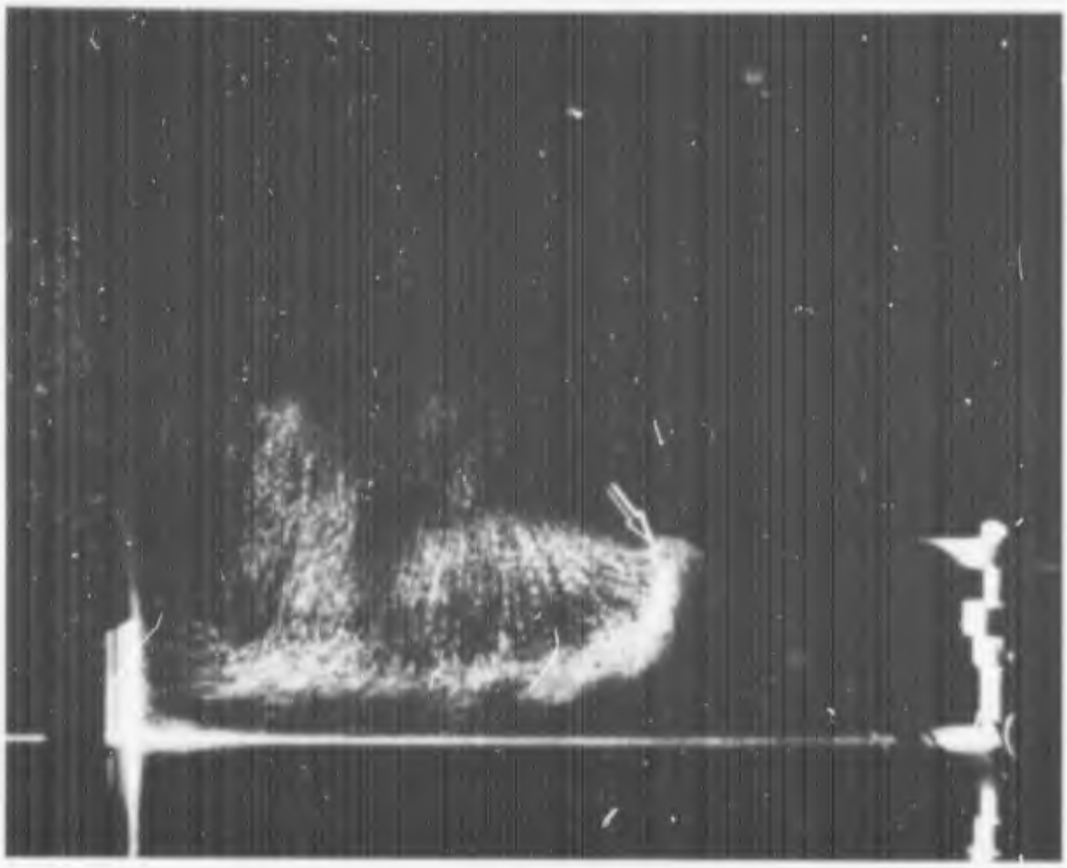

Fig. 38 Obstacle 8: Z/R = 0.500, D/R = 2.5; Group 3, recirculation, $h_o > h_j$, Type B.

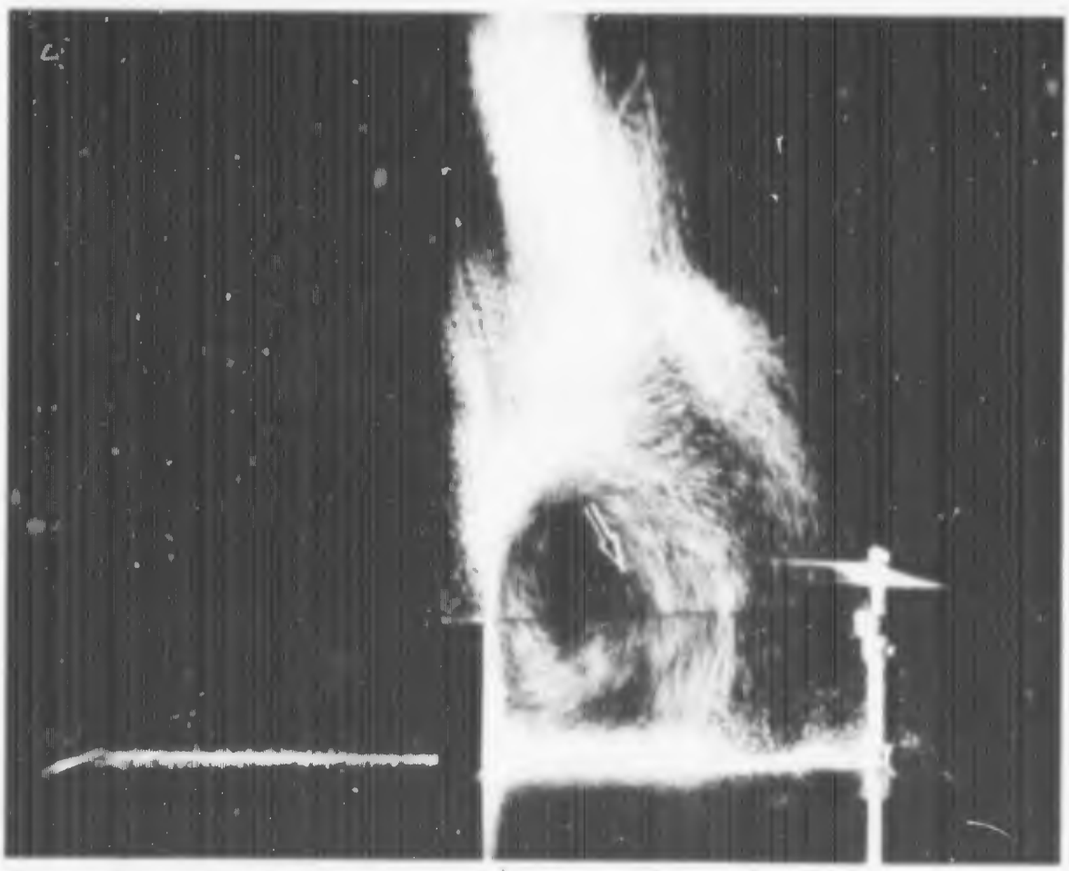

Fig. 39 Obstacle 11: Z/R = 0.667, D/R = 1.5; Group 3 recirculation, $h_o > h_j$, Type A.

indication of vortex type flow extending aft from both vertical edges.

Location 2: The "bow wave" is less prominent, while the vortex type flow from the vertical aft edges is more pronounced (Figure 41).

Location 3: Tangential flow parallel to the front face of the obstacle, apparently indicating the core of the recirculating flow. The vortex type flow from the vertical aft edges does not change appreciably (Figure 42).

Locations 4 & 5: The flow picture deteriorates -- some of the tangential flow seems to be maintained along with some of the vortex type flow from the vertical aft edges (Figures 43 and 44).

End-On Photographs

These pictures show a vortex extending back from each of the vertical aft edges of the obstacle (Figure 45), thus supporting the observations made above. However, the vortices dissipate within a short distance (Figure 46) aft of the obstacle.

Control photographs taken with obstacle 3 (h_o = 1", w_o = 3" and d_o = 1") in place of obstacle 11 and under the same conditions as listed above, exhibit a rather turbulent flow pattern moving straight back without any vortex type flow from the vertical aft edges (Figure 47).

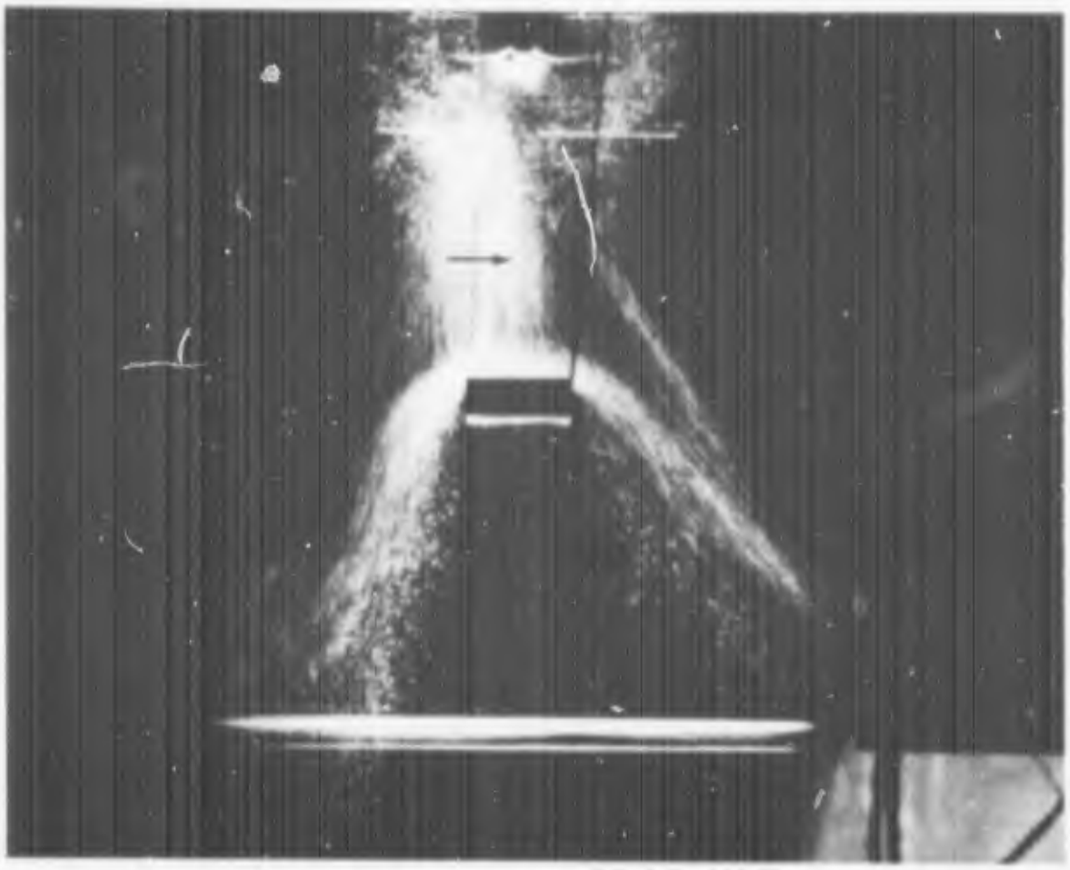

Fig. 40 Obstacle 11: Z/R = 0.667, D/R = 1.5; Group 3, recirculation, $h_o > h_j$, Type A, Location 1.

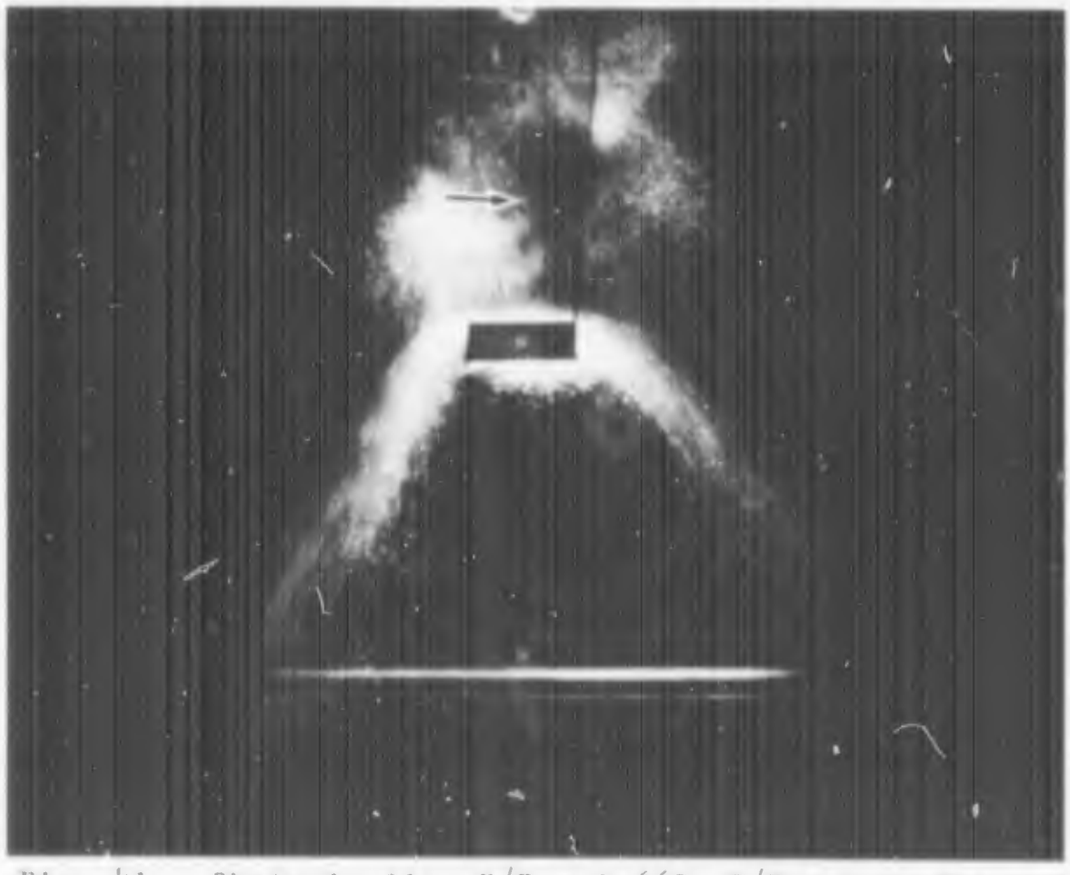

Fig. 41 Obstacle 11: Z/R = 0.667, D/R = 1.5; Group 3, recirculation, $h_o > h_j$, Type A, Location 2.

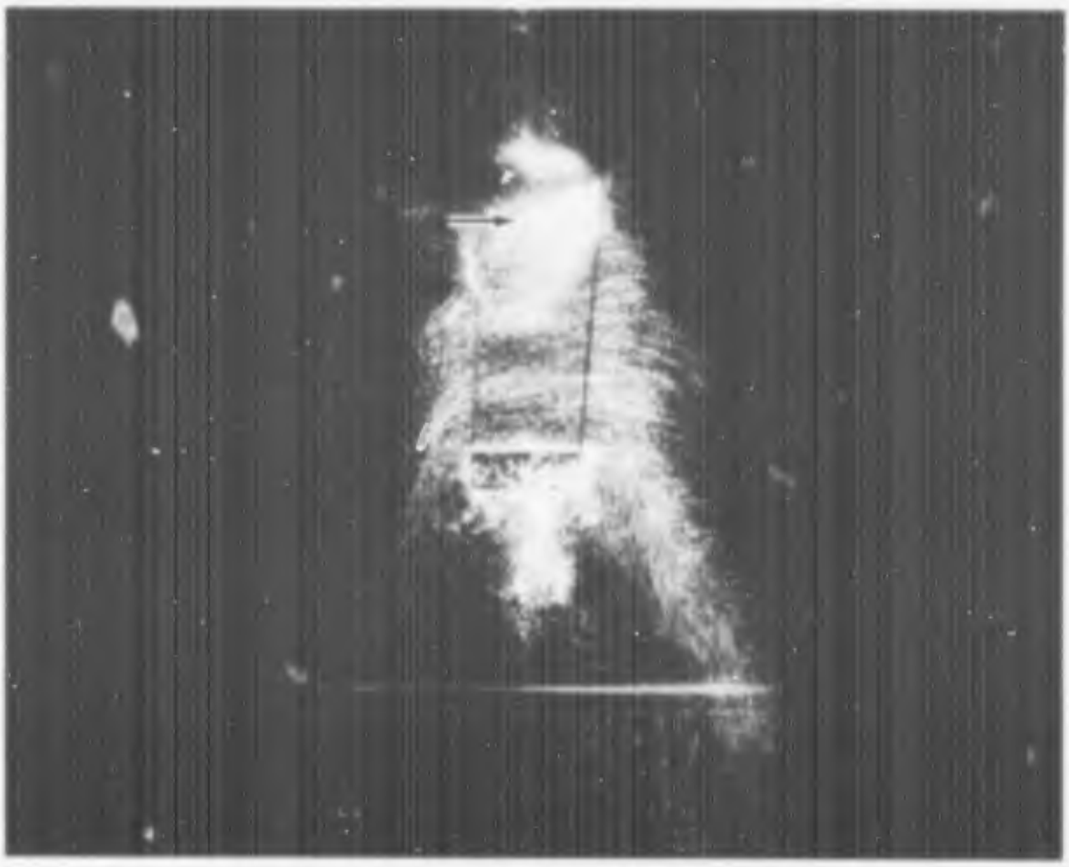

Fig. 42 Obstacle 11: Z/R = 0.667, D/R = 1.5; Group 3, recirculation, $h_o > h_j$, Type A, Location 3.

Fig. 43 Obstacle 11: Z/R = 0.667, D/R = 1.5; Group 3, recirculation, $h_o > h_j$, Type A, Location 4.

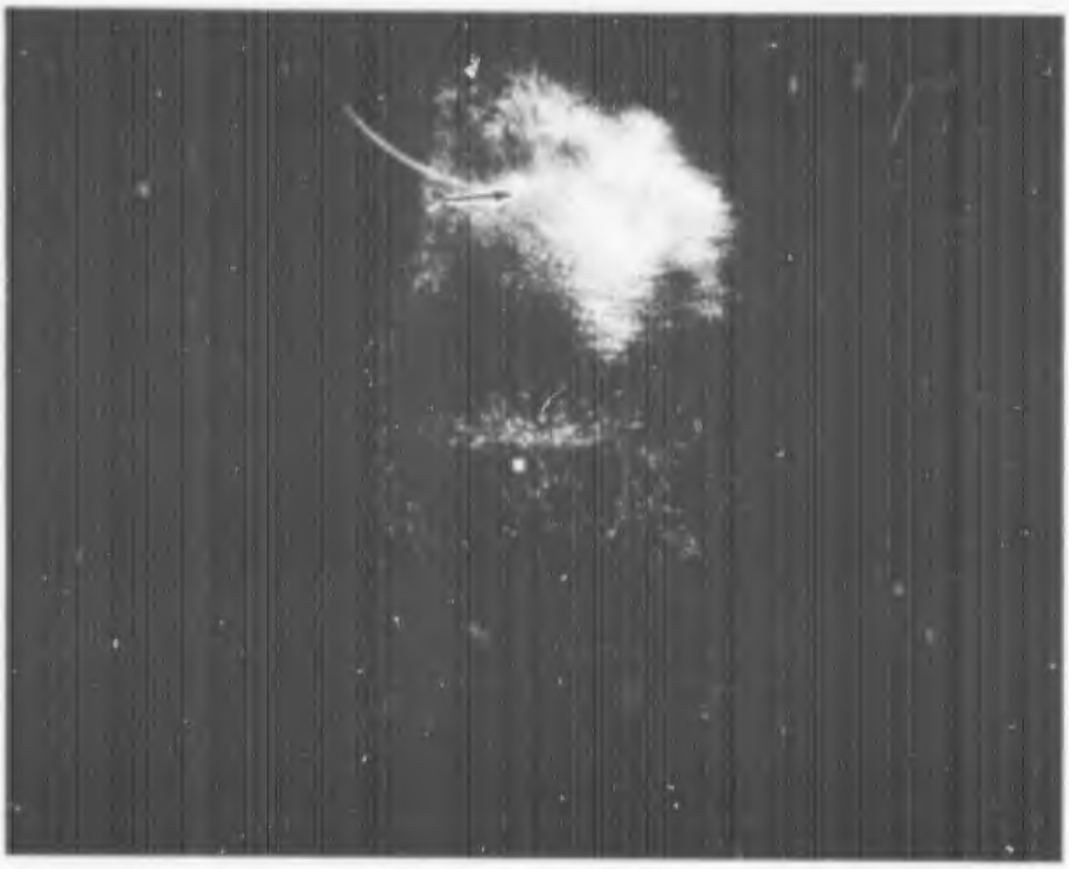

Fig. 44 Obstacle 11: Z/R = 0.667, D/R = 1.5; Group 3, recirculation, $h_o > h_J$, Type A, Location 5.

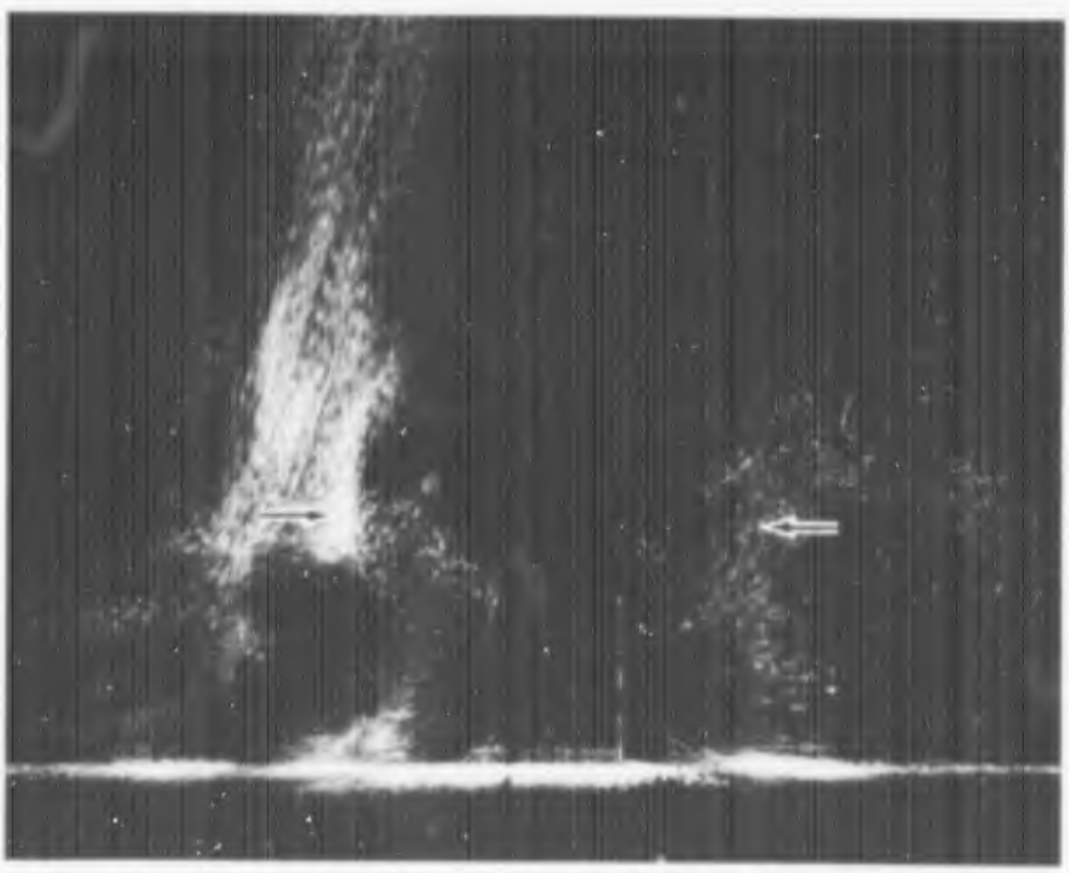

Fig. 45 Obstacle 11: Z/R = 0.667, D/R = 1.5; Group 3, recirculation, $h_o > h_J$, Type A, Location 1.

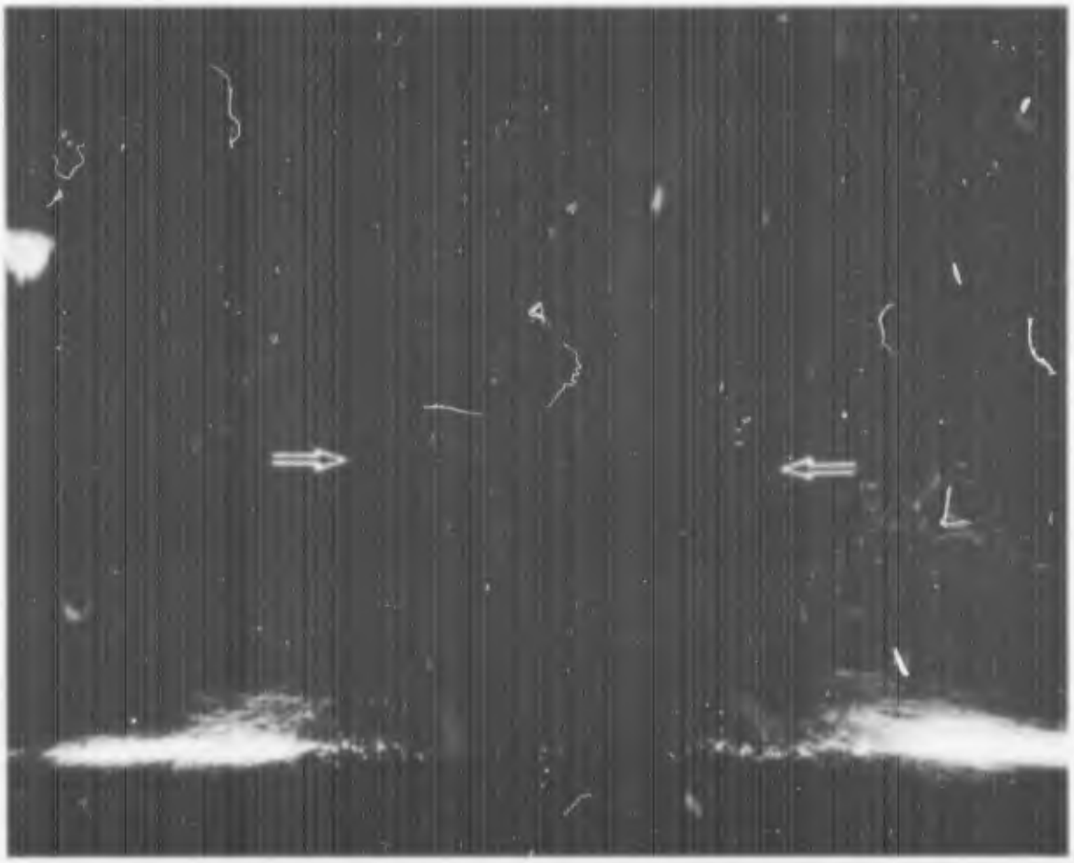

Fig. 46 Obstacle 11: Z/R = 0.667, D/R = 1.5; Group 3, recirculation, $h_o > h_j$, Type A, Location 4.

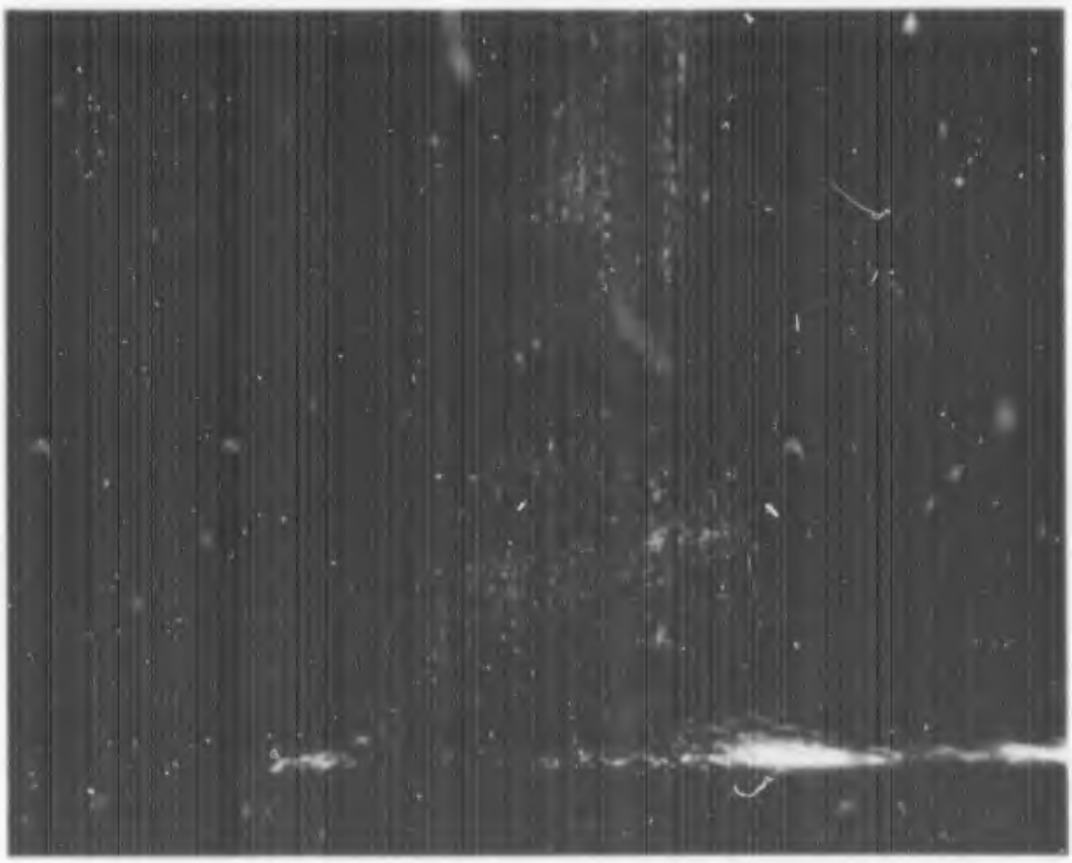

Fig. 47 Obstacle 3: Z/R = 0.667, D/R = 1.5; Group 1, no recirculation, $h_j > h_o$.

VI. CYLINDER-PRISM OBSTACLES

A certain number of runs was repeated so as to determine the influence a rounded top edge exerts upon recirculation.

The dimensions of obstacle 20 are listed in Section IV. It was used either by itself (obstacle 20 + 0) or in combination with obstacles 3, 7 and 11 over the entire range of Z/R and D/R values. Care was also taken to provide for a smooth transition surface between the prism and the cylinder.

Furthermore, a few tests were conducted with obstacles 17, 18 and 19 (for their dimensions refer to Section IV). However, the investigation of the flow patterns due to the last three obstacles was abandoned in order to concentrate on one obstacle width (w_o = 3").

The introduction of the cylinder-prism obstacle into the flow field has apparently only one major influence -- the onset of recirculation is delayed.

Obstacle 7 induces recirculation inboard of the rotor tip through the rotor disc for $0.500 \leq Z/R \leq 1.000$, ($D/R \leq 2.0$), while no recirculation can be observed for the equivalent cylinder-prism obstacle (obstacle 20 + 3) and the above Z/R and D/R values (Figures 48 and 49). A closer study of the photographs indicates that the height of the wall jet h_j apparently does not exceed 1.5", i.e. h_j appears to be less than the distance from the ground plane to the tangent point of the upper edge radius of the obstacle.

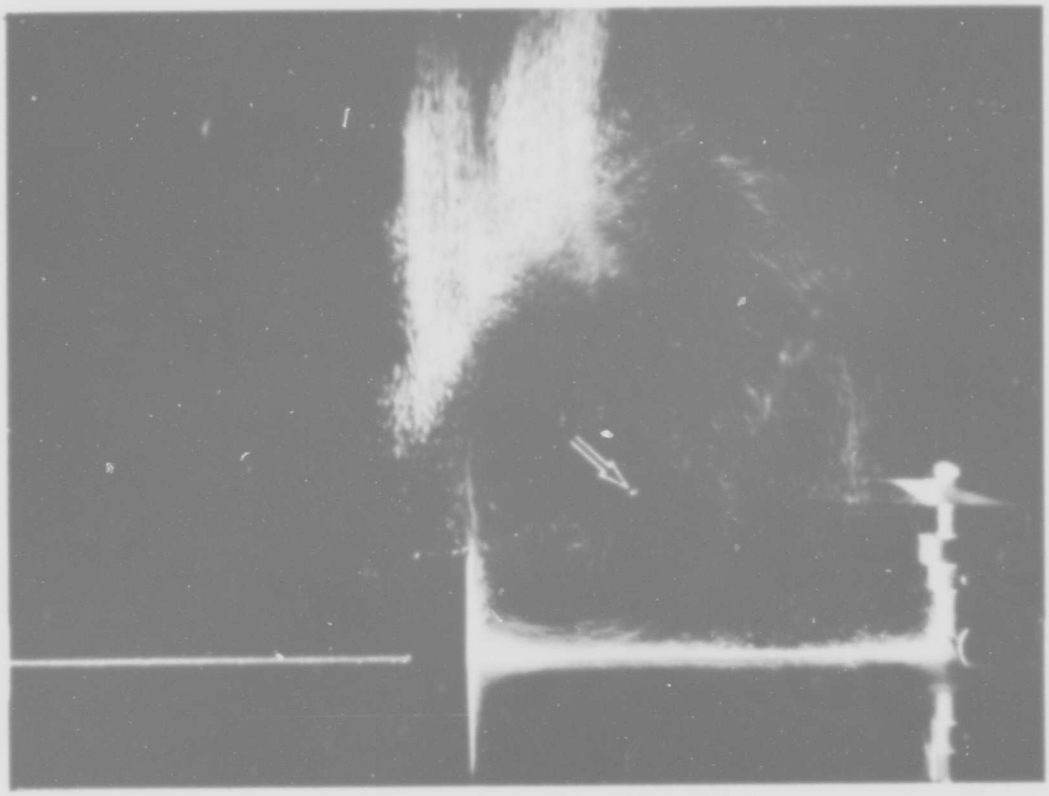

Fig. 48 Obstacle 7: Z/R = 0.500, D/R = 1.5; Group 3, recirculation, $h_o > h_j$, Type A.

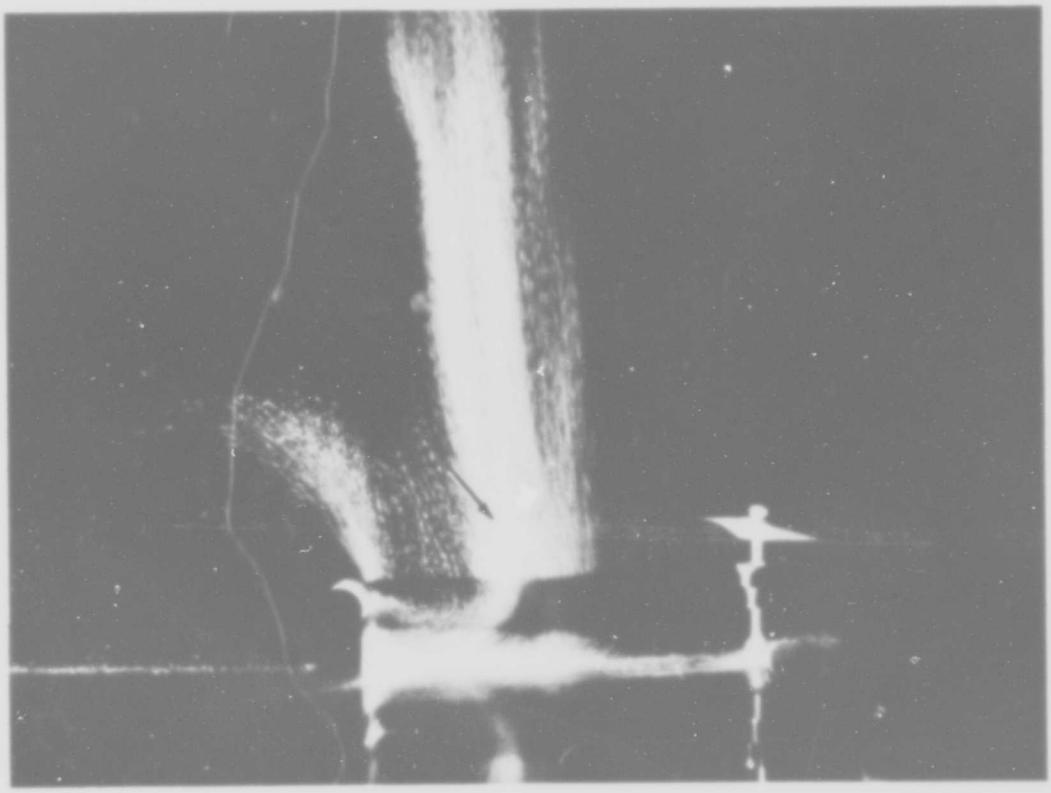

Fig. 49 Obstacle 20 + 3: Z/R = 0.500, D/R = 1.5; Group 2, no recirculation, $h_o > h_j$.

VII. WEDGE OBSTACLES

The purpose of the wedge obstacle tests was to prevent recirculation from entering the rotor disc or the rotor disc plane by trapping it underneath the lip of the wedge obstacles. The dimensions of the wedge obstacle, obstacle 21, are listed in Section IV and shown in Figure 6. It was used either by itself (obstacle 21 + 0) or in combination with obstacles 3, 7 and 11. The apex of the wedge always faced the rotor drive shaft. While Z/R was kept constant at 0.667, D/R was varied over the entire range.

The wedge facing the oncoming wall jet prevents recirculation through the rotor disc and the rotor disc plane for the test geometries listed above.

The effect of the wedge obstacle by itself (obstacle 21 + 0) on the wall jet is similar to that of a splitter plate (Figure 50)*. The major portion of the wall jet follows along the lower surface of the wedge and then spills around its base. There is apparently no change with increase in D/R.

Photographs of obstacle 21 + 3 in place indicate that the flow turns up at the forward face of the obstacle (Figure 51). However, it is not possible to observe on the photographs a turning of the flow through a full 180 degrees. There are no apparent changes with D/R.

---

*Note: The arrows in the wedge obstacle photographs indicate the position of the rotor tip and the apex of the wedge obstacle in the picture plane, respectively.

Fig. 50 Obstacle 21 + 0: Z/R = 0.667, D/R = 1.5; $h_j > h_o$.

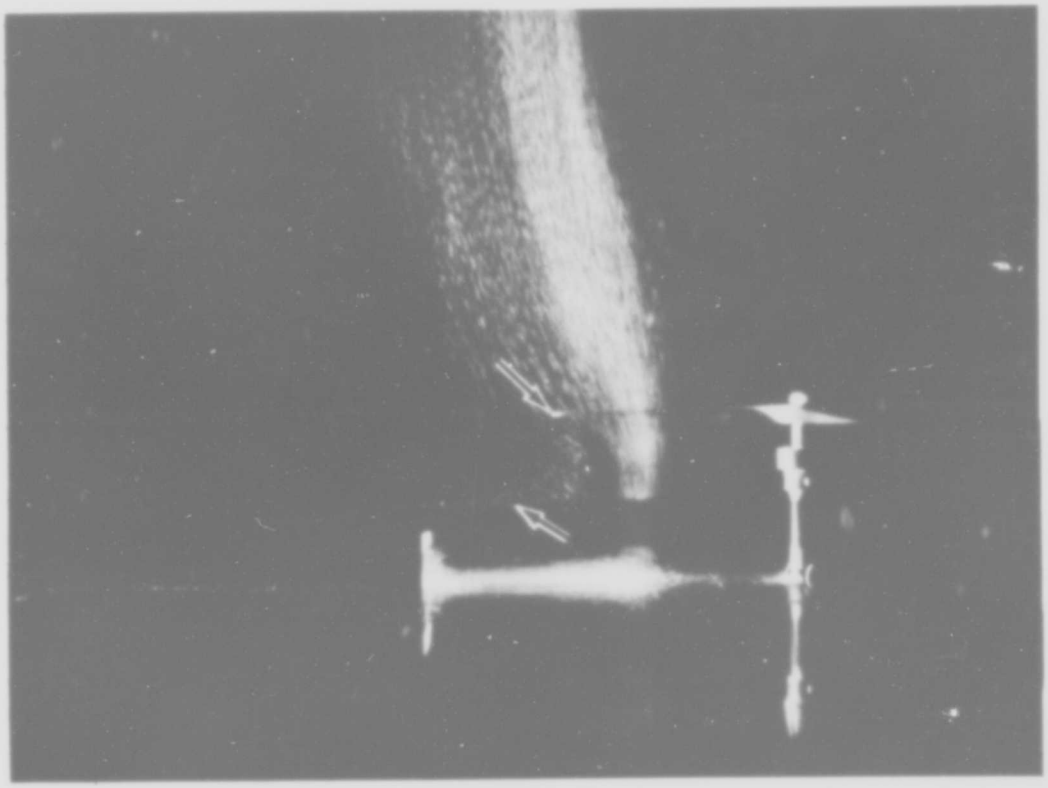

Fig. 51 Obstacle 21 + 3: Z/R = 0.667, D/R = 1.5; $h_o > h_j$.

Photographs of obstacle 21 + 7 in position show the beginning of recirculation below the bottom surface of the wedge (Figure 52). This recirculation is fully developed for obstacle 21 + 11 (Figure 53). Again there seems to be no change with increase in D/R.

It is interesting to note that the flow, having turned through 180°, will not follow the bottom surface of the wedge to its apex, but will remain more or less horizontal for a short distance or even deflect downward before turning again and re-entering the wall jet. No recirculation through the rotor disc or the rotor disc plane can be observed for all of the above conditions.

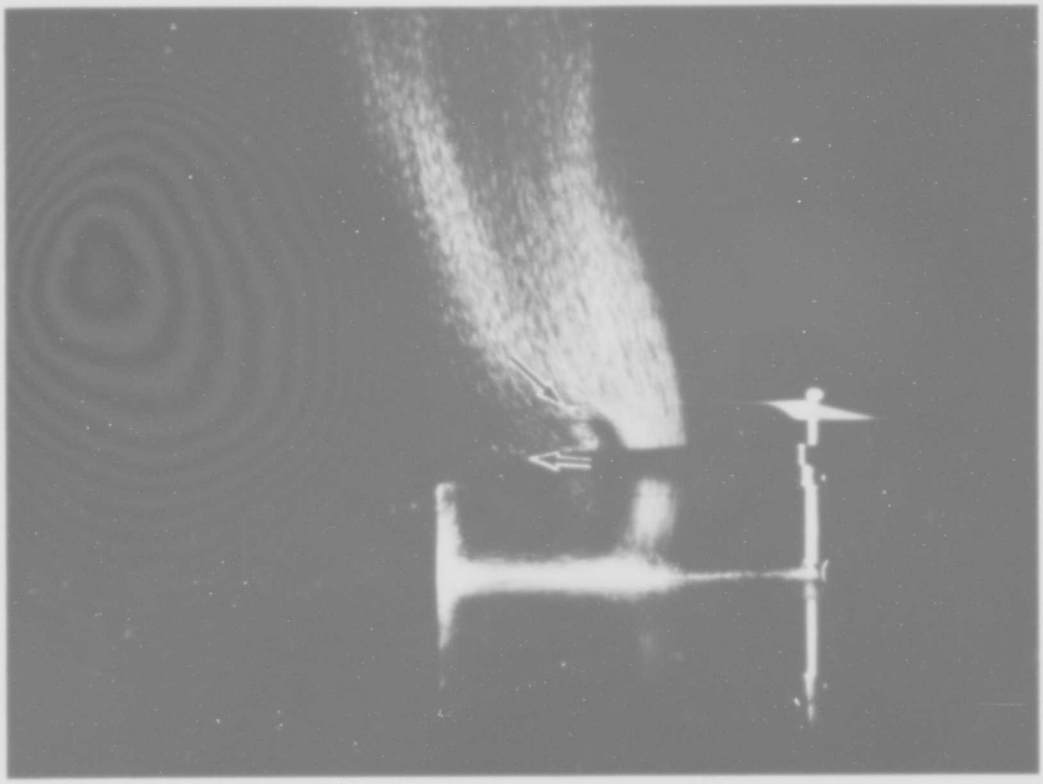

Fig. 52 Obstacle 21 + 7: Z/R = 0.667, D/R = 1.5; $h_o > h_j$.

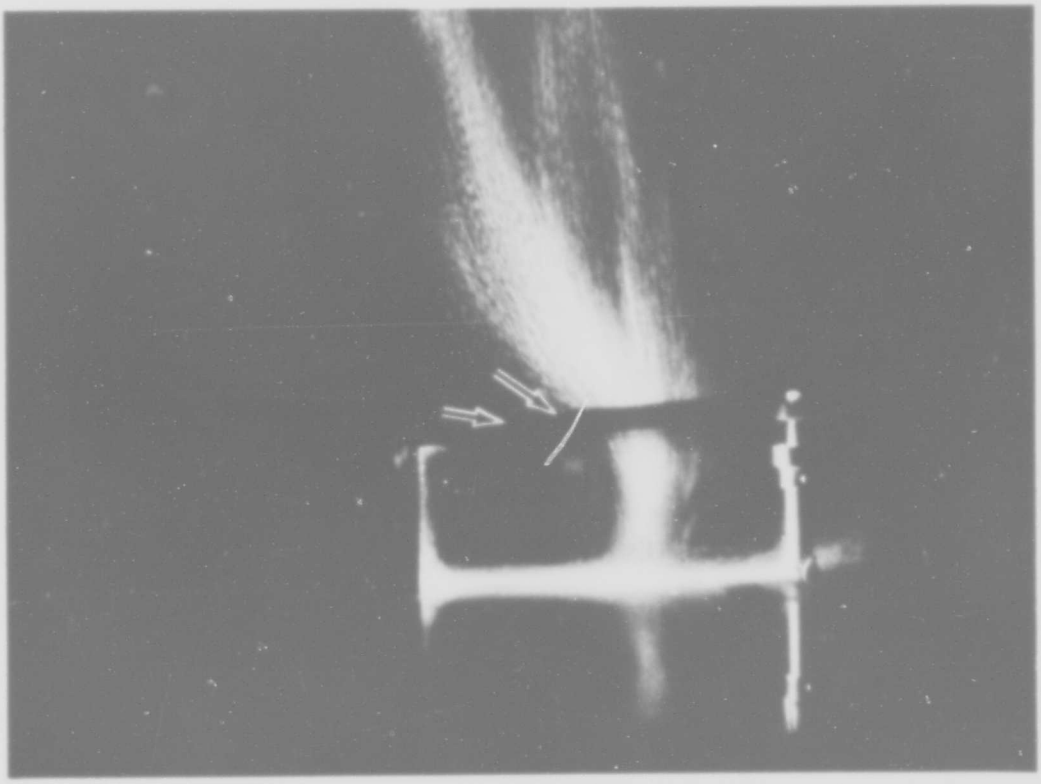

Fig. 53 Obstacle 21 + 11: Z/R = 0.667, D/R = 1.5; $h_o > h_j$.

VIII. ROD OBSTACLE

Attempts to observe the Coanda effect were inconclusive. Obstacle 22 (for dimensions refer to Figure 7) was designed for this particular purpose.

It appears that the radius of curvature of the circular lucite cylinder is too small and that, therefore, the flow separates from the bottom tangent point of the rod (Figure 54).

Modified obstacles (larger radius of curvature) will be built and their flow fields studied at a later date.

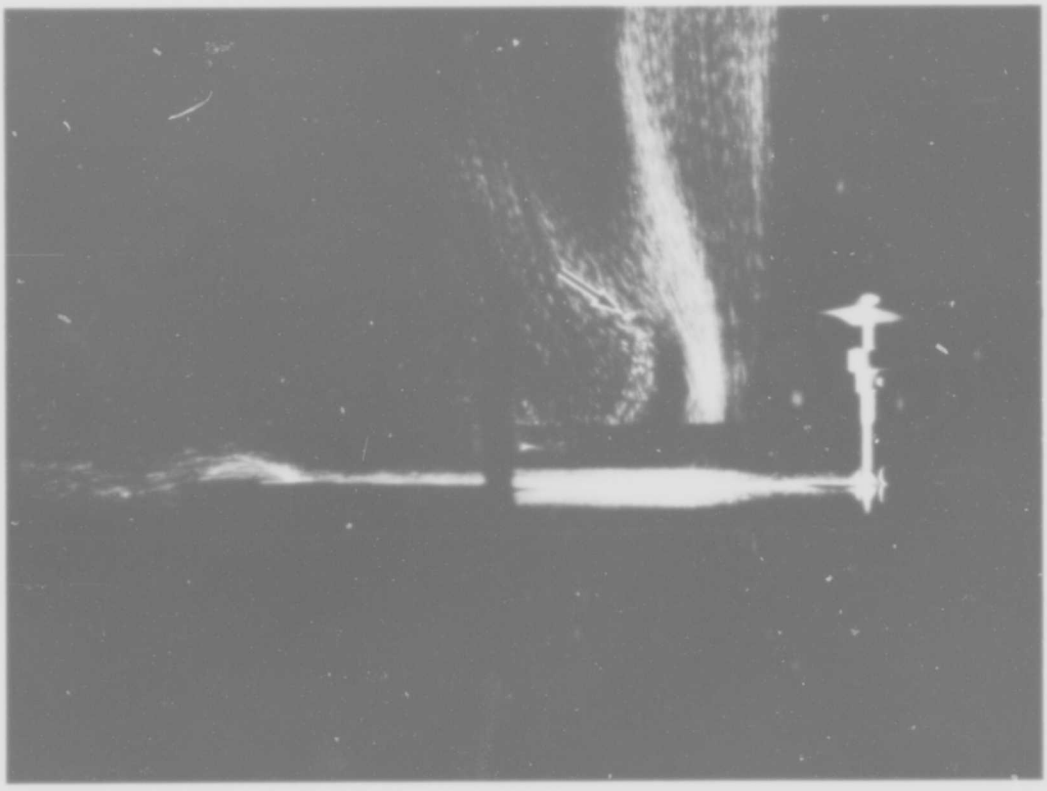

Fig. 54 Obstacle 22: Z/R = 0.667, D/R = 1.5; distance ground plane - centerline of rod = 1.0".

IX. RING OBSTACLES

There were, in addition to the previously listed obstacles, several ring obstacles made out of wood. These were:

Ring obstacle A : ID = 18"; OD = 20"; h_o = 1"

A': ID = 18"; OD = 20"; h_o = 2"

A": A and A' combined; h_o = 3"

B : ID = 24"; OD = 26"; h_o = 1"

B': ID = 24"; OD = 26"; h_o = 2"

B": B and B' combined; h_o = 3"

The reason for building these obstacles was to study the probable rotational symmetry of the flow. However, difficulties in visualizing the flow were encountered. It was impossible to observe a discreet development of flow patterns with these obstacles placed on the ground plane.

Sawdust introduced into the airstream above the rotor disc plane had the appearance of a swirling cloud, which seemed to occupy almost the entire volume between the sifter and the area on the ground plane enclosed by the ring obstacle. This was particularly pronounced for the 1" and 2" high obstacles, regardless of the respective obstacle inside diameters. It is hoped that additional test runs, scheduled for the near future, will aid in the understanding of this phenomenon.

Furthermore, the ring obstacles were employed in obtaining some power data. These measurements showed that by placing ring obstacles on the ground plane, concentric with the rotor, the power required to run the rotor would be reduced by a significant amount.

The reduction in power required is most likely due to recirculation inboard of the rotor tip, through the rotor disc. It seems reasonable to assume, based on the tests conducted with the prism obstacles, that the ring obstacles induce recirculation. The recirculating flow has a certain momentum which is higher than that of the flow being induced from the surrounding volume into the rotor disc. It imparts some of its higher momentum to the flow approaching the rotor disc and at the same time displaces a certain percentage of the approaching slower flow, thus reducing the work load of the rotor, which in turn reduces the power absorbed by the rotor from the drive motor, a synchronous electric motor running at constant RPM. The above should be particularly true for ring obstacles A', A", B' and B".

The limited data available at the present time indicate that power required varies, for a given D/R, inversely with the obstacle height h_o. A graph of percent reduction in power required vs the frontal area facing the wall jet (Figure 55) demonstrates this dependence clearly.

Flow visualization runs as well as power required and velocity survey data were limited to Z/R = 0.667. An extension to additional Z/R values along with various additional obstacle heights and diameters is scheduled.

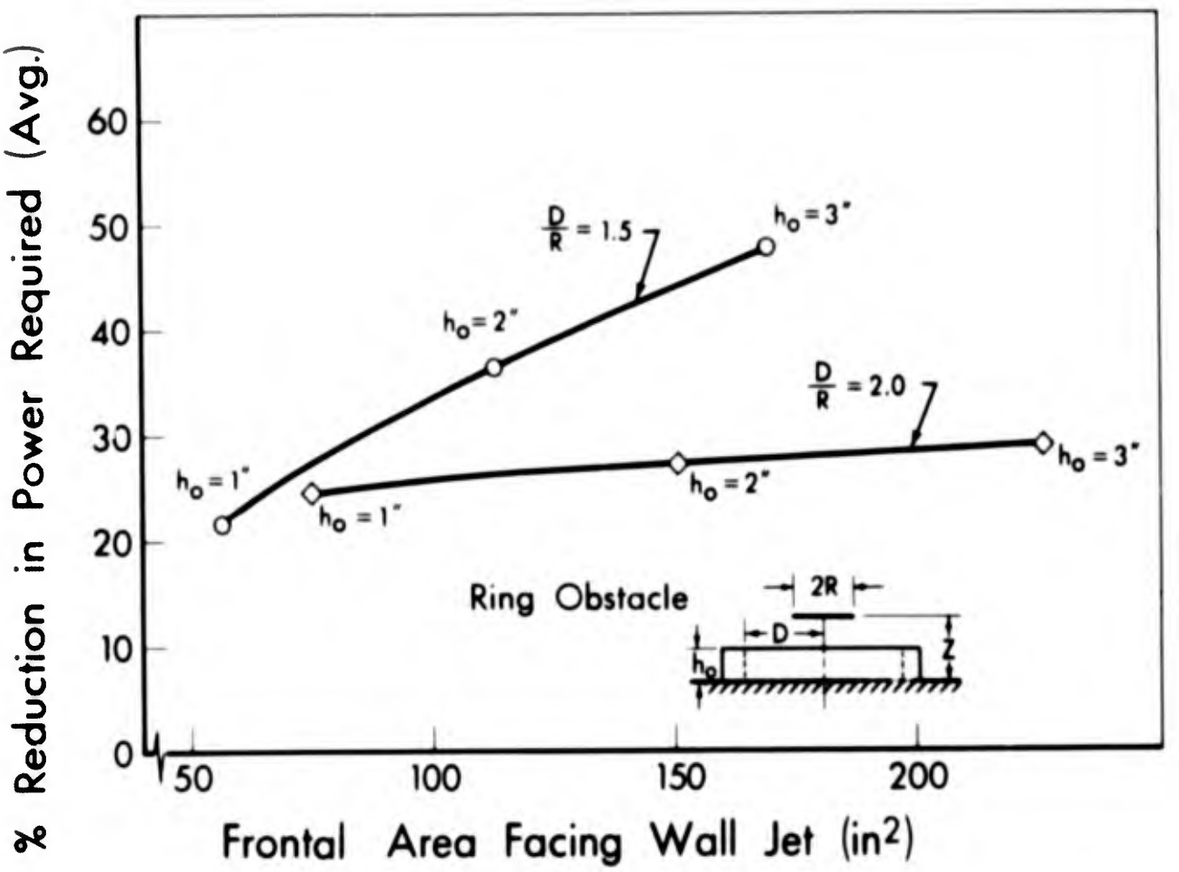

Fig. 55 % reduction in power required vs. frontal area.

X. DEAD AIR DOME

E. A. Fradenburgh[11] refers to a roughly hemispherical volume between a point above the rotor disc and the ground plane as the "dead air dome". This volume is actually not a region of completely stagnant air, but only of slowly moving air.

He states that the dead air dome forms as $Z/R \rightarrow 1.000$. However, as mentioned previously[1], it was possible to observe the dome up to $Z/R = 2.000$. Furthermore, its over-all height appeared to be almost independent of Z/R.

Test runs encompassing the entire range of Z/R values confirm this observation (Figures 56, 57, 58, 59 and 60), with one exception, which occurs at $Z/R = 1.000$ (Figure 58). A summary of the data obtained from the test runs is shown in Figure 61.

A transition from a dead air dome extending above the rotor disc ($Z/R < 1.000$) to one remaining below the rotor disc ($Z/R > 1.000$) seems to take place at about $Z/R = 1.000$. Here the particles remain in the immediate vicinity of the rotor disc plane, i.e. they impinge on the rotor hub and are carried off to form the dead air dome without either penetrating the rotor disc or stagnating above it (Figure 58).

BLANK PAGE

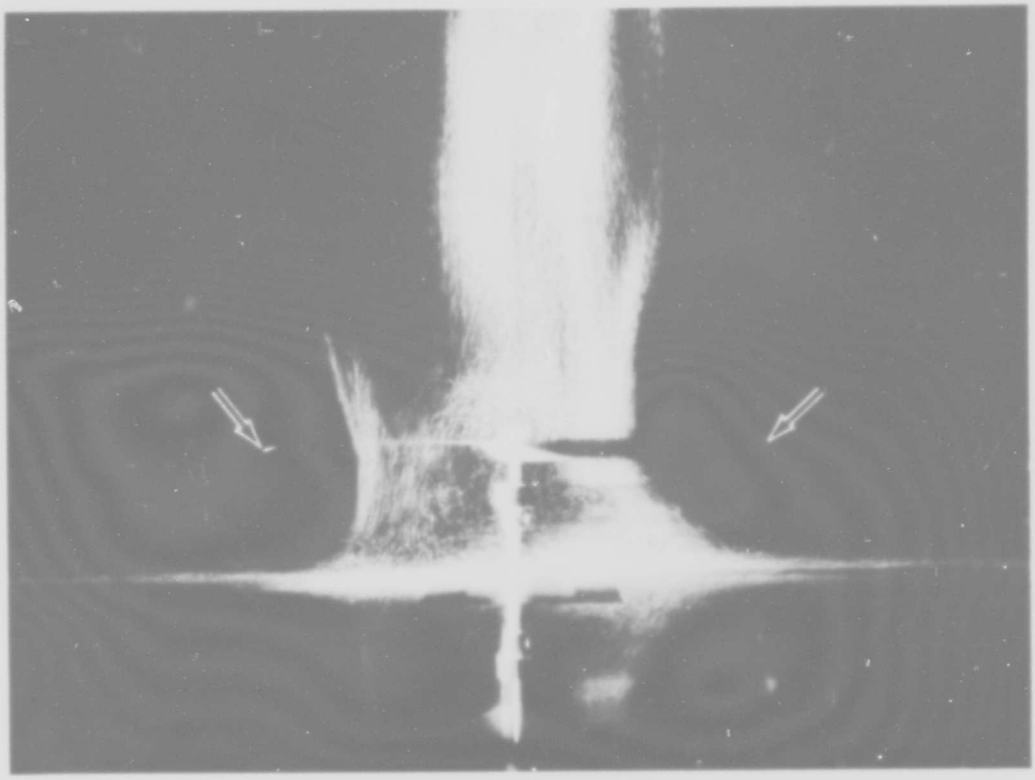

Fig. 56 Dead air dome, Z/R = 0.500.

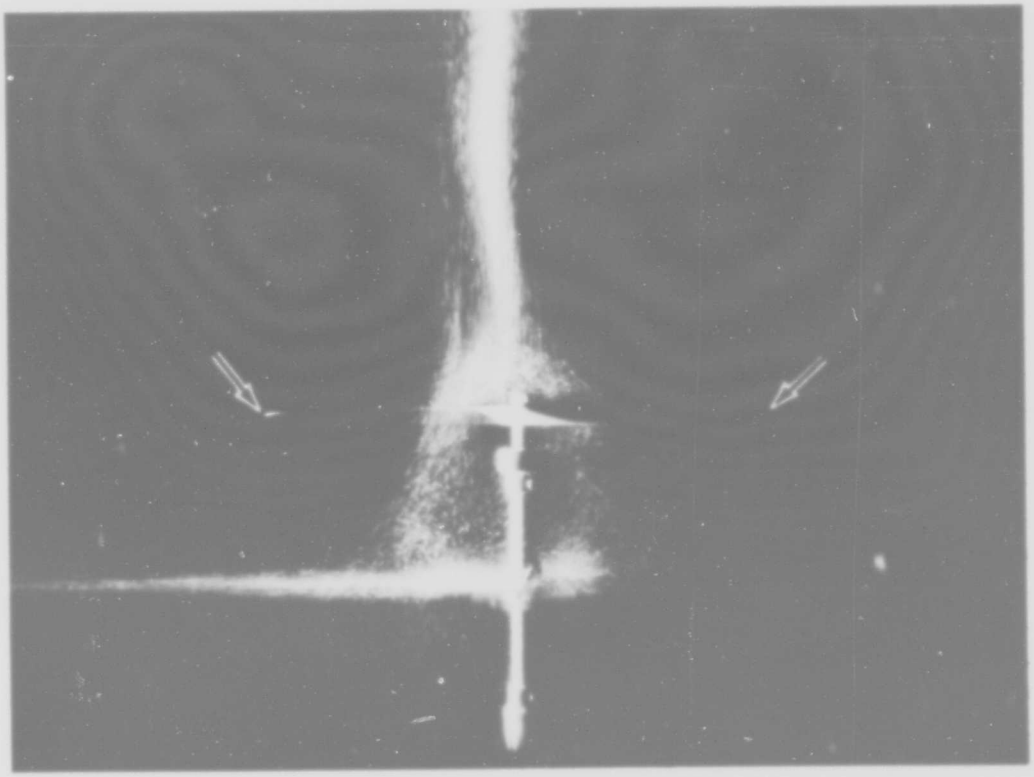

Fig. 57 Dead air dome, Z/R = 0.667.

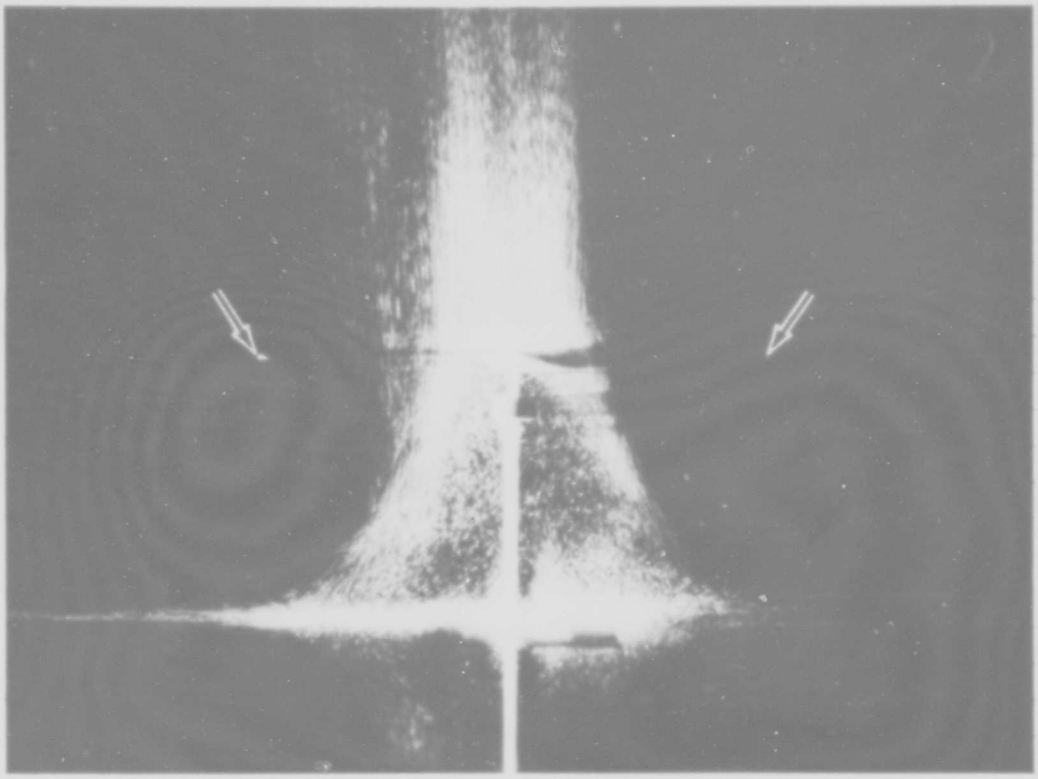

Fig. 58 Dead air dome, Z/R = 1.000.

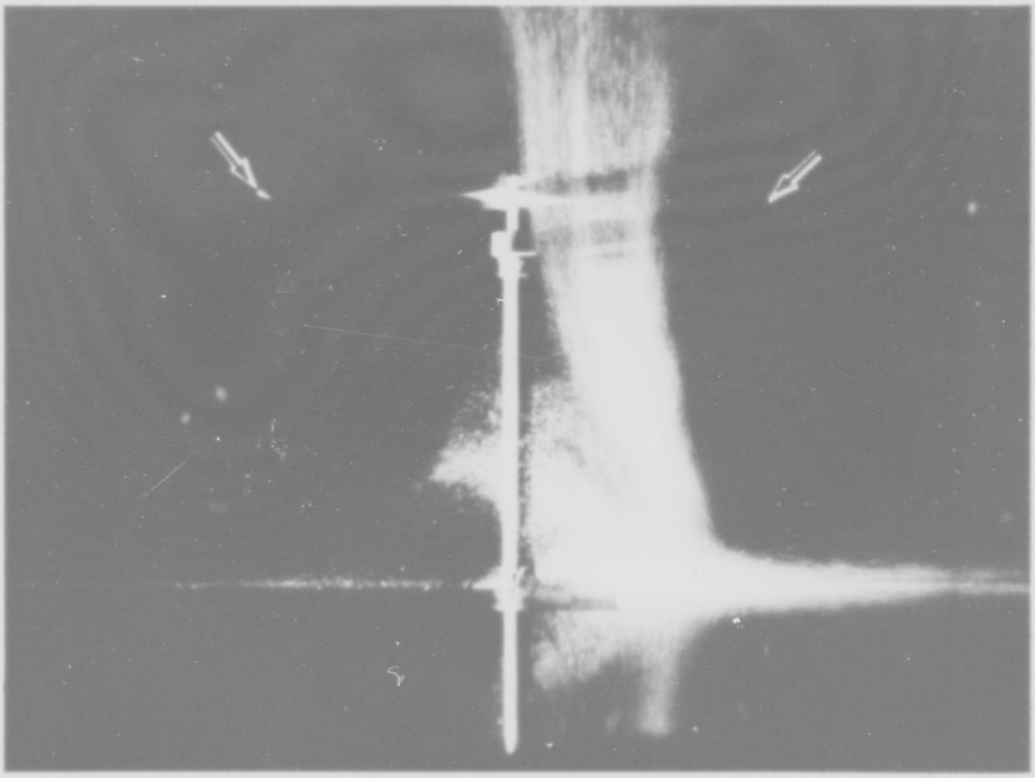

Fig. 59 Dead air dome, Z/R = 1.500.

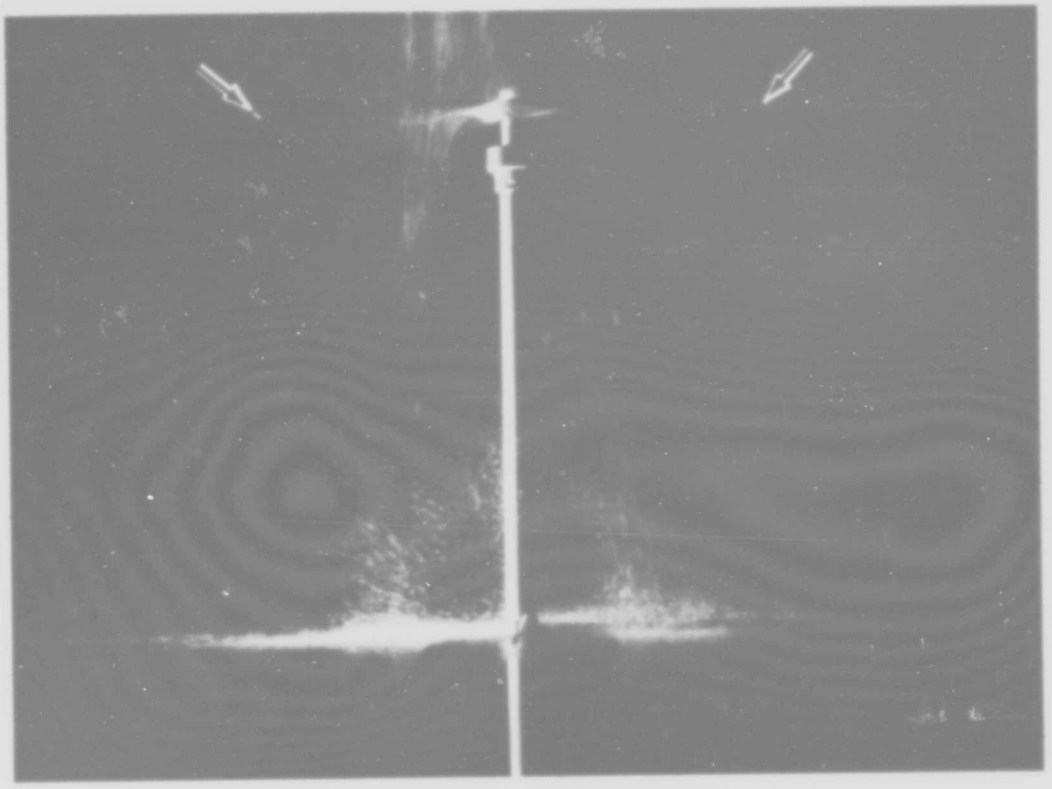

Fig. 60 Dead air dome, Z/R = 2.000.

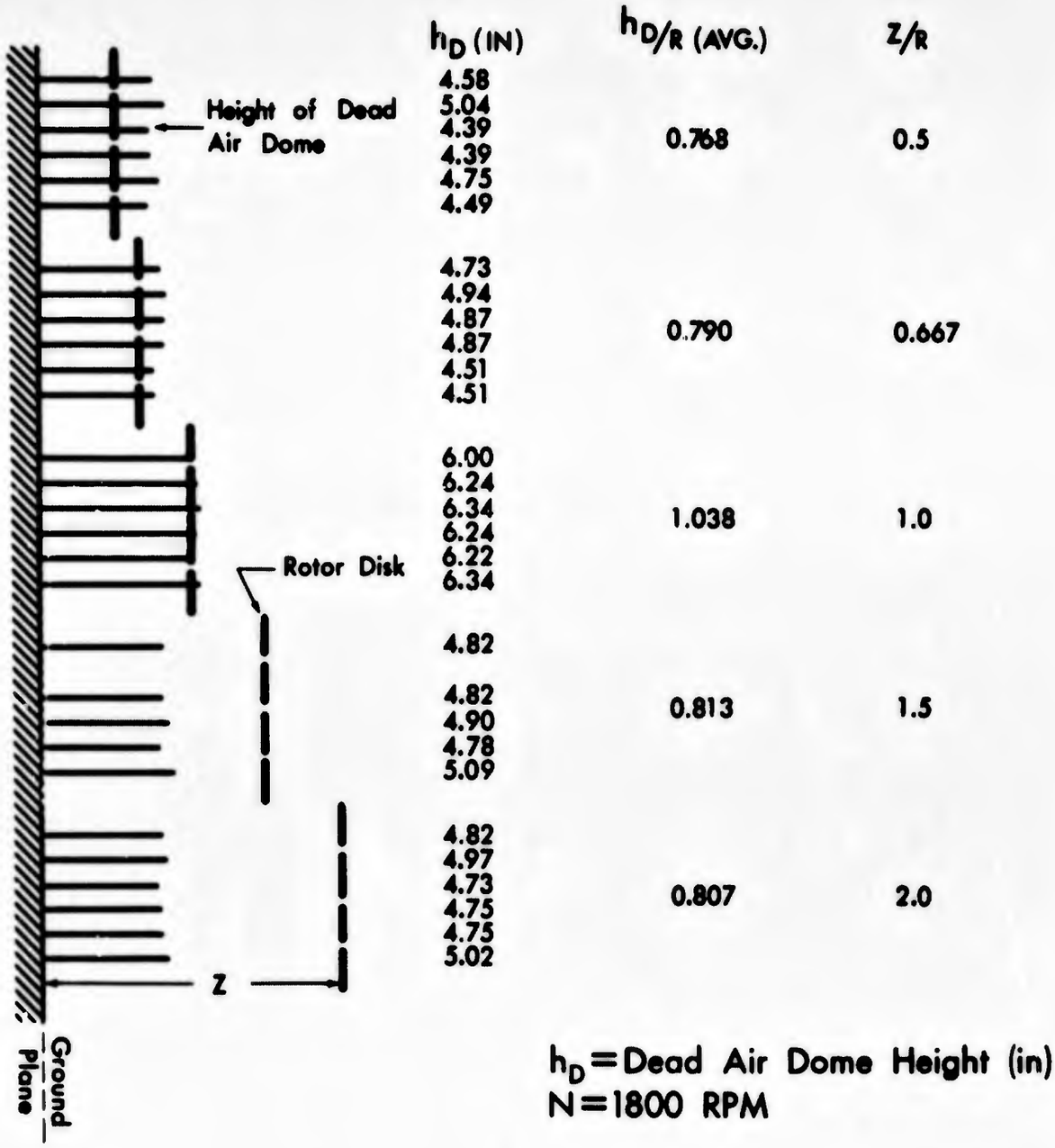

Fig. 61 Height of dead air dome h_D vs. rotor disc height Z.

XI. PERSISTENCE OF RECIRCULATION

A brief study of the persistence of obstacle-induced recirculation has been undertaken. The flow visualization photographs show, as expected, that recirculation does not persist (Figure 62).

The photographs were taken while the obstacle inducing recirculation was rotated from an upright to a horizontal position. They indicate clearly how the flow changes from recirculating to spilling once the obstacle reaches a cert in inclination with respect to the ground plane, thus reducing the effective height of the obstacle (Figure 62).

Obstacle 16, at Z/R = 0.667 and D/R = 1.5, was used for this initial investigation. Flow visualization pictures of obstacle 16 in an upright position (Z/R = 0.667 and D/R = 1.5) show the flow passing inboard of the rotor tip through the rotor disc (Figure 63). Photographs of the same obstacle in a horizontal position (identical Z/R and D/R) show that the flow spills over the obstacle (Figure 64).

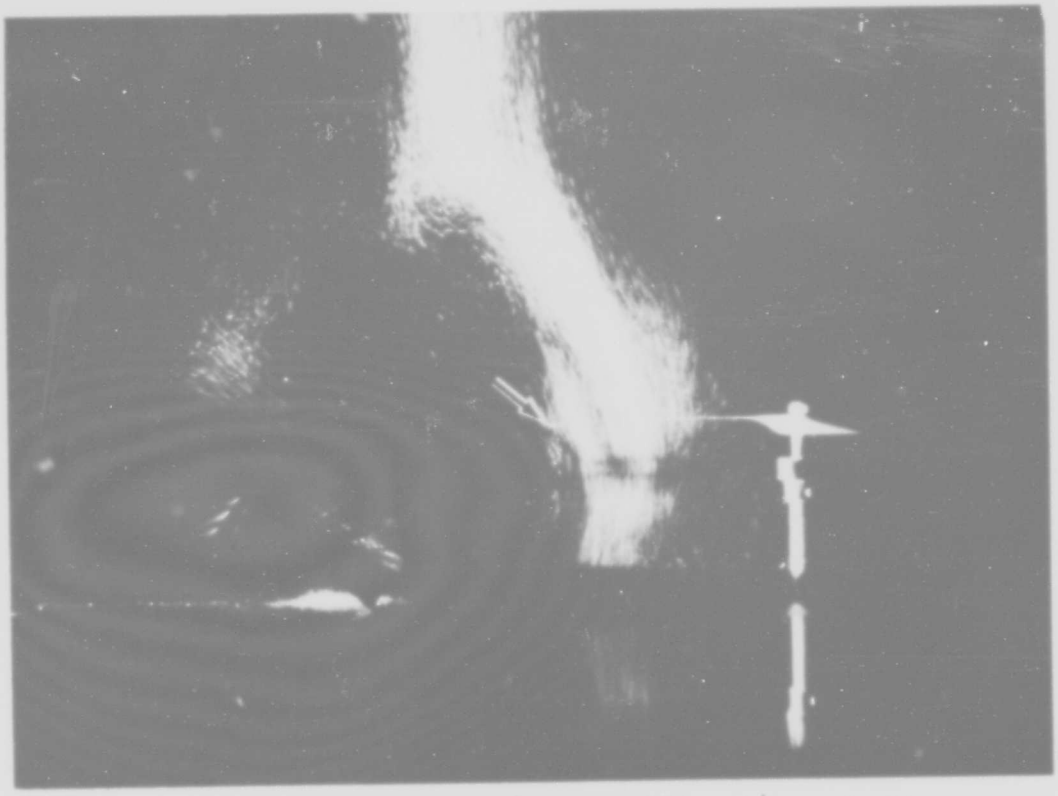

Fig. 62 Obstacle 16: Z/R = 0.667, D/R = 1.5.

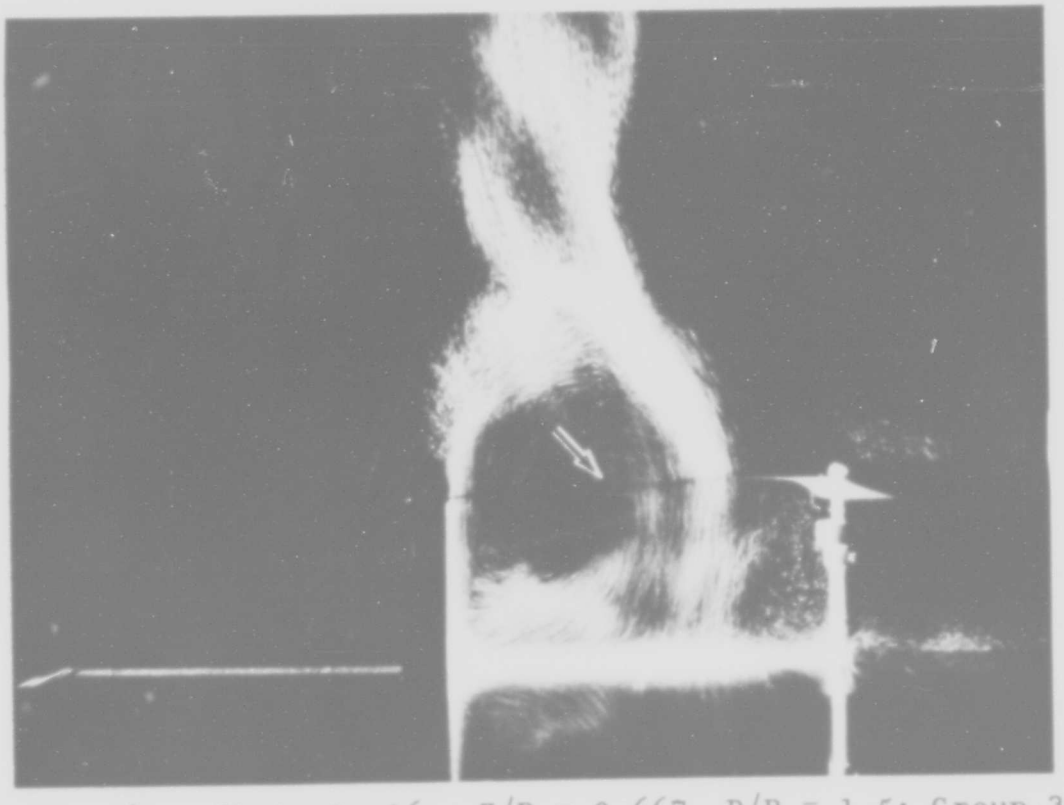

Fig. 63 Obstacle 16: Z/R = 0.667, D/R = 1.5; Group 3, recirculation, $h_o > h_j$, Type A.

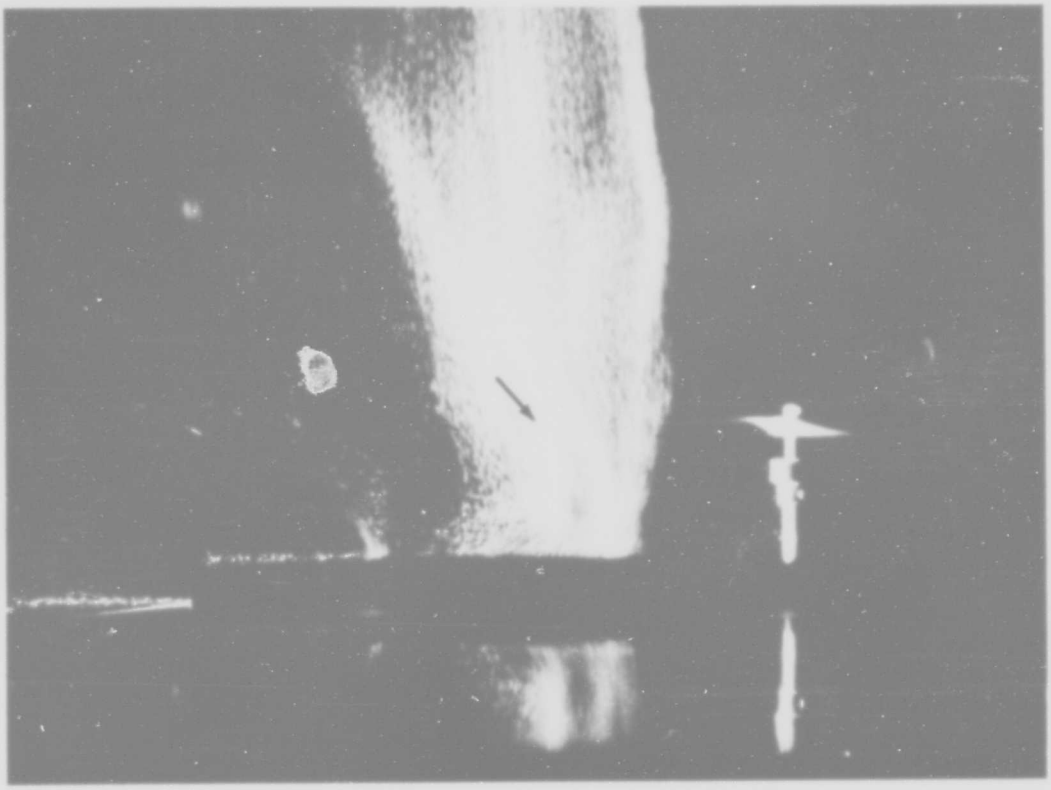

Fig. 64 Obstacle 16: Z/R = 0.667, D/R = 1.5.

XII. CONCLUSIONS

The primary requirement for recirculation to be induced by an obstacle on the ground plane is that the height of the obstacle be greater than the height of the wall jet approaching it. Recirculation will also not be induced if the obstacle is too far removed from the rotor drive shaft or the rotor disc is too far above the ground plane.

An obstacle with a rounded top edge will apparently delay the onset of recirculation.

Two major types of recirculation appear:

1) Recirculation inboard of the rotor tip with the recirculating flow passing through the rotor disc.
2) Recirculation outboard of the rotor tip with the recirculating flow either passing through or remaining below the rotor disc plane.

Wedges introduced above the ground plane into the recirculation will contain the flow and prevent it from entering the rotor disc or the rotor disc plane.

Ring obstacles placed concentrically (on the ground plane) about the rotor drive shaft lead to appreciable reductions in power required. The reduction is proportional to the obstacle height.

The height of the dead air dome seems to be independent of the height of the rotor disc above the ground plane, within the limits of the present study. The dead air dome falls into two categories:

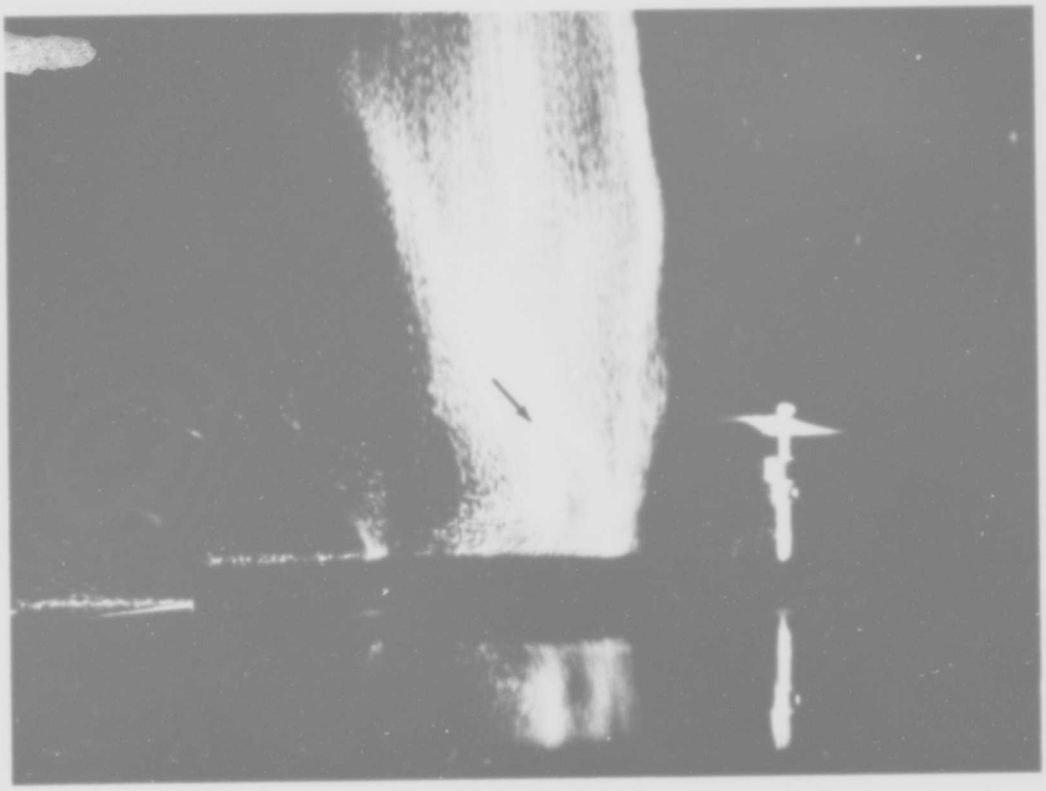

Fig. 64 Obstacle 16: Z/R = 0.667, D/R = 1.5.

XII. CONCLUSIONS

The primary requirement for recirculation to be induced by an obstacle on the ground plane is that the height of the obstacle be greater than the height of the wall jet approaching it. Recirculation will also not be induced if the obstacle is too far removed from the rotor drive shaft or the rotor disc is too far above the ground plane.

An obstacle with a rounded top edge will apparently delay the onset of recirculation.

Two major types of recirculation appear:

1) Recirculation inboard of the rotor tip with the recirculating flow passing through the rotor disc.
2) Recirculation outboard of the rotor tip with the recirculating flow either passing through or remaining below the rotor disc plane.

Wedges introduced above the ground plane into the recirculation will contain the flow and prevent it from entering the rotor disc or the rotor disc plane.

Ring obstacles placed concentrically (on the ground plane) about the rotor drive shaft lead to appreciable reductions in power required. The reduction is proportional to the obstacle height.

The height of the dead air dome seems to be independent of the height of the rotor disc above the ground plane, within the limits of the present study. The dead air dome falls into two categories:

1) above the rotor disc ($Z/R < 1.000$)

2) below the rotor disc ($Z/R > 1.000$)

There exists also a transitionary stage.

Obstacle-induced recirculation does not persist and will disappear as soon as the obstacle reaches a minimum effective height.

BLANK PAGE

A P P E N D I X I

Classification of Flow Visualization Photographs (Prism Obstacles):

GROUP 1: No Recirculation, $h_j > h_o$

Flow spills around obstacle

GROUP 2: No Recirculation, $h_o > h_j$

Flow spills around obstacle

GROUP 3: Recirculation, $h_o > h_j$

Type A: Recirculation inboard of rotor tip, through rotor disc

Type B: Recirculation outboard of rotor tip, through or below rotor disc plane

Type C: Recirculation through rotor tip, in rotor disc plane

Table III

Classification of Flow Visualization Photographs

(Prism Obstacles)

Z/R	0.500			0.667			1.000			1.500			2.000		
D/R	1.5	2.0	2.5	1.5	2.0	2.5	1.5	2.0	2.5	1.5	2.0	2.5	1.5	2.0	2.5
Obstacle	Type of Flow Observed														
1	1	1	1	1	1	1	1	1	1	1	1	1	1	1	1
2	1	1	1	1	1	1	1	1	1	1	1	1	1	1	1
3	1	1	1	1	1	1	1	1	1	1	1	1	1	1	1
4	1	1	1	1	1	1	1	1	1	1	1	1	1	1	1
5	3A	3B	3B	3B-2	3B-2	3B-2	3B-2	2	2	2	2	2	2	2	2
6	3A	3B	3B	3A	3B-2	3B-2	3B-2	2	2	2	2	2	2	2	2
7	3A	3A	3B	3A	3A	3B	3A	3A	3B	2	2	2	2	2	2
8	3A	3A	3B	3A	3A	3B	3A	3A	3B	2	2	2	2	2	2
9	3A	3B	3B	3C	3B	3B	3B	3B	3B	3B	3B	3B	3B	3B	3B
10	3A	3A	3B	3A	3B	3B	3A	3B	3B	3B	3B	3B	3B	3B	3B
11	3A	3A	3B	3A	3A	3B	3A	3A	3B	3B	3B	3B	3B	3B	3B
12	3A	3A	3B	3A	3A	3B	3A	3A	3B	3A	3A	3B	3B	3B	3B
13	3A	3B	3B	3A	3B	3B	3B	3B	3B	3B	3B	3B	3B	3B	3B
14	3A	3A	3B	3A	3B	3B	3A	3B	3B	3B	3B	3B	3B	3B	3B
15	3A	3A	3B	3A	3A	3B	3A	3A	3B	3B	3B	3B	3B	3B	3B
16	3A	3A	3B	3A	3A	3B	3A	3A	3B	3C	3A	3B	3B	3B	3B

A P P E N D I X I I

VELOCITY SURVEY

A brief velocity survey was conducted. It consisted of four data runs, i.e. two each with the orifice of the total head tube at 1.25" and 3.32" above the ground plane, respectively.

The data of the fourth run include effects due to ring obstacle A placed on the ground plane. A graph (Figure 65) shows the results, which seem to be in reasonable agreement with the theoretical value for the induced velocity (neglecting ground and recirculation effects -- Appendix III).

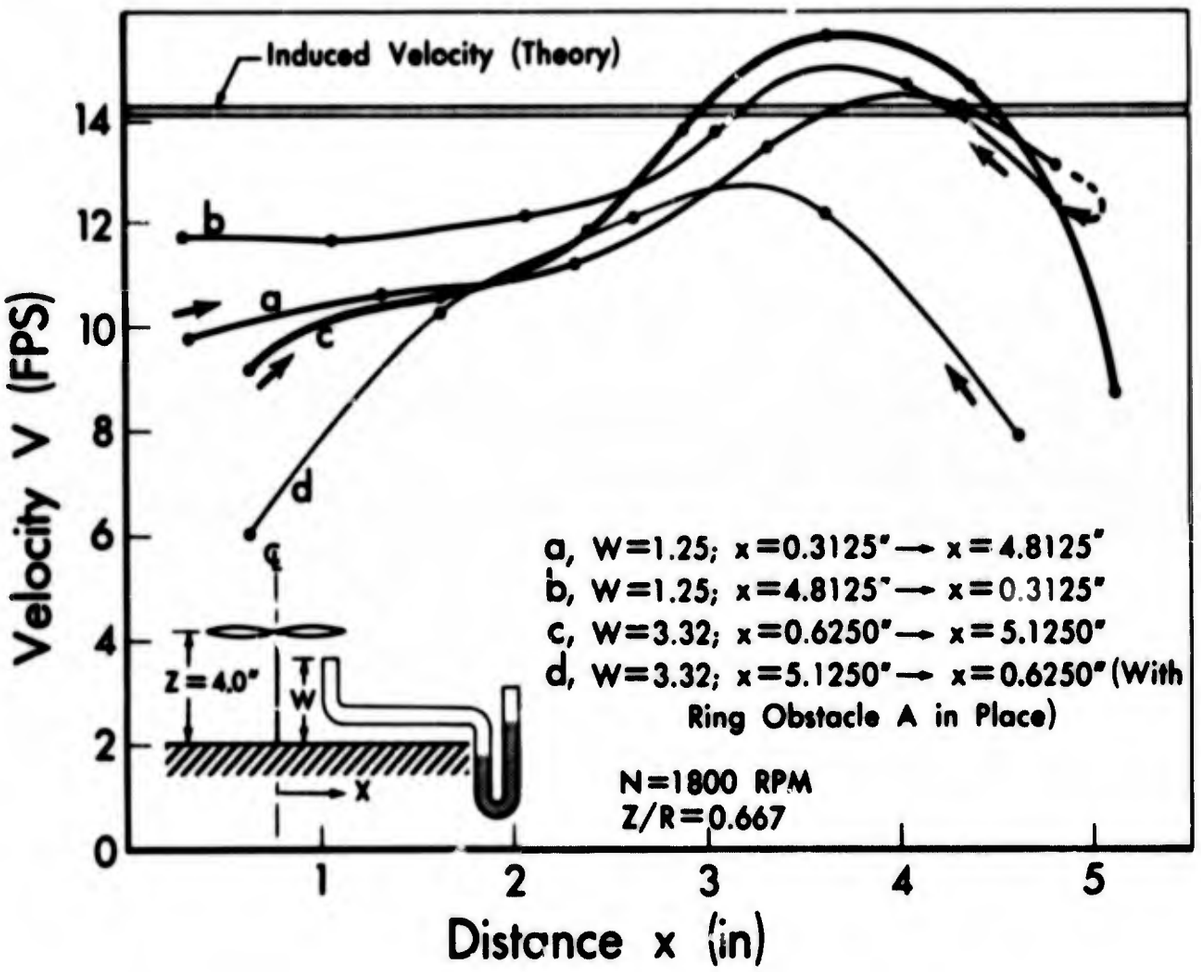

Fig. 65 Velocity below rotor disc vs. distance from rotor drive shaft centerline.

A P P E N D I X I I I

ROTOR DRIVE AND ROTOR PARAMETERS

Rotor Drive

Rated:	Power	P_o =	0.05 HP
	Voltage	E =	115 VAC (60 Hz)
	Power	P_1 =	110 W
	Current	I =	1.5 A
Measured:		N =	1800 ± 10 RPM
	Voltage	E =	110.29 ± 0.02 VAC
	Current	I =	1.200 ± 0.024 A
Calculated:	Efficiency	η =	33.896%
	RMS Voltage	=	70.3297 ± 0.0128 V
	Power	P =	0.03836 ± 0.00077 HP

Rotor (Reference 12)

Figure of Merit	M =	0.5 (assumed)
Density (at S.L.)	ρ =	0.002378 lbf sec^2 ft^{-4}
Kinematic Viscosity (at S.L.)	ν =	1.564 x 10^{-4} ft^2 sec^{-1}
Thrust	T =	$(2\rho\pi R^2P^2M^2)^{1/3}$
	=	0.7462 ± 0.0099 lbf
Disc Loading	=	$T/\pi R^2$
	=	0.950 lbf ft^{-2}
Power Loading	=	T/P
	=	19.45 lbf HP^{-1}
Induced Velocity	V_i =	$(T/2\rho\pi R^2)^{\frac{1}{2}}$
	=	14.13 ± 0.09 fps

Tip Speed $U = \frac{\pi N}{30} R$

$= 94.25 \pm 0.525$ fps

Reynolds Number $Re = UR/\nu$

$= 301,311 \pm 1,678$

REFERENCES

(1) Timm, G. K., "Visualization Studies of Obstacle-Induced Recirculation in the Flow Field About a Model Propeller Operating Within the Ground Effect Regime (Interim Report)", Boeing Scientific Research Laboratories, F.S.L. Technical Memorandum No. 31, April, 1964.

(2) George, M. and Fraundorf, E., "Downwash Impingement Tests of an 1/9 Scale Model of the Boeing 147 Aircraft", Dynasciences Corporation Report No. DCR-155, November, 1964; prepared for The Boeing Company, Vertol Div., Morton, Pa.

(3) Graham, M. E., Boeing Scientific Research Laboratories, Flight Sciences Laboratory, verbal communication.

(4) Graham, E. W., "Notes on Experimental Work in Jet Impingement and on Turbulence in Vortices", Boeing Scientific Research Laboratories, F.S.L. Technical Memorandum No. 32, April, 1964.

(5) Graham, E. W., "Notes on Jet Impingement and on the Limiting Lift for a Finite Aspect Ratio Wing", Boeing Scientific Research Laboratories, F.S.L. Technical Memorandum No. 34, August, 1964.

(6) Graham, E. W., "Questions and Comments on the Maximum Lift, Jet Mixing and Jet Impingement Problems", Boeing Scientific Research Laboratories, F.S.L. Technical Memorandum No. 37, January, 1965.

(7) Iwan, L. S., "Visualization Studies of Recirculation in the Flow About a Rotor Operating Near the Ground", Boeing Scientific Research Laboratories, F.S.L. Technical Memorandum No. 17, September, 1963.

(8) Taylor, M. K., "A Balsa-Dust Technique for Air-Flow Visualization and its Application to Flow Through Model Helicopter Rotors in Static Thrust", NACA Tech. Note 2220, November, 1950.

(9) Wright, F. H., "The Particle Track Method of Tracing Fluid Streamlines", Jet Propulsion Laboratory, Calif. Inst. of Technology, Prog. Rep. No. 3-23, March, 1951.

(10) Timm, G. K., Trip Report, Boeing Scientific Research Laboratories, F.S.L. Memo 1-8220-202, November, 1964.

(11) Fradenburgh, E. A., "Flow Field Measurements for a Hovering Rotor Near Ground", Sikorsky Aircraft Div., United Aircraft Corp., September, 1958.

(12) Gessow, A. and Myers, Jr., G. C., Aerodynamics of the Helicopter, McMillan Publishers, New York, 1952.